CHALMERS
UNIVERSITY OF TECHNOLOGY

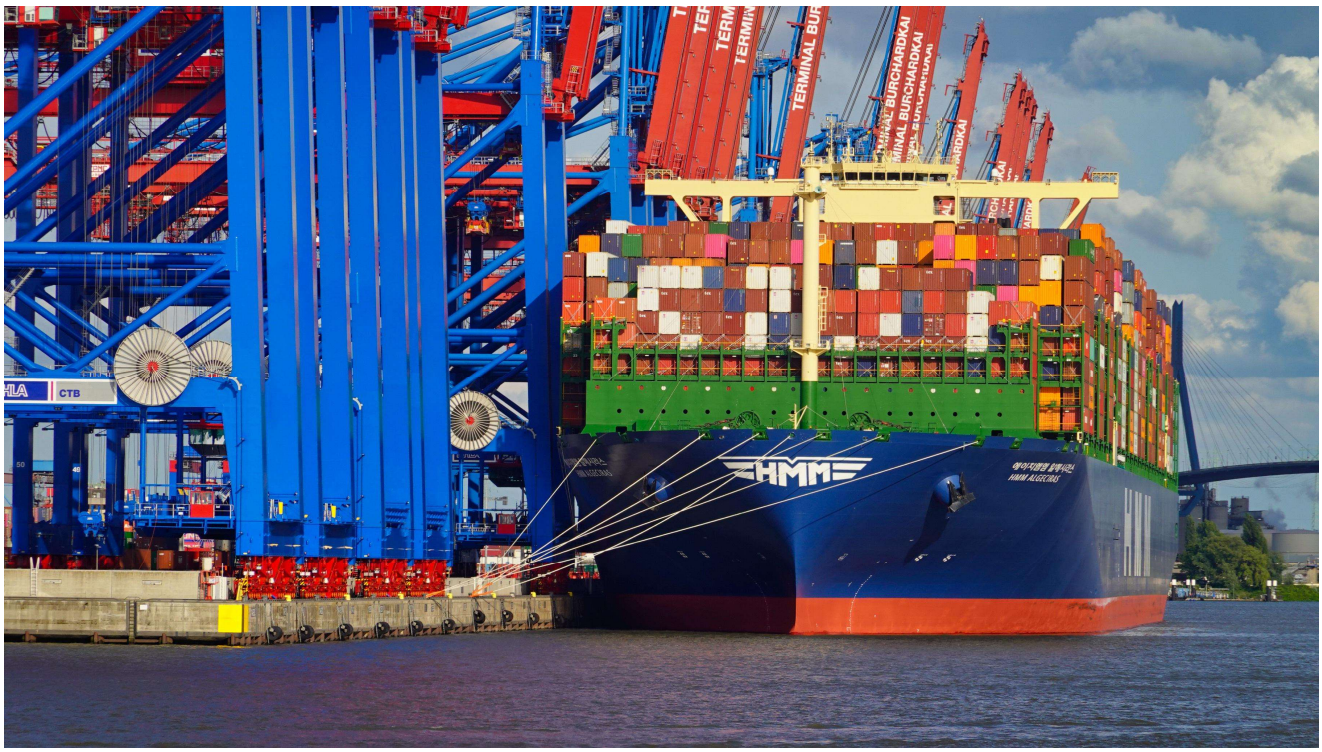


# Comparison of time domain simulation methods for ship mooring arrangements

Master's thesis in Naval Architecture within MSc Mobility Engineering

BASIL P. THOMAS
JOSÉ BORGES

DEPARTMENT OF MECHANICS AND MARITIME SCIENCES
CHALMERS UNIVERSITY OF TECHNOLOGY

Gothenburg, Sweden 2025
www.chalmers.se

MASTER'S THESIS IN MSC MOBILITY ENGINEERING

# Comparison of time domain simulation methods for ship mooring arrangements

Basil P. Thomas, José Borges

Department of Mechanics and Maritime Sciences
Division of Marine Technology
CHALMERS UNIVERSITY OF TECHNOLOGY
Göteborg, Sweden 2025

Comparison of time domain simulation methods for ship mooring arrangements

Basil P. Thomas, José Borges



Department of Mechanics and Maritime Sciences
Division of Marine Technology
Chalmers University of Technology
SE-412 96 Göteborg
Sweden
Telephone: + 46 (0)31-772 1000

Cover:
Moored container vessel, image by Horst Müller

Department of Mechanics and Maritime Sciences
Göteborg, Sweden 2025-08-13

Comparison of time domain simulation methods for ship mooring arrangements
Master's thesis in MSc Mobility Engineering
Basil P. Thomas, José Borges
Department of Mechanics and Maritime Sciences
Division of Marine Technology
Chalmers University of Technology

Abstract

Safe and effective mooring of ships at berth is a critical aspect of port operations, affecting crew safety and vessel integrity as well as operational cost and efficiency. It has become a common practice to plan ships mooring arrangements in advance using ship dynamics prediction tools. This study employs two prediction tools, one based on a fully nonlinear potential flow method and the other on a semi-empirical method, for simulating the dynamic behaviour of a moored ship in time domain. The simulations are carried out for a barge with a simple geometry, subjected to the primary environmental factors in ship mooring problems, namely wind, current and waves. The isolated and combined effects of these environmental factors on the ship dynamics are investigated by analysing the ship motions as well as mooring lines tensions. Overall, the results obtained from the employed tools were comparable, while the semi-empirical method offered substantially faster calculations (lower computational costs) than the potential flow method. However, the study reveals that the lack of suitable models to account for quay wall effects on the moored ship within the semi-empirical method can adversely affect the dynamic behaviour predictions, hence significantly impact the assessment of mooring line arrangement performance.

Key words: Mooring Line Arrangements, Simulations, Time domain mooring analyses, Potential flow, Semi-empirical model

# Contents

# Preface

In this study, semi-empirical and potential flow simulations have been carried out on a barge model. The study involved the following simulation software; SEAMAN and Shipflow Motions. The project is carried out in RISE Maritime (formerly SSPA), Gothenburg, Sweden between January and May 2025.

We would like to express our deepest gratitude to our supervisors, Dr. Jan Östh and Dr. Mohsen Irannezhad from RISE Maritime. Their ongoing support, guidance and assistance over the duration of the thesis has been critical in achieving this result. We are grateful to RISE Maritime for providing us with this opportunity to carry out such an interesting project.

We would also like to present our heartfelt gratitude to the following people for their unwavering support and guidance:

- Full Professor Jonas Ringsberg from Department of Mechanics and Maritime Sciences, Chalmers University who served as examiner and academic supervisor for the project. We appreciate the assistance and guidance we received from him in all matters related to the thesis. It has proven vital in directing and refining our study.
- Martin Kjellberg from RISE Maritime, who helped not only in all matters concerning Shipflow Motions simulations but also provided vital insights into the subject matter. We deeply appreciate his kind availability.
- Claes Eskilsson from RISE Maritime, who gave valuable insights into the mooring line modelling and for introducing us to the MoodyMarine tool. This has further extended our understanding of the different approaches to the mooring problem, even though we ended up not using this tool.
- Erland Wilske, Christine Sonntag and Olov Lundbäck from RISE Maritime for providing valuable insights and guidance relating different topics that contributed to us having a holistic understanding of the mooring problem and the different elements involved.
- Michal Orych, from Flowtech International who extended valuable support and assistance in utilisation of Shipflow motions tool for our study.

Finally, we would like to thank our friends and family for all the support extended throughout this challenging phase of our Masters education. This project would not have been possible without you all.

Göteborg 2025-08-13

BASIL P. THOMAS, JOSÉ BORGES

# List of acronyms

Below is the list of acronyms that have been used in the thesis listed in alphabetical order:

| | |
|---|---|
| AWA | Apparent Wind Angle |
| AWS | Apparent Wind Speed |
| CAD | Computer Aided Design |
| CFD | Computational Fluid Dynamics |
| CS | Control Surface |
| CV | Control Volume |
| DOF | Degrees of Freedom |
| DWT | Deadweight Tonnage |
| FEM | Finite Element Method |
| FFT | Fast Fourier Transform |
| FPS | Floating Production Systems |
| GIS | Geographic Information System |
| HMSF | High Modulus Synthetic Fiber |
| ISO | International Organization for Standardization |
| ITTC | International Towing Tank Conference |
| MBL | Minimum Breaking Load |
| MEG | Mooring Equipment Guidelines |
| MODU | Mobile Offshore Drilling Units |
| MSL | Mean Sea Level |
| MV | Motor Vessel |
| OCIMF | Oil Companies International Marine Forum |
| P&I | Protection and Indemnity Insurance |
| PCTC | Pure Car and Truck Carrier |
| PIANC | World Association for Waterborne Transport Infrastructure |
| RISE | Research Institutes of Sweden |
| RoPax | Passenger RoRo vessel |
| RoRo | Roll-on Roll-off vessel |
| SPM | Single Point Mooring |
| STS | Ship-to-Ship |
| SWL | Safe Working Load |
| VLCC | Very Large Crude Carrier |

# List of figures

# List of tables

# 1 Introduction

In the morning of the 13th of March of 2021, mooring lines securing the MV Endurance broke as a result of deteriorating environmental conditions (BSU, 2025). MV Endurance – a car carrier with American flag – was moored in Bremerhaven, Germany, when the accident happened. A strong wind gust of approximately 50 knots coming from south-west made it impossible to hold the vessel in place and caused line breakage, starting from the "head" lines (connected to the bow), and resulted in the ship colliding the pier. Figure 1.1 - a illustrates the event and location of damages caused by excessive movement of the vessel on the port structures. These damages include a destroyed lifebuoy holder and drag marks on the pier from the ramp (Figure 1.1 - 1), contact with the pier (caused a block of concrete to burst out), pontoon (damaged the wooden deflectors) and dock (teared off of a fender and deformed of the dock) (Figure 1.1 - 2), bollard cap destroyed (Figure 1.1 - 3) and contact with a building on land (Figure 1.1 - 4).

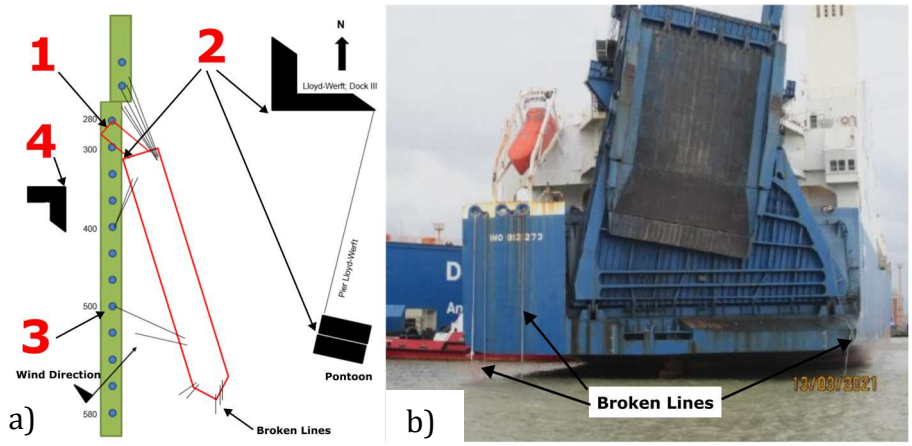


*Figure 1.1 MV Endurance's accident in Bremerhaven. a) Sketch containing the location of damages. b) Broken lines resulting from the accident. Adapted from the technical report by the Bureau of Maritime Casualty Investigation, (BSU, 2025).*

In addition to the damages caused to the port structures, the vessel suffered damage from the accident as well: a 0.8m-long crack in the hull on the port side, a hole in the bulbous bow, a dent in the stern, starboard side, with paint abrasions over a length of roughly 1.5m. The ship was not holding cargo, so no cargo damage was reported for this casualty. Although the captain tried to prevent these events by adding extra lines in time to resist the strong wind conditions predicted by the forecast, ultimately the report deemed the accident to be caused by human factor, as it was a result of parting of the poorly maintained ropes that were used in mooring. Figure 1.1 - b shows the resulting broken lines.

This example of accident in port is not unique and it is both the result of inadequate mooring equipment and harsh environmental conditions. Historically, mooring of ships was unproblematic, as most ports were located upstream from the river's mouth, where the ship was sheltered from stronger winds, waves and currents. The amount of goods transported with ships has increased substantially

in the 20th century causing an increase in demand for larger vessels. In the second half of the last century, the draft of the ships doubled, and the mass of ships increased from a maximum of 50 000 tonnes to more than 500 000 tonnes (Costa, 1987). This evolution forced port operations into deeper, more exposed waters, where the effect of environmental factors can cause significant ship motions.

Port operations, such as loading/unloading of cargo (for cargo vessels) and embarking/disembarking of passengers (for passenger vessels) require small ship motions. Reducing the motions of the vessel at berth leads to not only decreasing the amount of time the vessel is at port, but also to assuring the safety of the cargo, passengers and crew/port workers. In some extreme cases, external factors can cause motions to be so significant that loading/unloading is not only inefficient, but also impractical and unsafe. PIANC Working Group 24's report illustrates this with Figure 1.2 (PIANC, 1995). From point A to B is the case of small motions that do not affect the operation of the ship at all. From B to C, the gradual increase of motions results in loss of capacity to carry on loading/unloading operations. Finally, from C to D (and with motions larger than the ones represented with point D) it is impossible to carry out port operations.

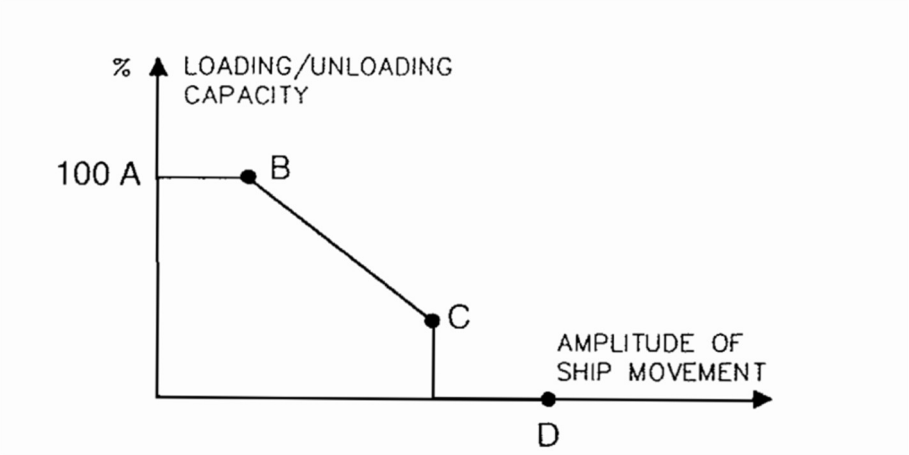


*Figure 1.2 Port operations capacity as a function of the amplitude of the movement of the moored ship. Adapted from (PIANC, 1995).*

To restrict ship motions effectively, it is important to design appropriate mooring systems. Mooring is defined by the Oil Companies International Marine Forum (OCIMF) as the "securing of a ship to a marine facility, terminal, berth or another ship using mooring lines" (OCIMF, 2018). Figure 1.3 illustrates a typical mooring pattern for a tanker ship as defined in OCIMF's Mooring Equipment Guidelines. The arrangement consists of breast lines, spring lines and head/stern lines. "Breast" lines should be as perpendicular to the ship's centreline as possible to restrict the ship in lateral motion. Ideally, they are placed as far as possible from midships. "Spring" lines should be as parallel to the ship's centreline as possible to restrict longitudinal motions. Finally, "head" and "stern" lines assist in restricting longitudinal motion as well. Like spring lines, head and stern lines are as parallel to the centreline of the ship as possible but connect the bow/aft to port bollards further in front of the ship or further aft, respectively.

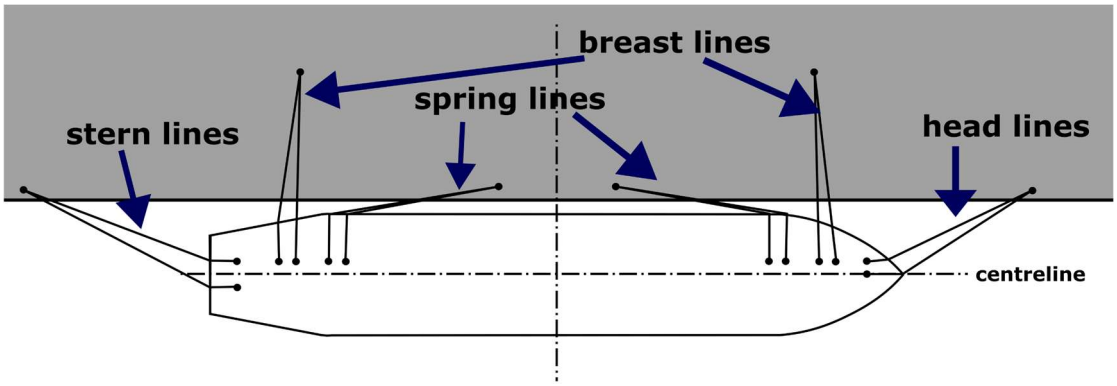


*Figure 1.3 Typical mooring line arrangement for a tanker ship: different types of mooring lines. Adapted from (OCIMF, 2018).*

Many elements and parts of the ship and berth are involved in the mooring process; examples of such equipment are shown in Figure 1.4. Mooring lines (Figure 1.4 - a) - sometimes connected to mooring tails (Figure 1.4 - b) - secure the ship to bollards (Figure 1.4 - c) or quick release hooks (Figure 1.4 - d) on the berths. These are routed through fairleads or chocks (Figure 1.4 - e), redirected by bitts (Figure 1.4 - f) and pedestal rollers (Figure 1.4 - g) and secured on the winches (Figure 1.4 - h) by reeling them in the drums. Fenders (Figure 1.4 - i) prevent the vessel from colliding with or rubbing against the concrete or wooden berth structure, thereby avoiding damage to the side shell of the ship and to the port structure. This system of mooring lines and fenders balances the external forces acting on the ship to provide the stability needed to carry out port operations.

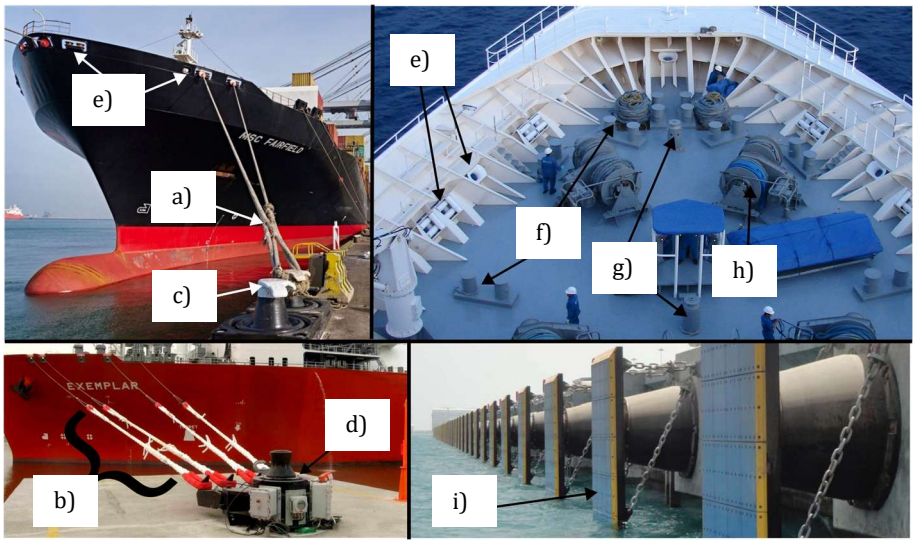


*Figure 1.4 Mooring equipment.*

In addition to the conventional mooring equipment that has been described, new mooring tools are being developed and used in some ports. These include vacuum mooring systems – in which vacuum pads use suction to restrict the motion of the vessel - and magnetic mooring systems – where electromagnets connected to hydraulic arms provide the necessary resistance to movement. Although these systems have advantages over conventional mooring (Kuzu, 2017), these mooring systems rely on port-based infrastructure that is not yet widely used. These mooring solutions will be disregarded in this thesis.

The mooring arrangement is the combination of equipment used to moor the ship. Figure 1.5 shows – as an example - the mooring line arrangement of the MV Endurance when it was moored in Bremerhaven. Seven lines were available for the front (Figure 1.5 - a) and seven lines for the aft (Figure 1.5 - b) and they were arranged in a 5/2 configuration: 5 head/stern lines and 2 spring lines. The winches that should be used are also specified, as well as the bollards and the fenders.

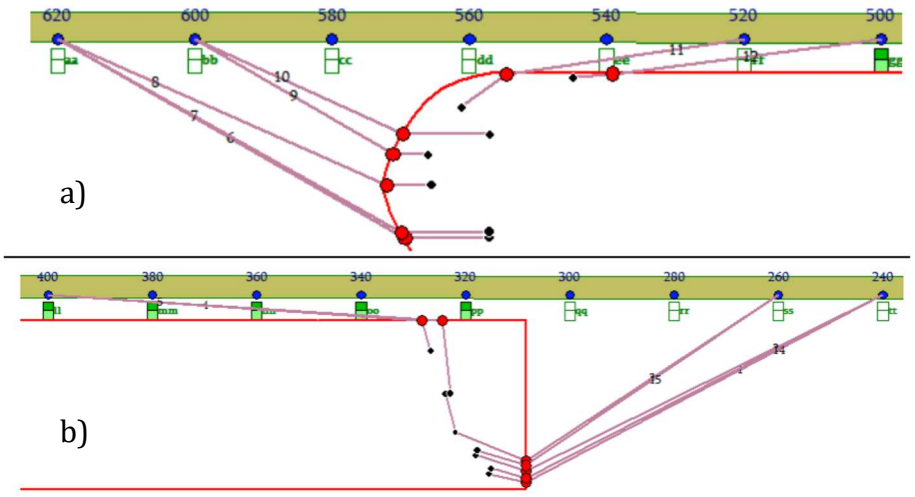


*Figure 1.5 Mooring arrangement of the MV Endurance before the accident: a) configuration in the bow, b) configuration in the aft. Adapted from (BSU, 2025).*

Mooring line arrangements are specific to each vessel and to each port. The size and type of the vessel influences the magnitude of the effect an environmental factor produces. For example, in a port where head currents are common and significant, a tanker will feel a larger effect from the current than a cargo ship, since the exposed area of tankers are often larger than the area from cargo ships – block coefficients for tankers range often from 0.78 to 0.88, while for cargo ships it ranges from 0.56 to 0.73 (Papanikolau, 2014). In another port, where winds are prevalent, a cruise vessel, with high freeboards and tall superstructures will be more affected by winds and gusts than a tanker, due to larger areas exposed to the wind.

Different types of vessels have different requirements when it comes to maximum amplitude of motions in port that allow safe port operations. PIANC's Working Group 24 suggest recommended motion criteria for safe working conditions in their report. Table 1.1 summarises these recommendations for different types of vessels (PIANC, 1995). Other authorities have also developed some vessel-specific guidelines e.g. the British Standards Institutes provides guidelines for motions for Ro-Ro ships as a design basis (BSI, 2007).

*Table 1.1 Recommended motion criteria for safe working conditions Adapted from (PIANC, 1995). Ranges depend on the available equipment on the vessel for port operations.*

| Ship Type | Surge (m) | Sway (m) | Heave (m) | Roll (°) | Pitch (°) | Yaw (°) |
|---|---|---|---|---|---|---|
| Fishing Vessel | 0.15 – 2.0 | 0.15 - 1 | 0.4 | 3 | 3 | 3 |
| Freighter, Coaster | 1.0 | 1.2 | 0.6-0.8 | 1-2 | 1 | 2-3 |
| Ferries, Ro-Ros | 0.1-0.8 | 0.1-0.6 | 0.4-0.8 | 1-3 | 1-2 | 1-4 |
| General Cargo | 2.0 | 1.5 | 1.0 | 3 | 2 | 5 |
| Container Vessel | 1-2 | 0.6-1.2 | 0.8-1.2 | 1-1.5 | 1-2 | 3-6 |
| Bulk Carrier | 1-5 | 0.5-2.5 | 1.0 | 2-3 | 2 | 2-6 |
| Oil Tanker | 3.0 | 3.0 | - | - | - | - |
| Gas Tanker | 2.0 | 2.0 | - | 2 | 2 | 2 |

In order to fulfil such motion criteria, increasing the stiffness of the mooring arrangement by adding extra mooring lines appears to be a valid solution. However, this is not only inefficient in the use of the mooring equipment, but it would also result in longer time in port. Besides, the addition of extra lines without consideration of the interaction between them can lead to an uneven distribution of load between the lines, thus making the system unpredictable in the event of extreme conditions. A good mooring arrangement has the right number of mooring lines, with a balanced distribution of load.

To maximize the efficiency of the lines, these should align with the direction they are trying to restrict (OCIMF, 2018). In a general setting, a good mooring arrangement must be able to hold all expected environmental conditions, with the fenders taking up the loads in the on-berth direction, the breast lines counteracting the loads in the off-berth direction, the spring lines opposing the loads parallel to the berth and all of them contributing to restrict vertical motion with their vertical components.

Wrong use of the equipment - and thus unbalanced distribution of exerted loads - can have serious consequences in the safety of the cargo, vessel and, especially, the crew, as it was shown with the example of the MV Endurance. Although in this

example there were no human casualties, an article from the Maritime Injury Centre states that between 2016 and 2021 mooring accidents have caused 858 injuries and 31 deaths (Maritime Injury Center, 2024). As an example, in a recent incident, in 2021, a crew member suffered a fatal head injury when a mooring rope slipped off a fairlead as it came under tension during a warping operation. Generally, to avoid similar situations, mooring equipment is marked, and snap back zones are demarcated to alert the crew and operators. As a last remark on incidents, cargo can also get damaged or lost because of a poor mooring arrangement as seen from the report by UK P&I Club (2009).

Environmental conditions at port are often predictable making it possible to plan an effective and efficient mooring arrangement prior to arrival in port. Several principles for planning a good mooring arrangement have been outlined in section 1.6.2 of (OCIMF, 2018).

An efficient way to plan and evaluate mooring arrangements is to make use of prediction tools. These tools employ mathematical models and perform numerical computations to simulate the physical phenomena involved in the mooring of ships. Today, mooring simulations have become valuable methods in evaluating effectiveness of different mooring line arrangements in various environmental conditions. A mooring simulation tool can take, e.g. the line arrangement, the lines' properties, ship and port data, and environmental factors as inputs and, after performing the computations, can assess the considered mooring arrangement with respect to the lines' tension and the ship motions, for example.

Moored ships are mainly affected by waves, current and wind, as depicted in Figure 1.6, even though these can be suppressed to some extent by port structures like breakwaters or wind shelters. These environmental factors can sometimes fluctuate with frequencies close to the natural frequencies of the harbour resulting in harbour oscillations and large vessel motions (Dong, 2022). Moreover, the shallow water effects as well as bank and cushion effects add complexity to the problem. These phenomena originate from port structures – like a quay or shallow port- and cause forces of considerable value on the moored ships when the fluid is displacing near it (which can be not only a result of current, but also of passing ships). Finally, the mooring lines and fenders used to attenuate the motions have non-linear mechanical behaviour. Most of these physical factors can be captured with different accuracies by prediction methods with different fidelity levels.

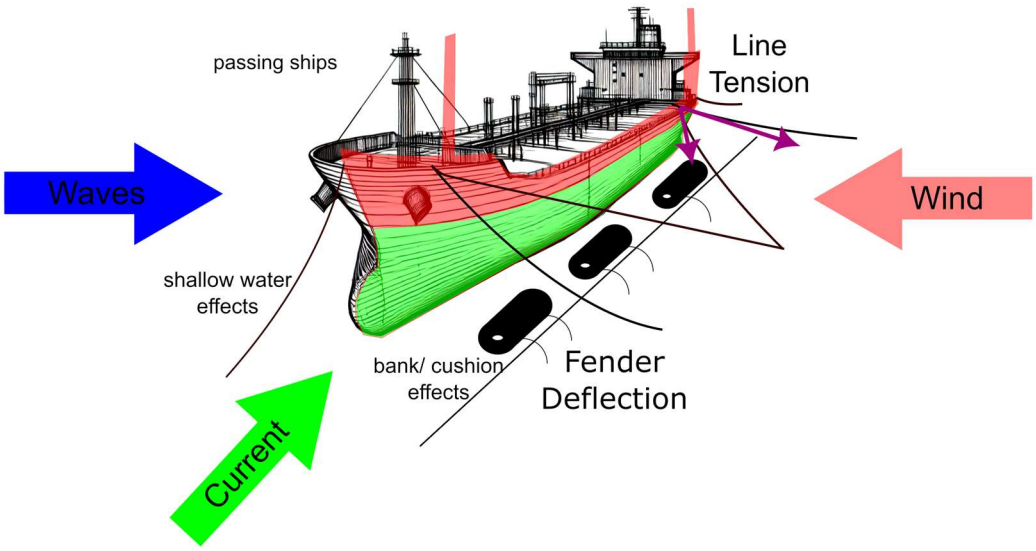


*Figure 1.6 Different factors to account for in mooring simulations.*

Tools based on empirical or semi-empirical methods are often valuable in obtaining quicker predictions, by relying on statistical correlations derived from measurements and in the use of analytical formulations. On the other hand, numerical methods based on Computational Fluid Dynamics techniques (CFD) or potential flow solvers require a considerably larger amount of computer resources and time, with the advantage of handling complex problems with less simplifications. These higher fidelity tools are often more reliable and more accurate at representing the physical phenomena involved in the mooring problem.

In the event of quickly deteriorating environmental conditions, as in the case of the MV Endurance, where heavy winds and gusts were announced one day prior, it is valuable to be able to quickly adapt to these situations and plan accordingly. Faster methods, such as empirical/semi-empirical methods, would be preferred in situations where time is a limiting factor. However, it is important to assure that these faster methods don't oversimplify the problem in such a way that renders the results useless and with unreasonably large errors.

## 1.1 Purpose

The purpose of this thesis is to evaluate and compare the performance of the computational models and numerical methods implemented in two different simulation tools for prediction of ships mooring line arrangements, namely a tool based on semi-empirical methods and a tool based on non-linear potential flow methods.

The time-domain results of the semi-empirical prediction methods employed in the in-house software simulation tool, SEAMAN, developed by RISE - SSPA Maritime Centre, are obtained and compared against the time-domain results obtained from a commercial potential flow solver, Shipflow Motions.

## 1.2 Scope and limitations

A barge with simple geometrical characteristics is chosen as the ship under study in this thesis, enabling a clearer analysis of the computational models and the resultant ship behaviour with respect to its mooring lines arrangement. Therefore, the conclusions drawn in this thesis can mainly be extended to ships and structures experiencing similar physical phenomena as the ones considered for the barge. However, these results are not extendable to e.g. floating offshore structures' mooring lines, where, for example, catenary behaviour of the ropes is important in determining the motions of the floating structure and the forces in the lines.

Although there exists measurements data – both from model scale and full-scale experimental studies - on mooring line tension and ship motions for different mooring line arrangements affected by different environmental conditions, such data was not used in this thesis. The reason lies on the fact that such datasets used in literature were either confidential or not replicable for confidential reasons. For instance, if the main particulars, loading conditions and design specifications of the moored ship are not known, it becomes impossible to replicate a representative simulation. Consequently, the validation practice, i.e. comparing the simulation results against experimental data, is not carried out on the results presented in the thesis.

Moreover, the choice of tools limits the analysis for the lack of reference of the error obtained from the software. It would have been preferred to have included tools that has been validated for mooring applications, such as Optimoor or MoodyMarine, and where the error obtained in relation to real life measurements has been quantified.

Both considered tools -the potential flow solver and the semi-empirical model - assume the ship to be a rigid-body, i.e. the deformation of the body is not accounted for during the simulations. Even though there have been developments of models based on the flexible hull idea, this is commonly accepted as a valid assumption in manoeuvring theory (Soares, 2011) as the contribution from the deformations is small when compared to a characteristic length of the model.

By using potential flow simulations to simulate mooring we are also accepting the assumptions made by potential flow theory. Disregarding the viscous effects in mooring calculations in which the velocity of the ship is often small might produce larger errors than in seakeeping/manoeuvring simulations where the ship moves at higher velocities. For small motions, the boundary layer plays an important role. The error stemming from lack of consideration for viscous effects in the calculation is decreased by considering these factors artificially, through IITC friction estimation models. The assumption that viscous effects are mostly negligible in the simulation calculations is therefore accepted in this thesis.

Further simplifications are made in the semi-empirical tool. Strip theory is used to calculate wave forces and added mass and damping coefficients. Strip theory assumes the ship domain can be approximated by a set of strips, for which forces

are calculated and linearly added to obtain a total force. It has been proved that strip theory produces valid estimations and hence it is considered a valid approach to these calculations. Strip theory calculations are described in greater detail in Section 2.2.3.3.

In this thesis, the focus was set on wind, waves and current as the dominant environmental excitation forces acting on the moored ship system. Other effects represented in Figure 1.6, such as passing ships, bank effects, cushion effects and shallow water effects, were not considered. Additionally, the modelling of these environmental factors was done without considering sudden changes in speed or direction – as often happens in extreme conditions. Although the waves at real sea are irregular and varying, in this thesis only the regular waves are considered. Moreover, the wind gust is not taken into account, thus constant wind speed and wind direction are considered in each simulation incorporating wind. Furthermore, non-varying water current velocity and direction is considered in each respective simulation.

## 1.3 Outline of the thesis

To achieve the objective of the thesis, a series of simple test case scenarios defined by isolating/combining various environmental conditions and the barge line arrangements are introduced and evaluated in both tools. The physical models considered are presented in Section 2. The corresponding computational models are described in Section 3. The study cases are explained in Section 4 and finally the results are presented and discussed in Section 5. Section 6 includes the final thoughts and suggestions for future work.

# 2 Mooring of ships

This chapter summarises the theory behind the mooring problem and that will be useful in the analysis of the results. The first subsection describes development of mooring simulations and research that has been done in regard to the modelling of different factors involved in mooring. The second subsection delves deeper in the theoretical formulations of these models. Special consideration is given to the description of the different forces on the ship, the ship motions, different mooring equipment and simulations methodologies currently in use.

## 2.1 Literature study

The mooring problem has been approached from multiple angles. Theoretical calculations along with experiments on models formed the first step in evaluating the mooring problem - as in the study done by Muga et al. (1971), where a barge model was tested in open sea conditions. The results were compared with theoretical calculations using slender-body approximations. The resulting calculations from the theoretical approach presented an adequate prediction of the motions of the barge. Bomze et al. (1974) explores an analytical approach to calculating the ship motions and mooring forces with a time series analysis using the Froude-Krylov hypothesis wherein it is considered that: firstly, the wave is not modified by the presence or motion of the ship, secondly, linear wave theory is applied and finally, the underwater portion of the ship is approximated as a rectangular block.

Studies have been performed to characterize the motions of ships at berth when affected by different effects. Response in waves is the most studied phenomena; these can be characterized as long-period waves -e.g. in (Molen, 2006)-, short-period waves (Sakakibara, 2008) damping (Boze, 1974) and wave drift forces (Faltinsen, 2015). Response in currents have been studied by Gómez-Pina and Ottesen-Hansen (PIANC, 1995). Wichers (1991) studied the effect of the wind, wave and currents – characterising them as the most relevant phenomena in ship mooring.

In the study by Ivar et al. (1988), a simulation model for analysis of motions of berthed vessels is described and simulations are performed in the time-domain. A simulation program called MOSSI-Q is used to carry out the simulation. The following assumptions are made to simplify the analysis.

- Responses to waves are modelled as linear responses
- Low frequency motions (in surge, sway and yaw) as affected by low frequency external forces are modelled as a set of coupled nonlinear second order differential equations solved in the time domain
- Responses from the wave and low frequency forces are superimposed to obtain the total motion

Kwan et al. (1991), in their study regarding mooring of Floating Production Systems (FPS) and Mobile Offshore Drilling Units (MODU), compares applications

and limitations of frequency and time domain analysis and compares with conventional quasi-static analysis methods. It was noted that quasi-static approach neglects the mass, damping and fluid acceleration effects. However, these effects are captured in the dynamic analysis of the mooring system. The comparison of results in the study shows that the tensions calculated in the mooring ropes using the dynamic analysis are as much as 19 times larger than those calculated using the quasi-static method. The study also identifies four non-linearity effects that influence the mooring line behaviour.

- Non-linear stretching of the mooring line especially when the mooring lines are manufactured from synthetic fibres.
- Non-linear deformation of the cross-section of the mooring line
- Fluid loading effect on the mooring line which produces a drag force proportional to the relative velocity between the fluid and the line.
- Bottom effects, which describes the portion of the mooring line in contact with the sea floor

The last two non-linearities can be neglected in the case of mooring of ships to berths as the mooring lines are rarely immersed in the water, and in air the drag can be neglected. Moreover, the mooring lines are not in contact with the seafloor for this application. The non-linearities in stiffness are solved by recalculating the stiffness for every step based on the elongation of the line. The study also shows that frequency domain analysis can produce acceptable line tensions provided the non-linearities are properly linearized. The use of frequency domain analyses has however decreased in favour of time domain simulations since this study was published, for the lack of detail the frequency-domain simulations provided in its results.

Wichers and Kat (1991), in their study carried out numerical simulations for a tanker in a single point mooring arrangement (SPM). The effect of wind, current and wave drift forces were analysed in sway, surge and yaw degrees of freedom. The analysis was carried out for different loading conditions, and it was noted that effect of increased wind force in the case of the vessel in ballast condition results in increased instability. The study also noted that further study is required in analysing the wind gust characteristics at sea and its effects on vessels or platforms. The study, having been conducted on low speed currents, neglects the free surface effects.

Rosa-Santos et al. (2014) studied the influence of the type of fender and pre-tensioning of mooring lines in reducing the ship motions. Experiments were carried out using a small-scale model of the vessel. The results showed that friction provided at the contact between the vessel and the fenders along with the pre-tensioning provided increased dampening to the ship motions.

The effect of shallow water on the forces and motions of a moored vessel was studied by Faltinsen et al. (2015), using second order perturbation method with the incident wave slope as the small parameter. It was concluded that the added mass and damping coefficients increased with decrease in depth. It was also found that the longitudinal drift forces increase with decreased depth.

As for mooring line tension prediction, Wang et al. (2022) carried out a study to compare a few different mooring analysis methods used to predict mooring forces. The methods considered were using classification society rules, OCIMF formulas and using the commercial Optimoor software. The study concluded that the results obtained using these methods were comparable.

The lack of an industry standard regarding methods used to assess the mooring problem was also identified in the present literature study. Each method has its own merits and downfalls. The choice of the method of analysis should rather reflect on the effect that forms the focus of this study or the purpose for which the analysis is carried out.

## 2.2 Forces on the ship

One of the goals of the mooring simulations is to obtain an accurate prediction of the motions of the moored ship. To calculate the motions of the moored ship, knowledge about the forces that are causing the motion of the moored ship is needed. In this section these forces, and their modelling are considered in detail.

The description of the forces includes a mention of how it affects the motions along different degrees of freedom (DOFs). The ship has 6 degrees of freedom: surge (movement along the x-axis, Figure 2.1 - 3), sway (movement along the y-axis, Figure 2.1 - 2), heave (movement along the z-axis, Figure 2.1 - 1), roll (rotation around the x-axis, Figure 2.1 - 6), pitch (rotation around the y-axis, Figure 2.1 - 5) and yaw (rotation around the z-axis, Figure 2.1 - 4). These movements are usually defined at the centre of gravity (COG) of the ship.

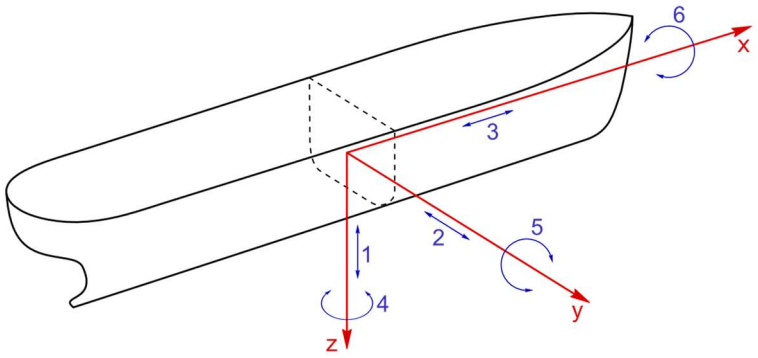


*Figure 2.1 Degrees of freedom represented in a body-centred coordinate system.*

### 2.2.1 Hydrostatic forces

When the ship - or, in general, a body - is placed on the water, the reaction force that counteracts gravity is a result from displacing the particles of the fluid. Archimedes principle describes this phenomenon and can be formulated as "The weight of the volume of water displaced by a floating body is equal to the weight of that body" (Biran, 2003). The hydrostatic force can be defined as:

$$F_{hydrostatic} = \rho_{water} \cdot g \cdot \nabla = m_{body} \cdot g \,, \tag{2.1}$$

where $\rho_{water}$ is the density of the water, $g$ is the gravitational acceleration, $\nabla$ is the volume of fluid displaced and $m_{body}$ is the mass of the body placed on the fluid.

The gravitational force acts through the COG of the ship, while the buoyant force acts through the centre of buoyancy, which is the centroid of the submerged volume. Improper load distribution can shift the COG away from the vertical line through the centre of buoyancy, resulting in a static heel (list) or trim. In such cases, hydrostatic restoring moments act when the ship is disturbed, attempting to return it to equilibrium. During dynamic ship motion, such as in waves, the submerged shape of the hull changes, leading to continuous variation in the location of the centre of buoyancy. This variation gives rise to time-dependent restoring moments in roll and pitch, which influence the ship's dynamic response. The change in the submerged shape of the hull can also cause lack of or excess buoyancy, which produces a restoring force in the vertical direction, affecting heave.

### 2.2.2 Hydrodynamic forces

The set of forces considered under this category comprise of the forces that arise because of the interaction between the ship and the water. These are usually divided into added mass and damping forces.

The added mass force is an inertial force, representative of the acceleration of the surrounding water by the ship. It is a resistive force that acts against the movement of the ship, causing it to have force and moment components in all 6 degrees of freedom. Because of its proportional relation to acceleration, it is called "added mass" as it is equivalent to considering a bigger mass (Muga, 1971). This force is a result of hydrodynamic pressure variations proportional to the acceleration of the body in a certain direction (Faltinsen, 1990).

The damping forces represent the effect of dissipating energy due to wave generation (radiation damping), viscosity (viscous damping) and eddy-making (vortex shedding). The damping force is proportional to velocity and has force and moment components in all six degrees of freedom (Muga, 1971). It is worth mentioning that for the study of roll motion, the effects from viscous damping and eddy making are particularly significant, whereas these phenomena are often neglected for the other degrees of freedom due to their relatively smaller impact.

These hydrodynamic forces can be expressed mathematically through

$$F_k = -A_{kj}\frac{d^2\eta_j}{dt^2} - B_{kj}\frac{d\eta_j}{dt} \,, \tag{2.2}$$

where the subscripts $k\,, j = 1, 2, \ldots, 6$ refer to the different DOFs, $\eta$ refers to motion in a specific DOF and $A_{kj}$ and $B_{kj}$ are, respectively, the coefficients of added mass and damping. There are 36 added mass coefficients in total and 36

damping coefficients in total. These coefficients depend mostly on geometry, but also on ship speed and oscillating frequency. Some of the coefficients can have null value and, for cases where the floating structure does not have speed on the longitudinal direction and there is no current, it is possible to show that $A_{kj} = A_{jk}$ and $B_{kj} = B_{jk}$.

An approximation of the three-dimensional coefficients can be obtained by combining the two-dimensional added mass and damping coefficients with strip theory calculations. In these calculations, the underwater part of the ship is divided into strips, the coefficients are calculated for those sections and thereafter integrated along the strips. Strip theory assumes that the variation of the flow in the cross-section is much larger than the longitudinal variation of the flow, which is a valid assumption for most of the ship hull (for normal merchant ships); it fails however at the fore and aft ends of the ships. To avoid lengthy calculations for all the coefficients, numerical methods were developed to calculate estimations for the two-dimensional coefficients. Lewis forms are such examples, where the non-dimensional added mass and damping coefficients are obtained through correlations with the beam-draught ratio $B/D$, the sectional area coefficient $\sigma = A/(BD)$ , where A is the submerged cross sectional area, and a non-dimensional frequency of oscillation $f = \omega\sqrt{D/g}$ . Figure 2.2 is an example of such a curve for heave added mass, when $\omega \to \infty$ and for the case of infinite water depth.

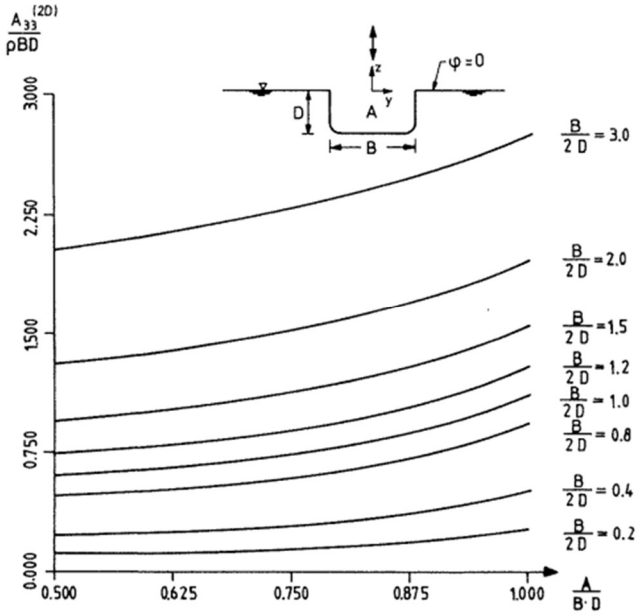


*Figure 2.2 Lewis forms for heave, depending on sectional area coefficient and beam-draught ratio, for frequency ω → ∞. Adapted from (Faltinsen, 1990).*

### 2.2.3 Environmental excitation forces

Environmental factors often affect the ship operation at sea. These factors also play a crucial role in impacting the moored ships. The dominant environmental excitation forces applied to moored ships are originated from current, wave and wind. Other factors, some of which are shown in Figure 1.6, as well as more specific ones such as ice and tides, are not considered in this thesis.

#### 2.2.3.1 Wind

Wind loads result from the interaction between the flow of the wind and the floating body. The effect of the wind becomes considerable in the case of large, exposed bodies, such as ships with a high freeboard or ships with large superstructures (PIANC, 1995). This is the case of, for example, large Pure Car and Truck Carriers (PCTCs) and RoPax vessels (vessels for rolling cargo and passengers).

For the mooring of merchant ships, wind can have a beneficial effect, e.g. if the wind is pushing the ship into the fender, causing the friction between fenders and the ship to increase and hence reducing the motions (PIANC, 1995). It is, however, more common that the wind produces unwanted ship motions that reduce the efficiency of port operations. Wind can be especially problematic when it presents irregular behaviour, as in the case of wind gusts, which can cause unbalanced rapid tensioning of the mooring lines. These events are often unpredictable and dangerous to crew and cargo.

Wind affects mainly sway, roll and yaw motions and, for some values of wind speed, there is a risk of dynamically induced motions due to resonance with the ship's natural frequencies (PIANC, 1995).

The forces generated by wind are originated from differences in pressure around the body. The added pressure on one side is a result of the variation of linear momentum of the fluid. This variation can be obtained by means of the linear momentum equation of fluid mechanics (White, 2003), by considering a fixed control surface (CS) close to the surface of the body and the fixed control volume (CV) enclosed by it:

$$\sum \boldsymbol{F} = \frac{d}{dt}\left(\int_{CV} \boldsymbol{V}\rho \, dV\right) + \int_{CS} \boldsymbol{V}\rho \, (\boldsymbol{V} \cdot \boldsymbol{n}) dA \,, \tag{2.3}$$

where $\boldsymbol{V}$ is the fluid velocity and $\rho$ is the fluid density. The force vector sum presented on equation (2.3) includes the surface forces on the fluid enclosed by the control surface plus all the body forces acting on the masses within the control volume. Ships often have complicated geometries when it comes to areas exposed to wind loads. Therefore, the accurate calculation of wind forces can only be done experimentally or with the help of CFD. Such methods can model the change in fluid velocity accurately and take into account other mechanisms like turbulence that can influence pressure distributions in the body and hence contribute to the wind force. More sophisticated models for force calculations would include coupled finite element methods (FEM) to those of CFD to calculate deflection of the structure under the load of the fluid. Nonetheless, as mentioned in Section 1.2, the ship in this thesis is assumed to be a rigid body, thus such flexibilities and deflections of the ship structure are overlooked.

Due to the complexity in obtaining accurate wind force prediction, empirical methods are often used (Faltinsen, 1990) and have been deemed reasonably

accurate for the purpose of assessing seakeeping motions. Wind force is usually calculated for a specific direction using equation (2.4) (PIANC, 1995):

$$F_w = \frac{1}{2} \cdot \rho_a \cdot A \cdot V_r^2 \cdot C \ , \tag{2.4}$$

where $A$ is the area of the ship subjected to the wind, $V_r$ is the relative wind velocity and C is the empirically determined wind coefficient for the considered direction. Isherwood (1973) determined the value of this coefficient for different types of merchant ships for the surge, sway and yaw motions. This empirical constant is determined by inverting equation (2.4) and using force data obtained from testing, according to the formulas:

$$C_X = \frac{F_X}{\frac{1}{2} \cdot \rho_a \cdot V_r^2 \cdot A_T} \ , \tag{2.5}$$

$$C_Y = \frac{F_Y}{\frac{1}{2} \cdot \rho_a \cdot V_r^2 \cdot A_L} \ , \tag{2.6}$$

$$C_K = \frac{M_X}{\frac{1}{2} \cdot \rho_a \cdot V_r^2 \cdot \frac{A_L^2}{L_{OA}}} \ , \tag{2.7}$$

$$C_N = \frac{M_Z}{\frac{1}{2} \cdot \rho_a \cdot V_r^2 \cdot A_L \cdot L_{OA}} \ . \tag{2.8}$$

In equations (2.5) to (2.8), $A_T$ represents the transversal area, $A_L$ represents the lateral area, $F_X$ is the wind force in the x-direction (in N), conversely $F_Y$ is the wind force in the y-direction (in N), $M_X$ is the roll moment and $M_Z$ is the yaw moment (in Nm).

Sustained wind conditions describe wind with stationary direction, intensity and duration (Bureau Veritas, 2022). Intensity of the winds - described by the velocity of the latter and denoted $U_{Wm}(z, T)$ - is the averaged mean velocities at a height $z$ above the Mean Sea Level (MSL) over a specified duration of time $T$.

The height at which wind is to be considered will influence the chosen value for the relative velocity, because of the variations in the wind speed due to the atmospheric boundary layer. The power law is usually considered as an acceptable model of this phenomenon (ITTC, 2014):

$$U_{Wm}(z_{ref}) = U_{Wm}(z) \left(\frac{z_{ref}}{z}\right)^{\frac{1}{7}}, \tag{2.9}$$

where $z_{ref}$ is a reference height for which the wind speed is defined and $U_{Wm}(z)$ is the wind speed at height $z$.

It is, finally, important to consider the modelling of the wind itself and its velocity. The wind can be modelled as time averaged wind (sustained wind conditions),

with the purpose of calculating steady wind forces, or as a fluctuating wind (transient wind conditions), due to gusts, in the case of considering dynamic load.

Transient winds are considered either when wind velocity and/or direction change abruptly. These are usually generated by gusts, that can be observed, according to the Beaufort Wind Scale, at 4 Bft (moderate breeze), but are more noticeable from 6 Bft (Strong Breeze) onwards. These gusts often last for less than 20 seconds.

Transient winds can also be caused by squalls, where wind velocity changes rapidly and where wind direction also changes. Squalls can last much longer than gusts and pose serious problems for the mooring of offshore structures as they are an extreme case of dynamic loading.

#### 2.2.3.2 Current

The effect of current has been studied over the years considering its impact on the design and operation of marine structures. ISO 19901-1 identifies different types of currents as follows (ISO, 2015):

- Tidal current
- Oceanic circulation current
- Storm generated current

As outlined in (Bureau Veritas, 2022), tidal currents are considered regular and predictable. Their effects are most prevalent in coastal waters. Oceanic currents create circulation of the water in the ocean, and they are significant in the open sea operational analysis. Storm generated currents, on the other hand, are less predictable and result from wind stresses and atmospheric pressure differences.

Current, along with wind and wave forces, presents one of the primary environmental loads a mooring system is arranged to handle. In the case of mooring analysis, tidal current is considered and modelled as a force acting on the surface of the vessel below water. As discussed in (Wichers, 1991), unless in exceptional cases, significant changes in current measurements only occur within months or days. In the presence of islands, however, current speed and direction vary with a higher frequency due to the creation of eddies of varying scale.

Current at a point is defined by its velocity and direction. When considering a column of water, there are two approaches that can be used. The first option is to consider a uniformly distributed current velocity and direction along the entire depth of the column. The second option is to consider a velocity gradient with changing depth which is commonly formulated by the power-law current profile - given by (ISO, 2015)-, equivalent to a boundary layer caused by the seabed:

$$U_c(z) = U_{C0}\left(\frac{z+h}{h}\right)^{\alpha}, \tag{2.10}$$

where $U_c(z)$ is the current velocity at depth $z$, $U_{c0}$ is the current speed at the surface, $h$ is the water depth and $\alpha$ is the power law exponent.

A few other current distribution profiles that are used as well are discussed in (Bureau Veritas, 2022).

*Additional effects on current*

Current interacts with surfaces or other environmental phenomenon producing different effects as outlined by Faltinsen (1990) and described below. These are general effects that result from the flow of the fluid and affect the current loads on the ship.

*Stretching of current:* In the presence of waves, the current profile is stretched since the height of the water column varies with the waves. This is captured by equation (2.11) for a regular Airy wave.

$$z_s = z + \eta \left( \frac{\sinh[k_0(z+h)]}{\sinh(k_0 h)} \right), \tag{2.11}$$

where $k_0$is the wave number and $z_s$ is the vertical position of a particle under a wave, z is the still water level position and h is the mean water depth. This change in height affects the current profile since the particles no longer stay at the same elevation.

*Free-surface effect*: The current flow split by the body produces vortex shedding as shown in Figure 2.3. The free surface prevents the development of a Karman vortex street in a similar fashion to a splitter plate. This results in a reduction of the drag force. Wichers et al, in their study, concluded that at low velocities, the effect of free surface can be ignored (Wichers, 1991).

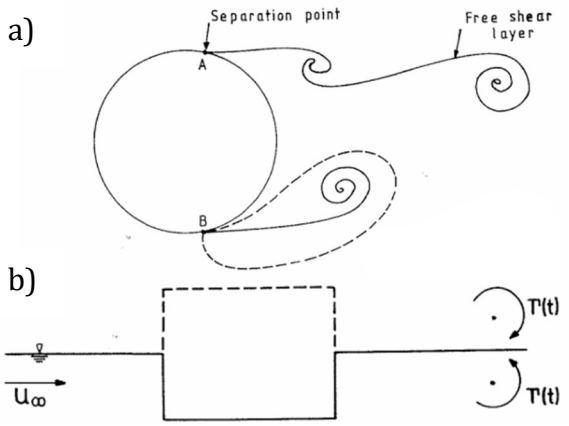


*Figure 2.3 Free-surface effect: a) vortex formation around a body surrounded by the fluid medium b) prevention of vortex formation due to free surface. (Adapted from Faltinsen, 1990).*

*Bilge radius effect:* Increased bilge radius results in decreased drag coefficient.

*Effect of Laminar or Turbulent flow:* Experiments were conducted for subcritical and transcritical flows and it was seen that a significant difference exists between the drag coefficients (Aarsnes, 1985). The observation was attributed to the flow separation characteristics in both the flows. Thus, based on flow separation characteristics captured by the model, the drag coefficient varies as well.

*Three dimensional effects:* Compared to the calculated forces using pure strip theory, it is found that three-dimensional flow effects result in a decreased drag force.

*Shallow-water effects***:** The under-keel clearance influences the current significantly. For smaller clearances the current increases up to six times as that in deep water (PIANC, 1995). As remarked in "Prediction of wind and current loads on VLCCs" (OCIMF, 1977), this is caused due to the blockage effect of the vessel which forces water to flow around the vessel rather than under the keel. The decrease in available space for the movement of the fluid results in an increase of the speed of the fluid.

*Bank effect from pier structures***:** Side structures also influence the effect of current on moored vessels. The effect is briefly described in (PIANC, 1995). Current flow in proximity to the quay surface produces an increased head of water. This in turn creates an off-berth flow which pushes against the moored vessel.

*Munk Moment***:** Munk moment describes an effect produced as a result of the motion of the vessel in a current environment. Bureau Veritas describes Munk moment as "part of the manoeuvring yaw moment $M_z$ which is not zero when the body is placed in a stationary current" (Bureau Veritas, 2022). Considering the low velocities involved the effect may be assumed to be of low significance.

As described, several effects come into play during the application of a current force. Although these effects are not dealt with in detail in the thesis, it is noteworthy to understand that sources of discrepancy between the results in different models could originate from these effects.

*Current induced force on bodies*

Current induces loads on bodies through the effect of friction and drag. The forces inducing surge, sway and yaw are formulated below and forms the primary effects on the body due to current.

$$F_{Cx} = \frac{1}{2}\rho_{water} LTC_{Cx}(\beta_R)U_R^2 \ , \tag{2.12}$$

$$F_{Cy} = \frac{1}{2}\rho_{water} LTC_{Cy}(\beta_R)U_R^2 \ , \tag{2.13}$$

$$M_{Cz} = \frac{1}{2}\rho_{water} L^2 T C_{Cz}(\beta_R) U_R^2 \ , \tag{2.14}$$

where L is the characteristic wetted length, T is the mean draught, $\beta_R$is the angle between the relative velocity vector and the x-axis of the coordinate system, $C_{Cx}, C_{Cy}$ and $C_{Cz}$ are the current drag coefficients. These coefficients are obtained as functions of $\beta_R$. $U_R$ is the magnitude of the relative velocity $= \sqrt{u_R^2 + v_R^2}$ - where $u_R$ and $v_R$ are the components of the relative velocity of the body to the water. These components are calculated with equations (2.15) and (2.16).

$$u_R = u - U_c cos\beta_C \ , \tag{2.15}$$

$$v_R = v - U_c sin\beta_C \ , \tag{2.16}$$

where $U_c$ is the current velocity and $\beta_C$is the angle of incidence of the current relative to hydrodynamic coordinate system ($\beta_C = \alpha - \psi$ , see Figure 2.4).

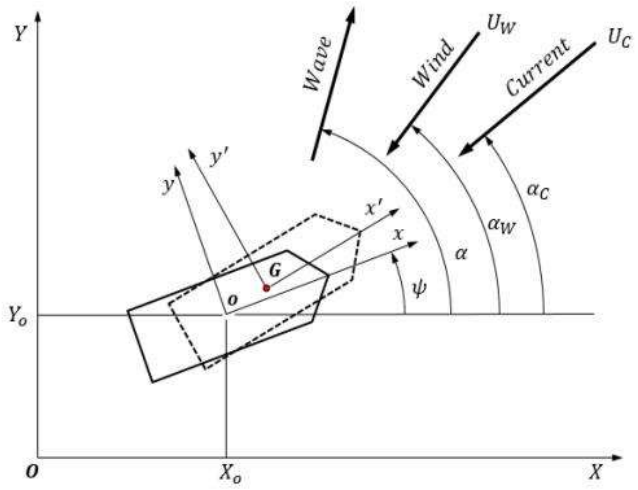


*Figure 2.4 Coordinate system and directions of environmental loads.*

### 2.2.3.3 Waves

Water waves are usually formed with wind friction between wind and the free surface creating shear, accelerating the fluid and creating a higher velocity at the free surface (which results in vorticity) (Bureau Veritas, 2022). Waves can be divided according to the period into short-period waves - with periods smaller than 20s - and long-period waves - with periods ranging from 30s to 5 minutes. The difference in period creates different physical phenomena. Mooring Equipment Guidelines highlights short period wave drift forces as a static phenomenon and longer period induced drift forces from swell waves and from other larger waves as a dynamic force (OCIMF, 2018).

For moored ships, waves are less important than wind and current. The standard environmental criteria defined by OCIMF in MEG4, that all ships above 16000 DWT should be able to withstand while moored, does not contain a wave load

element. Ports nowadays are often sheltered from wave action, thus the lack of consideration of waves when it comes to mooring. In fact, most of the action of short-period waves is cancelled by the existence of breakwaters and other partially reflecting elements in the port and its surroundings (PIANC, 1995). Short-period waves are responsible for exciting heave, pitch and roll motions and hence these motions are only problematic for exposed ports. Longer period waves on the other hand create horizontal motions on the ship – surge, sway and yawing – and are more difficult to dissipate than short-period waves. These waves usually contain elements with frequencies closer to the surge, sway and yaw natural frequencies of the moored ships and can create resonance phenomena (PIANC, 1995).

There are many theories used to describe waves mathematically. Linear wave theory (or Airy theory) will be used here to model the waves. This theory assumes the sea bottom to be horizontal and the free surface to have an infinite horizontal extent. The wave profile according to linear wave theory for both finite and infinite water depth is given by:

$$\zeta = \zeta_a \sin(\omega t - kx)\,, \tag{2.17}$$

where $\zeta$ is the elevation at position x, $\zeta_a$ is the wave amplitude, $\omega = \frac{2\pi}{T}$ is the circular frequency (with $T$ being the wave period), $t$ is the time variable, $k$ is the wave number and $x$ is the coordinate in the direction of the wave propagation. We consider a sea state with regular waves as a sea state where only one wave is modelled. If irregular waves were considered, the wave elevation would be expressed as the linear combination of the individual waves, which is possible by assuming linearity. The wave elevation of such irregular sea would be described by:

$$\zeta = \sum_{j=1}^{N} A_j \sin(\omega_j t - k_j x + \epsilon_j)\ , \tag{2.18}$$

with $A_j = \sqrt{2 \cdot S(\omega_j) \cdot \Delta\omega}$ and $S(\omega)$ being the wave spectrum.

There are two types of forces and moments to consider in the presence of waves (Faltinsen, 1990):

1. The first type consists of forces and moments on the body when the body is forced to oscillate with the wave excitation frequency. This means there is nothing restricting the motion of the body and there are no incident waves. These correspond to the added mass and damping loads described in Section 2.2.2 and to the restoring forces described in Section 2.2.1.
2. The second type corresponds to loads on the body when it is restrained from oscillating and there are incident waves. These are usually named wave-excitation loads and are made up of Froude-Krylov and diffraction forces and moments, which are described in this section.

Because of linearity, these two types of forces can be added to obtain the total hydrodynamic forces and moments.

The Froude-Krylov force corresponds to the force resultant from the undisturbed pressure field caused by the undisturbed wave and the diffraction force will correspond to the force resulting from the disturbance the body introduces in said pressure field. The derivation of these forces for a cylinder with dimensions considerably smaller than the characteristic wavelength of the undisturbed wave leads to the formulation of the Morrison equation, which is important in the context of moorings for offshore structures. However, a more generalized version of this derivation can be seen in the following, taking the assumption into account that the wavelength is considerably larger than the body.

$$F_i = -\iint pn_i ds + A_{i1}a_1 + A_{i2}a_2 + A_{i3}a_3 \,, \tag{2.19}$$

where p is the pressure in the undisturbed wave field, **n**=$(n_1, n_2, n_3)$ is the unit vector normal to the body surface defined to be positive into the fluid, $a_1, a_2$ and $a_3$ are the components of acceleration along the x-, y- and z- axes of the undisturbed wave field, and $A_{ij}$ are coefficients similar to the added mass coefficients that represent the diffraction forces. These last terms represent the change in the undisturbed pressure field due to the presence of the body. This integral should be evaluated over the average wetted surface of the body in order to obtain the value of this load.

Strip theory and equation (2.18) are often used in conjunction to obtain the wave excitation forces.

### 2.2.4 Mooring line and fender forces

Mooring lines and fenders are arranged to counter the environmental loads acting on the vessel. As discussed in the first chapter, the mooring lines can be classified according to their orientation and position in relation to the ship. Spring lines are longitudinally aligned and restrain the vessel in aft and forward directions, while breast lines are transversely aligned and restrict the transverse movement of the vessel away from the berth. While mooring lines take up off-berth and longitudinal forces in tension, fenders take up on-berth forces in compression. Apart from spring and breast lines, head and stern lines may also be set up in case of directional environments (in cases where the environmental loads are known to be predominant in a certain direction). They are most applicable in berths having vicinity to rivers.

Mooring Equipment Guidelines outlines several principles to be followed to obtain an effective mooring arrangement (OCIMF, 2018). Several factors that affect the effectiveness of a mooring arrangement are also discussed. Among those are the vertical and horizontal angles the lines are oriented at. With increasing vertical angle, the component acting in these horizontal degrees of freedom decreases and the effectiveness of the lines decreases. As for the horizontal angles, it is concluded that breast lines oriented as perpendicular as possible to the vessel and as far aft

and forward as possible along with spring lines oriented as parallel as possible to the vessel forms the best combination.

*Mooring lines*

The most critical characteristic of a mooring rope is its stiffness. The choice of selection of mooring line is dependent on the nature of operation and environmental conditions. (OCIMF, 2018) outlines the following considerations in the selection of mooring ropes of different stiffness.

- Low stiffness ropes, given their capability to absorb higher dynamic loads, are best suited for Ship-to-ship (STS) operations, or at terminals subjected to waves, swell and passing ship forces.
- In general, low stiffness is not ideal as it allows for too much motion for the moored ship.
- Movement induces energy to be stored in the ropes and snap back zones are to be set accordingly. This risk is higher in ropes with lower stiffness.
- The stiffness of the lines used also influences the distribution of the loads along the mooring arrangement.

The most common types of lines used are steel wire, High Modulus Synthetic Fiber (HMSF), Polyester/Polypropylene and Nylon. see Figure 2.5 presents typical elongation curves for ropes with these materials. Note the non-linear behaviour of the stiffness of the materials. Steel wires present the higher stiffness, meaning they should not be used in mooring line arrangements together with Polyester or Nylon ropes, as the steel wires will take most of the load. Mooring line tails often have smaller stiffness than the lines and combining a tail with the line allows for a better control of the desired stiffness of the line-tail system.

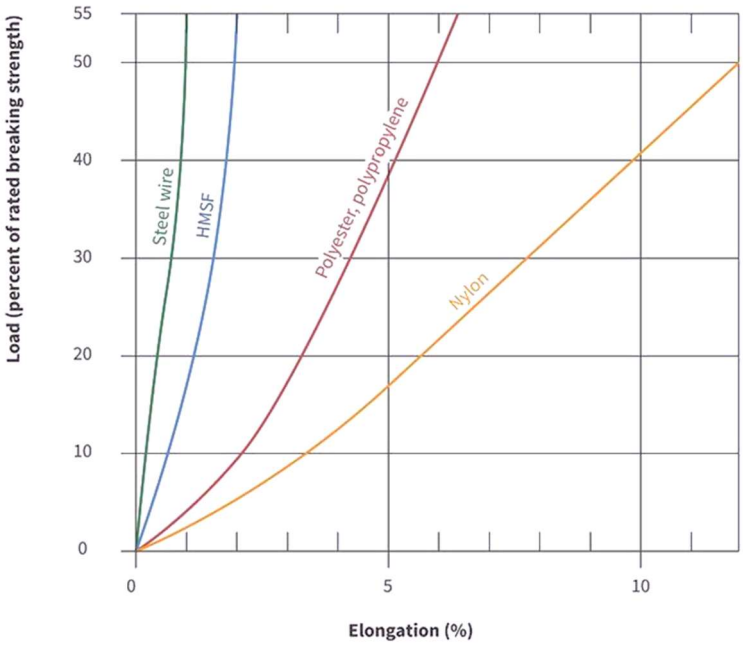


*Figure 2.5 Mooring rope types and stiffness. Reproduced from (OCIMF, 2018).*

A linear simplified approach to stiffness is done by considering the cross-sectional area, A, and Young's modulus, E, as constants under extension. This solution would approximate the curves observed in Figure 2.5 to straight lines. However, the stiffness of mooring ropes changes with percentage elongation as well as age and rate of elongation. While deteriorative ageing is modelled by reduced Minimum Breaking Load (MBL), changing stiffness due to the state of the rope in terms of its elongation and strain rate is handled in different ways. To accommodate for changing stiffness with change in length, the stiffness is recalculated with the increased length and reduced area. The stiffness can be calculated as follows,

$$k_i = \frac{EA_i}{L_i}\ , \tag{2.20}$$

where $i$ represents the instantaneous values. However, in multistrand fibre ropes, the mooring line dynamics is affected by the interaction between the fibres as well. At increased strain rates, the stiffness is higher. Thus, to completely capture the dynamic effects of a mooring rope, multiple such non-linearities needs to be considered by including the evaluation of a damping term.

Mooring line loads act as point loads on vessels. The point of action can be limited to a single point such as a fairlead, which would simplify the calculations and is enough to calculate ship motions. However, the force from mooring lines is transferred at several points that includes the fairleads, intermediate rollers - if any is used - and finally to the port bollard in one end and to the winch in the other. The tension along the length of the line will thus vary in the different segments.

Pre-tension of mooring lines is another important parameter. In the study by Ziylan et al. (2024), it was learned that the dynamic loading effects are significantly reduced when a pretension of 10% of the Minimum Breaking Load (MBL) is applied.

*Fender forces*

The fenders are the interface between the berthing/moored vessel and the port facility. In the berthing process, fenders absorb the ship's kinetic energy and dissipate the reaction forces into the port structure. When the ship is moored, the fenders are expected to protect both the vessel and the supporting structure in the case of unwanted ship motions.

During berthing and during mooring, fenders act as non-linear compression springs, as the force with which they act on the vessel depends on the deflection of the fenders. Manufacturers often provide the corresponding load-deflection curves.

*Equilibrium*

The mooring line forces are obtained by balancing the external forces applied to the tensions and fender forces as described by Ziylan et al. (2024) as follows.

$$\sum F_x = F_x + \sum_1^q (k_q X - P_q) \sin a_q + \sum_1^m k_m (Y + L_m sin\theta) cos a_m = 0 \quad , \tag{2.21}$$

$$\sum F_y = F_y + \sum_1^m k_m (Y + L_m sin\theta_m) \sin a_m - \sum_1^n k_n (Y + L_n sin\theta) L_n + \sum_1^q k_q X cos a_q = 0 \quad , \tag{2.22}$$

$$\sum M = M_{xy} + \sum_1^m k_m (Y + L_m sin\theta) L_m \sin a_m - \sum_1^n R_n (Y + L_n sin\theta) L_n + \sum_1^q k_q L_q cos\theta cos a_q = 0 \, , \tag{2.23}$$

where,

$F_x$ - longitudinal external forces,
$F_y$ - transverse external forces,
$M_{xy}$ - moment at ship centre,
m - number of breast lines,
n - number of fenders,
q - number of spring lines,
X - surge of vessel,
Y - sway of vessel,
$\theta$ - yaw angle of vessel,
k - stiffness coefficient,
$a$ - horizontal angle of mooring line,
R - reaction force in fender,
L - distance from centerline

Equation (2.21) denotes the force balance equation along surge direction, and it is seen that the fender force component is absent in this case. This is suggestive of a fender arrangement parallel to the quay wall and centreline of the ship. Equations (2.22) and (2.23) denotes the force balance equations in sway and yaw directions and in both formulations, fender force components are found.

### 2.2.5 Other forces

While current, wind, wave and mooring equipment forces form the primary forces that concern mooring in a general setting, several other forces may also be at play. (OCIMF, 2018) outlines a few sources of such secondary forces as follows.

- Tides
- Interaction of passing ships
- Ice
- Changes in draught, trim or list

Tide loads were not considered as they act with a very low frequency and with a gradual variation which make the effect of the tides practically insignificant when considering mooring of ships during port operations. Similarly to tide loads, ice

loads usually act with very low frequencies, as ice takes time to form around the vessel; these loads are also considered practically insignificant. The effect of passing ships in the harbour is similar to an unsteady current and waves acting on the moored ship. The effect is dependent on the speed of the passing ship. Finally, changes in draught, trim or list – that can be a result of port operations, loading and unloading – can often be planned for and efficiently handled with the management of the mooring system.

## 2.3 Ship motions

A ship at sea is subject to move in translation in 3 directions and to rotate around its 3 axes, as was mentioned in Section 2.2. The formulation of the equations of motion for ships begins with Newton's second law of motion:

$$\sum F = m \cdot a \ . \tag{2.24}$$

Equation (2.24) must be written in matrix form for vectorial quantities, where the force vector includes forces felt by the ship along the axes, together with the moments acting in each of the rotation degrees of freedom. The mass matrix will contain the mass of the ship for the linear motion equations and the respective moments of inertia for the rotational motion equations. Including these considerations in equation (2.24) and writing acceleration as a double derivative of position and angles, the vectorized form of Newton's second law for ship motions is obtained:

$$\sum \boldsymbol{F} = \boldsymbol{M} \cdot \ddot{\boldsymbol{x}} \ . \tag{2.25}$$

The sum of forces in equation (2.25) includes all the forces that were previously discussed in Section 2.2. Often the equations of motions for ships group the added mass, damping and restoring forces together and equate them to the exciting forces. Hence,

$$\sum_{k=1}^{6} \left[ \left( M_{jk} + A_{jk} \right) \cdot \ddot{\eta}_k + B_{jk} \dot{\eta}_k + C_{jk} \eta_k \right] = F_j \quad (j = 1,2, \dots, 6) \,, \tag{2.26}$$

where $M_{jk}$ are the components of the generalized mass matrix for the structure, $A_{jk}$ and $B_{jk}$ are defined as added mass and damping coefficients, $C_{jk}$ are the restoring coefficients, $\eta_k$ represents the ship motions and finally $F_j$ are the amplitudes of the exciting forces and moment-components with the force and moment-components given by $F_j$.

Motions are calculated in reference to an inertial reference frame, often located at the position of the ship in the beginning of the simulation. In case of body-centred calculation, different considerations needed to be made in relation to accelerated frames of reference. However, these are not used in the simulations analysed in the present study.

# 3 Numerical methods

In this section, the numerical methods used in this study are described in more detail. This is done for each employed tool separately, for a clearer presentation of such methods. In the case of mooring, the model includes the ship, the ropes, the port and the environmental conditions.

## 3.1 SEAMAN

SEAMAN is a system simulation tool using semi-empirical methods to predict the ships seakeeping and manoeuvring performance. The programming language includes both C++ in which the calculations are carried and a python interface for user input/output communications.

### 3.1.1 Barge model

In the semi-empirical tool, the barge is modelled by specifying the values of different ship geometrical characteristics and loading conditions that are then used in the semi-empirical calculations.

### 3.1.2 Mooring line

The mooring line properties of the line – such as the ones given in Table 4.3 - are used as inputs for mooring line force calculations. A mooring line is modelled as a spring-damper system in series. The value for the line stiffness is calculated through equation (2.20), in which the line's elasticity modulus and sectional area are given as inputs. The initial line length, which is the initial distance between the ship winch to the port bollard, is calculated by simulating the process of reeling-in line. The line is then pre-tensioned thus affecting the lines' length. The damping on the line is defined as a percentage of the stiffness of the line.

Instantaneous line tension, $F_{line}$, is obtained by calculating the instantaneous distance between the winch and the port bollard and comparing it to the initial line length, using the formula:

$$F_{line} = k \cdot \Delta L + c \cdot \dot{L} \ , \tag{3.1}$$

where $\Delta L$ is the variation in line length, c is the damping coefficient obtained through $c = \%_{damping} * k$ and $\dot{L}$ is the rate at which the line is being stretched.

These lines are connected on one end to winches onboard the ship and, on the other end, to port bollards. The winches are modelled to take a maximum tension and to allow a maximum hauling speed. The winch can operate with three different modes: constant tension, constant speed or locked (constant line length). The direction of $F_{line}$ is defined by the vector from the winch to the connected port bollard, and the point of application of the force is the point at which the winch is

defined. The coordinates of the winch in a body-centred reference frame centred (defined at $L_{pp}/2$, centreline and baseline) are given as input.

### 3.1.3 World model

The world includes the port facilities used in the mooring process. In the simulations carried out in this thesis, these facilities only include the quay itself and the port bollards on the quay.

The quay is modelled in SEAMAN with vector data (which is used by a geographic information system) that defines its geometry. The semi-empirical tool uses this geometrical data mainly to calculate the event of collisions. Other physical phenomena originated from the presence of the quay wall, e.g. bank/cushion effects, and wave reflection, are not considered in this method.

The port bollards are stationary (fixed) in the world inertial reference frame, and their coordinates are provided as an input. The port bollards (which are connected to the winches onboard) are defined by a Safe Working Load (SWL).

### 3.1.4 Environmental factors model

The modelling of the environmental factors is of interest to be able to understand the forces acting on the vessel and the resulting motions.

*Current*

Current is modelled in the semi-empirical tool by consideration of additional longitudinal and transversal terms, $u_c$ and $v_c$, together with the ship speed over ground, $u$ and $v$, when calculating the components of the ship's speed through water, $u_w$ and $v_w$, according to

$$u_w = u - u_c \ , \tag{3.2}$$

$$v_w = v - v_c - v_{wp} - p(KG - T_m)L \cdot \cos(\phi) - LCG \cdot r \ . \tag{3.3}$$

The additional components considered in the calculation of the transverse velocity component include $v_{wp}$, the wave particle velocity along the y-direction on the ship-centred reference frame, $T_m$ is the mean draught and $\phi$ is the roll angle. Current is also considered when calculating the turning rate through water of the ship.

$$r_w = r - r_c - r_{wp} \ , \tag{3.4}$$

where the subscript $c$ refers to current and $wp$ to wave particle velocity (RISE, 2016).

The linear and angular ship speed through water is then used in the manoeuvring forces and resistance computations.

*Wind*

In the simulations, wind is modelled with a constant speed and a constant direction. Consequently, the implemented gust model, that introduces spectrum-related variations in the speed and direction of the wind, is not used in the present study, as discussed in Section 1.2.

The wind force in the semi-empirical tool is calculated using equation (2.4). The coefficients $C_X$, $C_Y$, $C_K$ and $C_N$ are given as inputs for several incident angles and interpolated between these values for intermediate values. These coefficients need to be determined either experimentally or using another tool – in this thesis, CFD computations were made, and the respective coefficients were obtained.

*Waves*

Waves are modelled as regular long crested waves. Wave force in the semi-empirical tool is calculated based on Strip theory. Therefore, sectional data (sectional beam, sectional draught and sectional area) is given as input and for each section the different force and moment components are calculated. These values are then interpolated using a Simpson's rule.

The calculation of the force component in surge - $dX_{sec}$ - is shown as an example.

$$dX_{sec} = \rho_w A_{section} du_w \,, \tag{3.5}$$

where $A_{section}$ is the sectional area of the considered strip and $du_w$ is the wave induced water particle acceleration. This last term, for a regular and long-crested wave is determined by

$$du_w = \frac{h}{2}\omega^2 \cdot \cos(\theta_{wave} - n) \cdot \cos\left(\frac{\omega^2}{g} x_{w0} - \omega t\right) e^{-\frac{\omega^2}{g} t_{section}} \,, \tag{3.6}$$

where $h$ is the wave height, $\omega$ is the wave frequency, $(\theta_{wave} - n)$ is the wave direction relative to the ship, $x_{w0}$ is the horizontal position of the strip along the direction of motion of the wave and $t_{section}$ is the sectional draught.

Calculation of the other force and moment components - $dY_{sec}$, $dZ_{sec}$, $dK_{sec}$, $dM_{sec}$ and $dN_{sec}$ – are calculated using similar expressions that are not described in detail in this thesis. These detailed equations related to Strip theory can be found in relevant references, namely in (Kaplan, 1972).

### 3.1.5 Equations of motion

The notations for the 6DOF forces are $X$, $Y$, $Z$, $K$, $M$ and $N$ for surge, sway, heave, roll, pitch and yaw respectively. The notations for the 6DOF velocities are $u$, $v$, $w$, $p$, $q$ and $r$.

The equations of motion in the semi-empirical method are then given by

$$X_{\dot{u}}\,\dot{u} = X_{Total} \quad , \tag{3.7}$$

$$Y_{\dot{v}}\dot{v} + Y_{\dot{p}}\dot{p} + Y_{\dot{r}}\dot{r} = Y_{Total} \quad , \tag{3.8}$$

$$Z_{\dot{w}}\dot{w} + Z_{\dot{q}}\dot{q} = Z_{Total} \quad , \tag{3.9}$$

$$K_{\dot{v}}\dot{v} + K_{\dot{p}}\dot{p} + K_{\dot{r}}\dot{r} = K_{Total} \quad , \tag{3.10}$$

$$M_{\dot{w}}\dot{w} + M_{\dot{q}}\dot{q} = M_{Total} \quad , \tag{3.11}$$

$$N_{\dot{v}}\dot{v} + N_{\dot{p}}\dot{p} + N_{\dot{r}}\dot{r} = N_{Total}, \quad , \tag{3.12}$$

where $X_{\dot{u}}$, $Y_{\dot{v}}$, $Y_{\dot{p}}$, $Y_{\dot{r}}$, $Z_{\dot{w}}$, $Z_{\dot{q}}$, $K_{\dot{v}}$, $K_{\dot{p}}$, $K_{\dot{r}}$, $M_{\dot{w}}$, $M_{\dot{q}}$, $N_{\dot{v}}$, $N_{\dot{p}}$ and $N_{\dot{r}}$ are the coefficients describing the mass of the ship together with the added mass described in Section 2.2.2. The subscripts and variables named $\dot{u}$, $\dot{v}$, $\dot{w}$, $\dot{p}$, $\dot{q}$ and $\dot{r}$ correspond to the related DOF accelerations. Equations (3.9) to (3.14) describe both Newton's 2nd Law and the dominant coupling of the motions considered in the semi-empirical tool, namely the coupling between heave and pitch as well as the coupling between sway, roll and yaw.

The set of systems being used in a simulation define what forces act on the body and affect the motions. The forces included in the mooring simulations include the aforementioned wind and wave forces, as well as forces from the mooring lines, and finally the hydrodynamic hull forces. Not all forces include contributions in all DOF.

#### 3.1.5.1 Hydrodynamic hull forces

The hydrodynamic hull forces include different coupling terms for different DOFs. These forces are not considered for the heave and pitch degrees of freedom.

*Surge*

The hydrodynamic hull force contribution in surge follows the equation

$$X_h = (\Delta + X_{vr})vr + X_{vv}v^2 + X_{rr}r^2 + X_{res} + X_{SW}, \tag{3.13}$$

where $\Delta$ is the ship displacement, $X_{vr}$, $X_{vv}$ and $X_{rr}$ are empirical second order coefficients that specify how the coupling of the sway and yaw impact motion in the longitudinal direction, $X_{res}$ corresponds to the resistance force and finally $X_{SW}$ is the shallow water contribution (which is not calculated in this thesis). It is worth mentioning that the current forces acting on the surge direction impact the value of $X_{res}$ by affecting the value of speed through water as mentioned in equations (3.2) and

(3.3). In the semi-empirical method, estimated resistance values at various speeds are given as input. Therefore, the instantaneous resistance of the ship at its instantaneous speed is derived from interpolation on the given input. The resistance force acts on the ship COG.

*Sway*

The hydrodynamic hull force contribution in sway is derived from,

$$Y_h = (Y_{uv} + Y_{uuv}u)uv + Y_{ur}ur - \Delta * ur + Y_{uur}u^2r + Y_{nl} + Y_{SW}, \qquad (3.14)$$

where $Y_{uv}$ and $Y_{uuv}$ are hydrodynamic coefficients for the sway force due to side drift, $Y_{ur}$ and $Y_{uur}$ are hydrodynamic coefficients for the sway force due to turning rate, $Y_{nl}$ is the nonlinear sway force contribution and $Y_{SW}$ corresponds to the force from shallow water effects in the sway direction.

*Roll*

For roll,

$$K_h = (K_{ur} + K_{uur}u)ur + z_G ur + K_p p + K_{p|p|}p|p| + K_{up}up + (K_{uv} + K_{uuv}u)uv + K_{v|v|}v|v| + K_{r|r|}r|r| \ , \qquad (3.15)$$

where $K_{ur}$, $K_{uur}$, $K_{up}$, $K_{uv}$ and $K_{uuv}$ are hydrodynamic coefficients, $K_{p|p|}$, $K_{v|v|}$, $K_{r|r|}$ and $K_p$ are damping coefficients and $z_G$ is the z-position of the COG.

*Yaw*

Finally, for yaw, the formulation of the hydrodynamic hull forces is,

$$N_h = (N_{uv} + N_{uuv}u)uv + N_{ur}ur - \Delta x_G ur + N_{uur}u^2r + N_{nl} + N_{SW}, \qquad (3.16)$$

where $N_{uv}$ and $N_{uuv}$ are hydrodynamic coefficients for the yaw moment due to side drift, $N_{ur}$ and $N_{uur}$ are hydrodynamic coefficients for the yaw moment due to turning rate, $Y_{nl}$ is the nonlinear yaw moment contribution and $Y_{SW}$ corresponds to the force from shallow water effects in the rotation around the z-axis.

#### 3.1.5.1 Artificial damping force

One feature of the semi-empirical tool created to handle initial instabilities of the mathematical model of the mooring lines is an artificial damping force. It is called "damping" as it is calculated based on the speed of the vessel. Results obtained without resorting to this damping component showed in many cases unreasonable results as well as divergent behaviour.

This artificial force component acts in the surge, sway, roll and yaw degrees of freedom. It acts in the opposite direction of the velocity over ground and is calculated according to the formula:

$$F_{damping} = -\nabla \rho g * C_{damping} * v_{sog} \ , \tag{3.17}$$

where $C_{damping}$ is a damping coefficient and $v_{sog}$ is the speed over ground of the ship. The value used for $C_{daping}$ in the simulations analysed in the results section is 1e-1.

Note the damping force was only used for simulations with mooring lines, as the semi-empirical tool did not create the numerical instabilities without the lines.

### 3.1.6 Computational solver

The semi-empirical tool uses a Runge-Kutta 4th order method to solve the ordinary differential equations resulting from the combination of the several user-defined systems.

Runge-Kutta methods are used in solving simultaneous ODEs by calculating intermediate values between the current value of the function and the value corresponding to the following time step.

Consider $y(t)$ is a function that varies with $t$, the initial value of $y$ is $y(t_0) = y_0$ and the derivative of $y$ is defined as a function of $t$ and of $y$ itself, $dy/dt = f(t, y)$. Runge-Kutta method defines, for a time step $h > 0$:

$$t_{n+1} = t_n + h \ , \tag{3.18}$$

$$y_{n+1} = y_n + \frac{h}{6}(k_1 + 2k_2 + 2k_3 + k_4) \, , \tag{3.19}$$

where $k_1 = f(t_n, y_n)$ , $k_2 = f(t_n + \frac{h}{2}, y_n + h\frac{k_1}{2})$ , $k_3 = f(t_n + \frac{h}{2}, y_n + h\frac{k_2}{2})$ and $k_4 = f(t_n + h, y_n + hk_3)$. The value of the function at the next step, $y_{n+1}$, is approximated considering the slope of the function. This iterative process facilitates determining the behaviour of the function $y(t)$. Similarly, this method is used in mooring line simulations to determine velocities and positions – as their derivative, acceleration, is known through a balance of forces.

## 3.2 SHIPFLOW Motions

The commercial tool Shipflow Motions, developed by FLOWTECH International AB, is a fully non-linear unsteady potential flow solver for free surface flows. In this thesis, it represents a higher fidelity model approach to the mooring problem.

There is assumed to be a scalar quantity, $\phi$, that describes the motion of the fluid. This is referred to as the velocity potential. For the potential flow solver, an inviscid, incompressible and irrotational flow is assumed and the velocity potential is defined by setting its gradient equal to the fluid velocity.

$$\nabla\phi = \left(\frac{\partial\phi}{\partial x}, \frac{\partial\phi}{\partial y}, \frac{\partial\phi}{\partial z}\right) = (u, v, w) = \vec{u} \ , \tag{3.20}$$

Substituting $\vec{u}$ in incompressible continuity equation gives,

$$\nabla\vec{u} = 0 \, , \tag{3.21}$$

$$\nabla . \nabla\phi = 0 \, . \tag{3.22}$$

Equation (3.19) forms the Laplace equation for the velocity potential, $\phi$, which is the governing equation in potential flow. For free surface calculations a fluid domain follows the horizontal position of the body.

The following boundary conditions are applied for the free surface and body surfaces.

- Kinematic free-surface boundary condition: The fluid particle at the free surface remains at the surface.
- Dynamic free-surface boundary condition: The resultant force normal to the free surface is zero. i.e., pressure at the free surface equals the atmospheric pressure.
- Body surface boundary condition: No fluid flow occurs across a rigid body surface, i.e., the fluid velocity normal to the surface at the body surface is zero.

The manoeuvring forces along surge, sway and yaw are calculated based on the following set of equations.

$$X = \ X_{vr}vr + X_{rr}r^2 + X_{vv}v^2 \ , \tag{3.23}$$

$$Y = Y_{ur}ur + Y_{uv}uv + Y_{uur}u^2r + Y_{uuv}u^2v + Y_{nl} \ , \tag{3.24}$$

$$N = N_{ur} + N_{uv}uv + N_{uur}u^2r + N_{uuv}u^2v + N_{nl} - N_M \, , \tag{3.25}$$

where X, Y and N are non-dimensional surge, sway and yaw forces and moments respectively, and $u, v$ and $r$ are non-dimensional surge, sway and yaw relative velocities. The non-dimensionalisation is carried out according to the bis system, the same as SEAMAN, with reference length as the length of the barge. $Y_{nl}$ is the non-linear side-force term due to crossflow drag given by

$$Y_{nl} = \frac{1}{2}\rho C_d \int_{AP}^{FP} T(x)v(x)|v(x)|dx \ \ . \tag{3.26}$$

$N_{nl}$ is the non-linear yaw-moment term given by

$$N_{nl} = \frac{1}{2}\rho C_d \int_{AP}^{FP} T(x)v(x)|v(x)|x_{lev}(x)dx \, , \tag{3.27}$$

where, $x_{lev}(x)$ is the local longitudinal distance to the centre of gravity.

$N_M$ is the Munk moment that accounts for the turning moment caused due to lift forces acting off the centre of gravity due to a drift angle $\beta$, and is given by,

$$N_M = -\frac{1}{2}(A_{22} - A_{11})(u^2 + v^2)\sin(2\beta) \quad . \tag{3.28}$$

Here, $A_{11}$ and $A_{22}$ are added mass in surge and sway respectively.

The induced resistance/forces on the hull in the longitudinal direction is calculated from the wave resistance from the potential flow solution and friction resistance from the ITTC-57 friction line. The side force is obtained from the hull generated forces due to lift and crossflow drag. The resistance components are defined as follows,

$$R_T = R_W + R_F, \tag{3.29}$$

where, $R_T$ is the total resistance consisting of $R_W$, the wave resistance calculated from pressure integration on panels and $R_F$, the friction resistance obtained as follows.

$$R_T = R_{F0} * (1 + k), \tag{3.30}$$

where, $k$ is the form factor and $R_{F0}$ is the flat plate skin friction calculated as,

$$R_{F0} = \frac{1}{2}\rho V_s^2 S C_F, \tag{3.31}$$

where, $C_F$ is the friction resistance coefficient, S is the wetted surface area and $V_S$, is the ship speed.

While the forces along the wetted area are calculated based on potential flow solutions and friction components, the wind force is calculated based on wind resistance coefficients $C_X, C_Y, C_K, C_N$ and the longitudinal and transverse area of the ship above the waterline. The coefficients, representing the forces along x and y axis and the moments around x and z axis respectively, are calculated using formulations presented for wind forces in Section 2.2.3.

### 3.2.1 Modelling of barge and mooring lines

The geometry of the ship used in the potential flow tool is defined with the help of a CAD (Computer Aided Design) file. A mesh consisting of quadrilateral panels is created from the geometry and imported into Shipflow Motions. The hull form and the deck geometry are inserted separately. An example of a mesh used in the simulations can be observed in Figure 3.1.

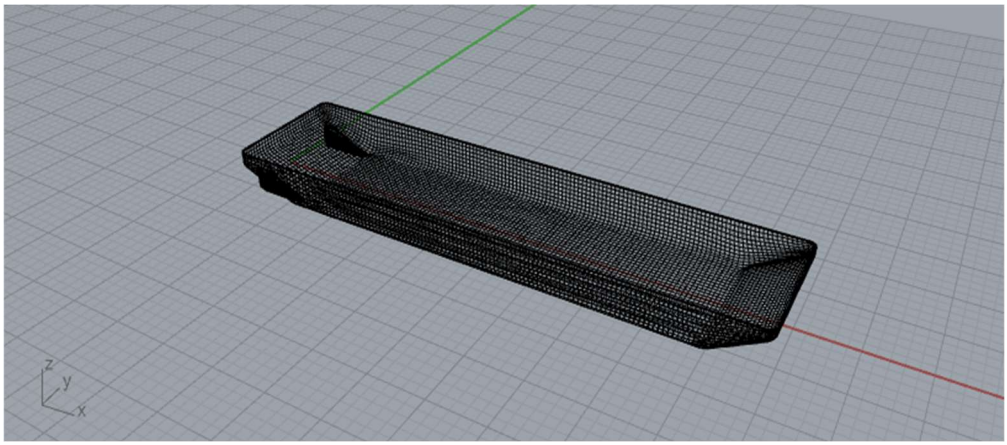

*Figure 3.1 Example of a mesh file used in the potential flow tool.*

Mooring line in the potential flow tool is defined by its end coordinates along with their conformities to the multi-body system, stiffness, damping and pretension. The force calculation follows a spring-damper assumption without considering hysteresis, similar to the modelling done on the semi-empirical tool (check Section 3.1.2).

### 3.2.2 Definitions of free surface and fluid domain

The computational domain considers a truncated free surface encompassing the bodies and extending two to four times the ship length to all sides. The free surface is discretised into panels (an example is shown in Figure 3.2 - a) with higher refinement levels closer to the hull (check Figure 3.3). A damping zone (an example is shown in Figure 3.2 - b) is also defined to prevent radiated or reflected effects originating from the truncated edges of the free surface (boundaries of the computational domain).

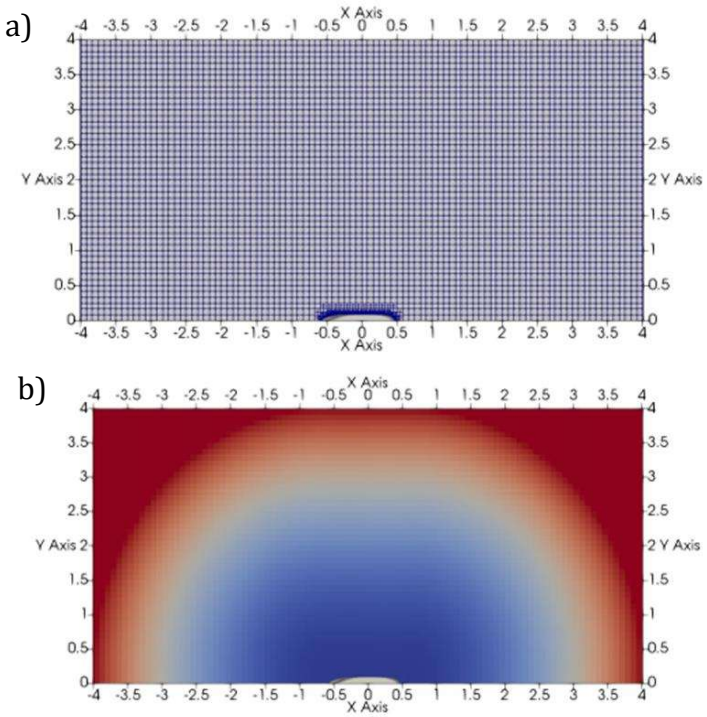


*Figure 3.2: Description of the free surface. Adapted from Shipflow Motions user manual, (FLOWTECH International AB, 2025). a) Free surface mesh (panels) b) Damping zone definition (red means more damping applied).*

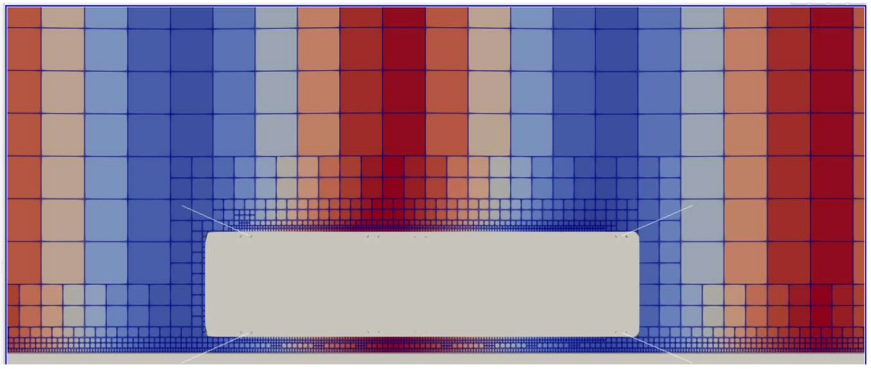

*Figure 3.3 Close up of the free surface panels refinement.*

The fluid domain is modelled as a compact domain bound by the truncated free surface, wetted surface of the vessel or any objects being observed and by the bottom surface.

### 3.2.3 Modelling of environmental loads

*Wave*

For the test cases selected, described further in section 4.3, regular long-crested waves are set to ensure motion responses can be easily discerned. Wave modelling is carried out using Stokes wave theory with fifth-order wave formulation. This differs from the linear Airy formulation used in the semi-empirical tool. The fifth

order formulation is expected to present a more accurate description of the real-world waves. (Sarkar, 2022) indicates that Airy wave theory produces slightly larger forces in an 'infinite' depth scenario. This can possibly be counted as a source of discrepancy between the calculated responses in the employed methods in this thesis.

*Current*

Current modelling is different in the potential flow tool as compared to the semi-empirical tool. This stems from the difference that instead of modelling the fluid medium with a velocity, the barge along with the world frame is given a velocity. Thus, a moving vessel - world frame is obtained with static fluid. The velocity given to the frame equals the current velocity in the direction opposing the intended current direction. The frame is accelerated to the current velocity. Once the required velocity is achieved, the external forces are calculated, and the vessel/world is accelerated or decelerated accordingly. Modelling is carried out such that the world is locked in all degrees of freedom and hence, will continue with the current velocity. The vessel is on the other hand is only constrained in selected degrees of freedom (as per test case). This results in the vessel responding to the forces generated due to the relative velocity between it and the fluid. This means that, in an unmoored free-floating simulation, the vessel will eventually decelerate to zero velocity (i.e. matches the fluid stream velocity). However, a moored vessel will continue to maintain a relative velocity with the fluid, since the mooring line forces maintain the position of the vessel relative to the world frame.

*Wind*

Wind forces and moments are evaluated based on the wind resistance coefficients that are calculated and provided as input to the code. Equation (2.4) is also used in the potential flow tool.

# 4 Study cases and model parameters

Five test cases, presented in Section 4.3, have been designed to assess and compare the two methods used in this thesis regarding the hydrodynamic models of the vessel as well as the mooring line characteristics. These assessments are made for the barge subjected to different environmental conditions, introduced in Section 4.1, aiming at providing an analysis study on the sensitivity of the results to the magnitude and nature of the applied forces. The mooring rope and characteristics selected for the investigations in this thesis are provided in Section 4.2. The post-processing approaches taken to analyse the obtained results are briefly introduced in Section 4.4.

## 4.1 Barge geometry and loading conditions

The ship used in the mooring simulations is a rectangular barge with the dimensions specified in Table 4.1. The details of the barge loading conditions are provided in Table 4.2.

*Table 4.1 Main particulars of the barge.*

| Particular | Symbol | Value |
|---|---|---|
| Length Between Perpendiculars [m] | $L_{pp}$ | 50 |
| Beam [m] | $B$ | 12.1 |
| Height [m] | $H$ | 3.5 |

*Table 4.2 Loading condition of the barge.*

| Variable | Symbol | Value |
|---|---|---|
| Displacement [kg] | $\Delta$ | $637.7\times 10^3$ |
| Longitudinal coordinate of COG (wrt. $L_{pp}/2$) [m] | $LCG$ | 0 |
| Transversal coordinate of COG (wrt. Centreline) [m] | $TCG$ | 0 |
| Height of COG (wrt. Baseline) [m] | $KG$ | 1.375 |
| Draught [m] | $T$ | 1.25 |

A barge is preferred for these simulations over a ship due to its simple geometry, hence allowing more efficient analysis. The barge includes two slanted surfaces, one on the bow and one on the aft, as can be observed in Figure 4.1. It also includes two fixed rudders in the aft slanted surface and eight pairs of onboard bollards to which the mooring lines connect to. Although a more sophisticated onboard mooring arrangement includes more equipment, e.g. winches, pedestal rollers, bits and fairleads as illustrated in Figure 1.4, such complexities are excluded from the current study. Consequently, the onboard bollards are assumed to be the winches to which the mooring lines connect to and are equivalent to “locked” winches.

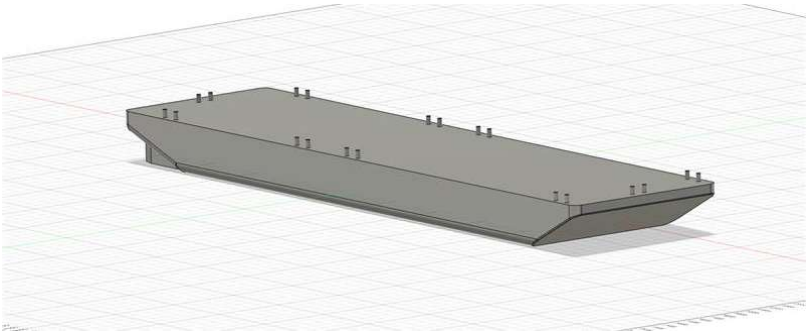

*Figure 4.1 Barge geometry and its simplified onboard mooring equipment.*

## 4.2 Mooring line selection

Generally, mooring ropes utilized in each vessel are selected based on various factors including the vessel displacement and the environmental and operational conditions the vessel encounters. However, for the simulations in this thesis, mooring ropes are selected arbitrarily based on manufacturer catalogues (Samson Rope, 2024) with the parameters outlined in Table 4.3.

*Table 4.3 Mooring line parameters*

| Parameter | Value |
|---|---|
| Diameter [m] | $80\times 10^{-3}$ |
| ISO 2307 Strength [tonnes] | 317 |
| Material | High Modulus Polyethylene (HMPE) |
| Axial stiffness [MN/m] | 6.3 |
| Axial damping [% of stiffness] | 2.5 |
| Density [kg/m$^3$] | 1088.93 |

The assumptions made regarding mooring lines were briefly discussed in section 1.2 and can be outlined as follows.

- The mooring rope is assumed to have linear elasticity
- Hysteresis effect is not considered

## 4.3 Environmental conditions

As discussed previously, in this thesis, the investigations are carried out on the forces originated from wave, current and wind as the primary environmental conditions affecting mooring of a vessel at berth. However, it is practically not feasible and ineffective to perform the simulations and respective analyses on all the possible combinations of such environmental factors. Therefore, a base environmental condition and a critical environmental condition are defined to narrow down the broad range of possible combinations of various environmental factors.

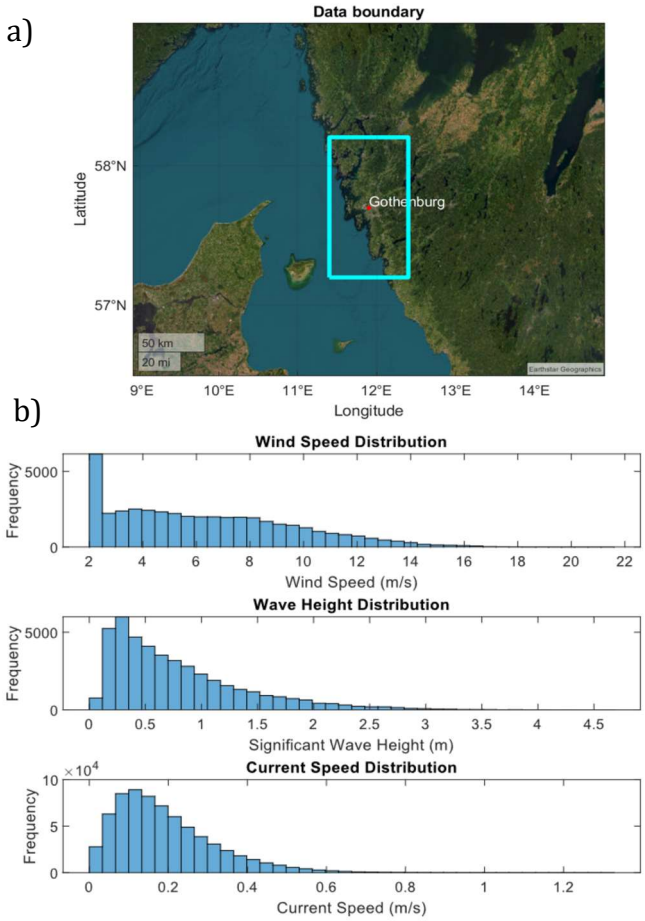


*Figure 4.2 Data used in the decision of the environmental conditions used in the model. a) Region where environmental data was collected. b) Distribution of wind speeds, significant wave height and current speed for the chosen region.*

The base environmental condition outlines the most occurring values of wind speed, current, and wave height and period that are obtained for the Gothenburg area (as described in Figure 4.2 - a). The statistical estimation is made considering the conditions from 2024 and is described in Figure 4.2 - b. This condition represents the environmental load scenario with highest probability of occurrence.

The critical environmental condition is defined as the combination of critical environmental factors in terms of mooring. MEG4 recommends some minimum environmental conditions that the mooring equipment onboard ships, above 16,000 DWT, should be able to withstand (OCIMF, 2018). These conditions are outlined in Table 4.4.

*Table 4.4 Standard environmental condition. Adapted from (OCIMF, 2018).*

| | Magnitude (knots) | Direction (degree) |
|---|---|---|
| Wind | 60 | Any direction |
| Current | 3 | 0/180 |
| | 2 | 10/170 |
| | 0.75 | 90/270 |

The fixed mooring equipment onboard should be sufficient to handle any combination of the wind and current mentioned in Table 4.4. In addition to the current and wind conditions recommended in the guidelines, a critical wave, the wavelength of which equals vessel length, is also considered.

Table 4.5 presents the applied base and critical environmental conditions in this study. Similar ranges of wind, current or wave directions are considered in the base environmental conditions as of the critical environmental conditions from guidelines.

*Note*: MEG4 outlines the critical environmental loads to ascertain the safety and integrity of the mooring equipment installed on a ship. However, the critical conditions considered in this study are chosen to perform an effective analysis and evaluation of the employed methods.

*Table 4.5 Environmental conditions applied.*

| Base Environmental Conditions | | | | Critical Environmental Conditions | | | |
|---|---|---|---|---|---|---|---|
| | Magnitude | | Direction(°) | | Magnitude | | Direction(°) |
| Wind | 2.25 m/s | | 0,10 & 90 | Wind | 30 m/s | | 0,10 & 90 |
| Current | 0.11 m/s | | | Current | 1.5 m/s | | |
| Wave | 0.3m | 4.25s | | Wave | 0.86m | 5.66s | |

## 4.4 Study cases

Four study cases are defined in a way that enables the study of the different phenomenon involved in isolation from each other and step-by-step build up complexity to culminate in the final case that represents the process of mooring of a merchant ship. In all case studies, the water depth is set as "infinite" (considerably larger than the dimensions of the barge).

### 4.4.1 Case 1a

The first case study is the barge in open sea (away from berth), with no mooring lines, while it is subjected to various environmental conditions with different degrees of freedom in each condition. A simplified sketch of this case study is shown in Figure 4.3.

This case study aims at providing assessment of the implemented basic ship hydrodynamics, i.e. ship motions in response to the environmental loads. The assessment is carried out in terms of the modelling accuracy and comparison of the ship motions in conjunction with the incorporated forces from the applied environmental conditions. The metric used in these assessments is relative and absolute difference in motions between the employed methods. The observations made in this case in terms of the hydrodynamic responses of the barge, e.g. six degrees of freedom motions, is used to identify potential sources of discrepancy

for the results obtained in the more complicated study cases, for instance the cases with mooring lines.

*Figure 4.3 Case 1a setup sketch: floating barge in open sea.*

The investigated environmental conditions in this case study includes the consideration of wave, wind or current, separately, in each respective simulation. The separation of environmental factors leads to isolating their exerted loads on the vessel, hence helps understanding the isolated effects on the ship hydrodynamic responses. Therefore, the simulations in this case study consists of the following environmental conditions scenarios, in which both the base and the critical conditions are considered.

*Waves*

The response of the ship to regular waves is analysed in three different simulations. The simulations conditions are distinguished based the considered wave direction, i.e., 0° (head wave), 10° (oblique wave) and 90° (beam wave).

A simulation in 0° (head wave) is carried out by fixing motions along surge, sway, roll, and yaw. This allows for an isolated assessment of the heave and pitch motions.

In the case of 90° (beam wave) simulation, the surge, sway, pitch and yaw degrees of freedom are fixed. This, in turn, allows for the assessment of the roll motion and can further ascertain the inferences made for heave motion in the 0° (head wave) simulation.

A simulation in 10° (oblique wave) is carried out with fixed surge and sway. This allows for assessment of the motions coupling without involving surge and sway.

*Current*

Similar to the assessments conducted for waves, the response of the vessel to current is also evaluated using three different simulations identified by three different directions, i.e. 0°, 10°, 90°.

For the simulation with current at 0°, sway, heave, roll, pitch and yaw are kept constrained and solely the surge motion is assessed.

For a 90° current simulation, surge, heave, roll, pitch and yaw are kept fixed. This facilitates the assessment of the sway motion of the vessel.

In the simulation with current at 10°, the vessel is constrained in heave, pitch and roll. Results from this simulation is assessed to evaluate the coupled surge and sway motions along with the yaw motion.

*Wind*

Three simulations are carried out in winds with directions identical to the directions and respective DOFs in the current scenario, thus analysing surge, sway and yaw motions. Owing to the low projected wind area, the heeling effect of wind is not assessed and is considered negligible.

### 4.4.2 Case 1b

This case study is the barge in open sea (away from berth), with two mooring lines (along surge direction), while it is subjected to various environmental conditions with different degrees of freedom in each condition. A simplified sketch of this case study is shown in Figure 4.4.

This case study aims at providing assessment of the implemented mooring line dynamics, i.e. the interaction between the rope behaviour and the ship motions in response to the environmental loads. The assessment is carried out in terms of the modelling accuracy and comparison of the ship motions and mooring line forces in different environmental conditions. The metric used in these assessments are relative and absolute difference in motions and mooring line forces between the employed methods. The observations made in this case in terms of the barge motions and line forces, is used to identify potential sources of discrepancy for the results obtained in the more complicated study cases.

Basically, the simplest case study with respect to the mooring lines would involve solely one single point mooring arrangement. However, the utilized tools in this thesis are not capable of modelling a single line scenario, due to the current implementation of mooring line pre-tensioning. Furthermore, consideration of a single mooring line introduces asymmetric conditions that may result in complicated ship behaviour and hence complex mooring line dynamics, which may need more sophisticated mooring line modelling. This is out of the scope of this thesis as the main focus here is on the ship mooring at berth, in which the ship motions are often small resulting in simpler line dynamics that could often be captured with simpler models. Therefore, the arrangement shown in Figure 4.4 is considered with two mooring lines, one at the bow and the other at the stern. The lines are set with a pretension of 80,000 N.

*Figure 4.4 Case 1b setup sketch: floating barge in open sea while constrained by two mooring lines.*

The simulations in case 1b (in both base and critical environmental conditions) are limited to two scenarios, one in waves (to study the response due to angular displacements) and the other in current (to study the response to linear displacements).

*Wave*

The interaction between the vessel and the mooring lines is analysed in a head wave 0° simulation, while fixing the sway, roll and yaw. Here, the mooring line tension along with coupled motions in surge, heave and pitch is assessed.

*Current*

Two simulations involving current scenario are analysed.

The first simulation is carried out in current flowing from 0° with the vessel motions along sway, roll and yaw constrained. This facilitates the assessment of the mooring line dynamics in a scenario that constitutes directional loading (in the direction of mooring).

Current from 10° acting on the vessel with motions restricted along heave, roll and pitch forms the second simulation. The purpose of this simulation is to assess the mooring line dynamics across the two methods in the case of an oblique load condition. In a practical mooring setup, lines are at an angle to the environmental load. Thus, this simulation helps ascertain that the coupling between hydrodynamic vessel responses and line modelling hold true for practical cases.

### 4.4.3 Case 2

This case study is the barge in open sea (away from berth), with four mooring lines (placed at the corners of the barge), while it is subjected to various environmental conditions but free in all degrees of freedom (6DOF). A simplified sketch of this case study is shown in Figure 4.5.

This case study aims to capture the four mooring line dynamics in more complex ship performance scenarios. This test case facilitates the assessment of the effect of having multiple lines contributing to restraining responses of the moored vessel to environmental loads. The metric to be used in assessing the accuracy of the

model will be relative and absolute error of the line force and ship motions, similar to case 1 b.

A single scenario considered in the simulations for this case study, which is the combinations of the wave, wind and current. Three simulations are carried out, identified by the directions 0°, 10°, 90°, while both the base and critical environmental conditions are considered.

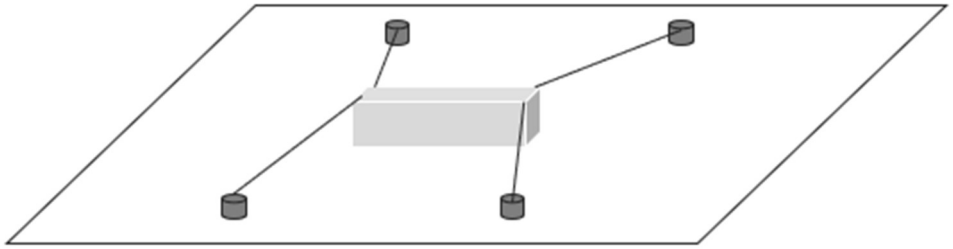

*Figure 4.5 Case 2 setup sketch: floating barge in open sea while constrained by four mooring lines.*

### 4.4.4 Case 3

This case study is the barge close to a berth (but no fenders), with four mooring lines (placed at the corners of the barge), while it is subjected to various environmental conditions but free in all degrees of freedom (6DOF). A simplified sketch of this case study is shown in Figure 4.6. Building on the previous case studies, in case 3, the quay wall is introduced, presenting an impermeable boundary condition for the fluid. The position of the bollards is unchanged from previous tests.

This test case aims to capture the influence of the quay structure on the ship performance with respect to its motions and mooring line forces. Examples of such berth proximity effects are the bank/cushion effect and effect of reflected waves. These effects are not implemented in the employed semi-empirical method, thus the simulations in the potential flow method can indicate the extent of such effects.

*Note:* For loading scenarios at 90°, current is not considered for the remaining simulations, because having currents perpendicular to a long quay wall is an impractical scenario.

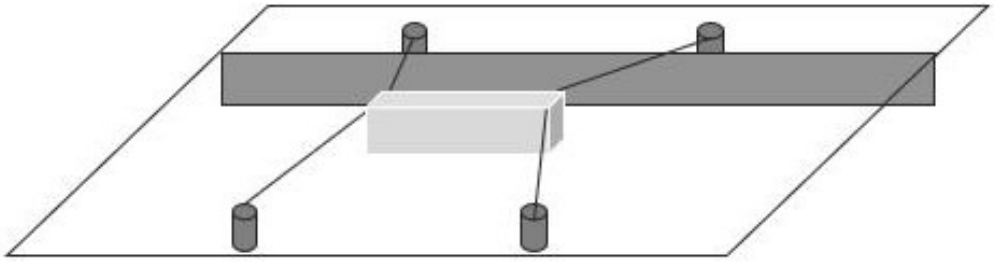

*Figure 4.6 Case 3 setup sketch: floating barge near berth while constrained by four mooring lines.*

## 4.5 Post-processing techniques

Both the tools employed, i.e. SEAMAN and Shipflow Motions, produce results in the form of timeseries that capture the vessel motions at the centre of gravity, as well as tensions in the mooring lines, fender forces, and other relevant parameters. Different environmental conditions with different constraints leads to different nature of results. For example, current forces ideally result in a nearly linear response in surge, sway and/or yaw, while a wave force results in sinusoidal variations in motions and tensions. Therefore, it is important to identify which values to compare for different scenarios.

For simulations involving just current or wind, a direct comparison of the displacement of the vessel in surge, sway and/or yaw directions is ideal. For simulations involving waves, there are several parameters that can be vary, namely, mean value, peak value, frequency and the response spectrum. Coupling with mooring forces only increases the variations in the results due to additional damping components.

Simulation convergence is another critical element before analysing the time series. Since the number and nature of scenarios vary greatly between simulations, it is unfeasible to establish a single convergence criterion that could be applied across all scenarios. Consequently, in this thesis, the convergence of the simulations is examined through a qualitative assessment, such as visual inspection of the time series plots.

To compare the oscillatory responses of the time series in waves, Fourier analysis is carried out as follows,

$$A(t) = A_0 + A_1 \cos(\omega t + A_{\epsilon 1}) + A_2 \cos(2\omega t + A_{\epsilon 2}) + \cdots, \qquad (4.32)$$

where $A_i$ is the *i*th harmonic amplitude of the response A and $A_{\epsilon i}$ is the phase component related to *i*th harmonic amplitude. $\omega$ is the wave frequency. The analysis is carried out over the last ten wave periods of the timeseries when the simulation is converged. The harmonic amplitudes reveal the magnitude of the oscillations at different frequencies and can provide additional insight into the response to waves. Fourier analysis is carried out using the Fast Fourier Transform (FFT) function in MATLAB and plots generated are shown in the Section 5. Noisy signals with multiple frequencies results in signals as shown in Figure 4.7 - a. Whereas, for signals that are uncorrupted, the plots obtained will depict magnitudes that can be clearly attributed to a set of frequencies as depicted in Figure 4.7 - b.

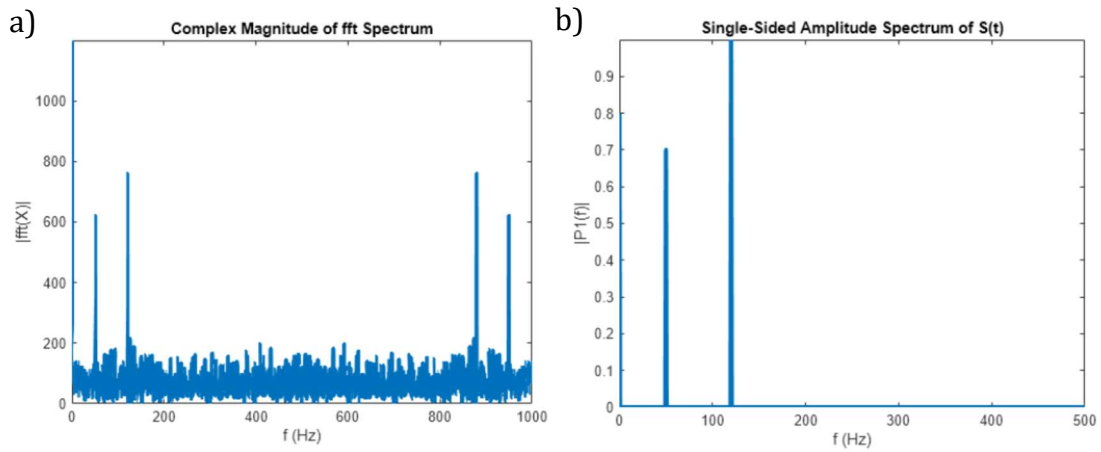


*Figure 4.7 FFT plots for: a) noisy/corrupted signals and b) uncorrupted signals (source: MATLAB documentation).*

# 5 Results and discussions

The following section describes the results of the simulations, and the evaluation of results produced using semi-empirical method against those produced using potential flow method. The results are presented based on the cases presented in Section 4.4.

In each case, the response of the ship to various selected sets of environmental conditions is studied. The chosen environmental conditions are derived from systematic combinations of different environmental factors provided in Table 4.5.

Note that for each case, the analysis is carried out for a selected time interval of the time series in each simulation. Accordingly, the "time" in the plots is offset time and represents the selected time interval for analysis and not the entirety of the simulation. Consequently, time=0 s does not necessarily mean the beginning of the simulation, but it means the beginning of the analysis time interval. This was done to exclude the initial part of the time series, which contains transient behaviour (before reaching stable solution and convergence), that is out of the scope of result discussion in this thesis.

## 5.1 Case 1a

The investigations in Case 1a (floating barge in open sea) include the application of wave, current and wind scenarios separately, in order to perform an evaluation of the ship responses considering the isolated effects from each of these environmental factors. It is aimed at assuring comparable basic hydrodynamic models in the employed tools before diving into more complex scenarios with mooring lines involved.

For each simulation in Case 1a, different degrees of freedom (DOFs) are selectively fixed or freed depending on the simulation scenario. Therefore, in each simulation a different combination of free and constrained motions is considered.

### 5.1.1 Response to wind

Response to wind is compared for 0° and 90° wind while free in a single DOF (free surge for 0° wind and free sway for 90° wind). Both scenarios are tested for winds at base and critical conditions.

*Wind at 0°*

In head winds, only surge motion was considered. The response of the vessel to 0° wind is shown in Figure 5.1.

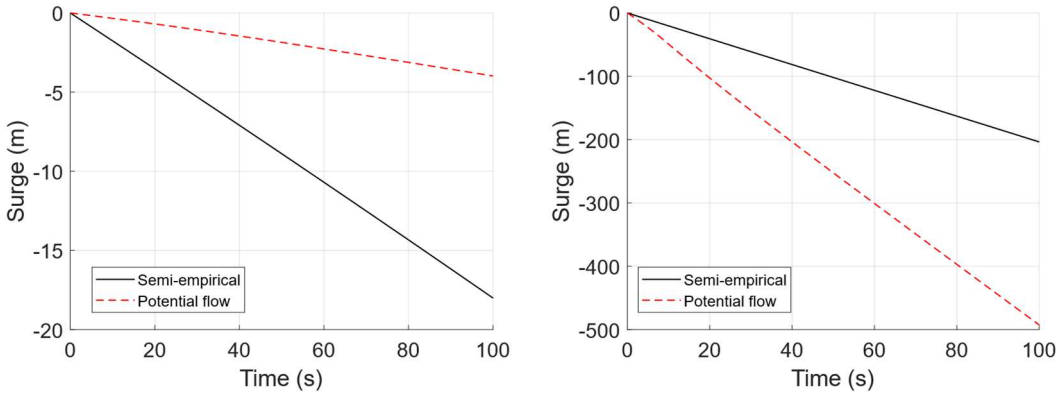


*Figure 5.1 Time-series of surge motion in case 1a with head wind and 1DOF (surge). Base condition (left) and critical condition (right).*

For this simulation, wind acts as an external force that pushes back the barge through the water (negative surge according to the defined coordinate system in Figure 2.1). The wind force is completely counteracted by the resistance force in the longitudinal direction, as no more DOFs are being considered in this simulation. Apparent wind speed (AWS) is the speed used in Equation (2.4).

Note that the barge picks up speed throughout the simulation (not shown), resulting in the continuous change of AWS and hence, changing the instantaneous wind force. These changes of AWS, wind force, ship speed and resistance force will continue until the forces reach equilibrium. It is expected that the final velocity achieved by the barge will correspond to the speed at which resistance is equal to the wind force. As an example, in the critical case, the semi-empirical tool predicts a final speed of -2.03 $m/s$, but the potential flow tool's predicted speed is -4.77 $m/s$. These can also be observed based on the surge motion time series in Figure 5.1. The final wind force, calculated according to Equation (2.4), is presented in Table 5.1.

*Table 5.1 Value of the final x-component of the wind force (in kN) in case 1a with head wind and 1DOF (surge).*

| | Semi-empirical | Potential flow |
|---|---|---|
| Base condition | -0.0972 | -0.123 |
| Critical condition | -19.6 | -16.1 |

The derived ship speed in each simulation is in line with the observed final wind forces in Table 5.1. For instance, in comparison to the results from the potential flow method, the results from the semi-empirical method reflects:

1. Larger magnitude of the ship speed and smaller x-component of the wind force in the base case,
2. Smaller magnitude of the ship speed and larger x-component of the wind force in the critical case.

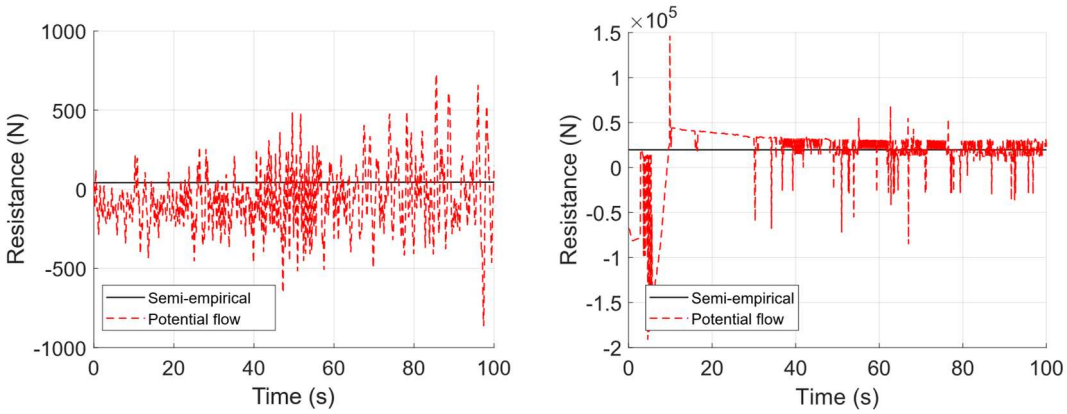


*Figure 5.2 Time-series of resistance force in surge direction in case 1a with head wind and 1DOF (surge). Base condition (left) and critical condition (right).*

The resistance force time-series, shown in Figure 5.2 reveals an oscillatory behaviour of resistance derived from the potential flow tool. It should be noticed that a moving ship in the employed potential flow method generates waves (wave making). Due to small ship speeds in the current simulations, the generated waves are very small, hence require extremely fine panels and thus extensive computational costs to capture them with a high level of accuracy. On the other hand, using large panels (with lower accuracy at capturing generated waves) may introduce oscillations into the resistance force calculations, as seen in Figure 5.2.

When the hydrodynamic forces are insignificant, the hydrostatic forces dominate the behaviour of the ship in time domain potential flow simulations. In such scenarios, the accuracy of hydrostatic force calculations becomes substantially important. In the employed potential flow method, the accuracy of the hydrostatic force calculations is directly affected by the ship and free surface panelisation. The panels are not ideal, consequently, there exist unphysical forces generated by such imperfect panelisations. These forces are often very small, but in scenarios where the hydrodynamic forces are insignificant, the unphysical forces may become considerable as they may continuously change the behaviour of the ship. The time-series of the hydrostatic force in longitudinal direction are shown in Figure 5.3.

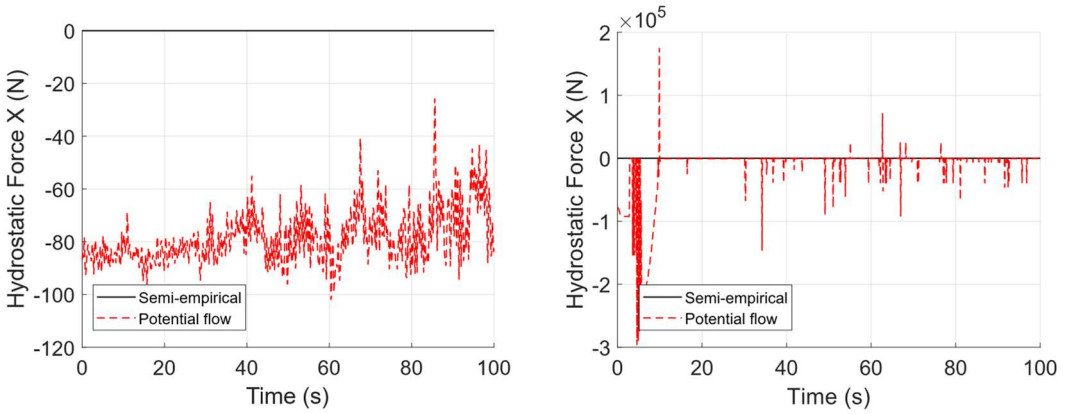


*Figure 5.3 Time-series of hydrostatic force in surge direction in case 1a with head wind and 1DOF (surge). Base condition (left) and critical condition (right).*

The average values of resistance and hydrostatic forces are presented in Table 5.2. The moving ship would have sinkage and trim due to the differences of pressure

at its fore and aft, but these degrees of freedom are fixed in the current simulations. Assuming insignificant contributions (from fixed sinkage and trim) in the longitudinal direction, there exists considerable hydrostatic forces from the utilized potential flow approach. This behaviour might also be intensified due to the generated waves by the moving ship, as discussed before. Therefore, the unphysical hydrostatic forces seen in the potential flow method might highlight a limitation of the applicability of this method in the current type of simulations' conditions.

*Table 5.2 Average values of different forces (in kN) in case 1a with head wind and 1DOF (surge).*

| | Semi-empirical | Potential flow |
|---|---|---|
| Resistance (kN) | | |
| Base condition | 0.0972 | 0.0629 |
| Critical condition | 19.7 | 16.2 |
| Hydrostatic Force (kN) | | |
| Base condition | 0 | 0.0785 |
| Critical condition | 0 | 12.7 |

*Wind towards 90° (coming from port)*

Beam wind was analysed considering the ship to be free only in sway.

Figure 5.4 contains the response of the vessel to beam wind in both the base and critical conditions.

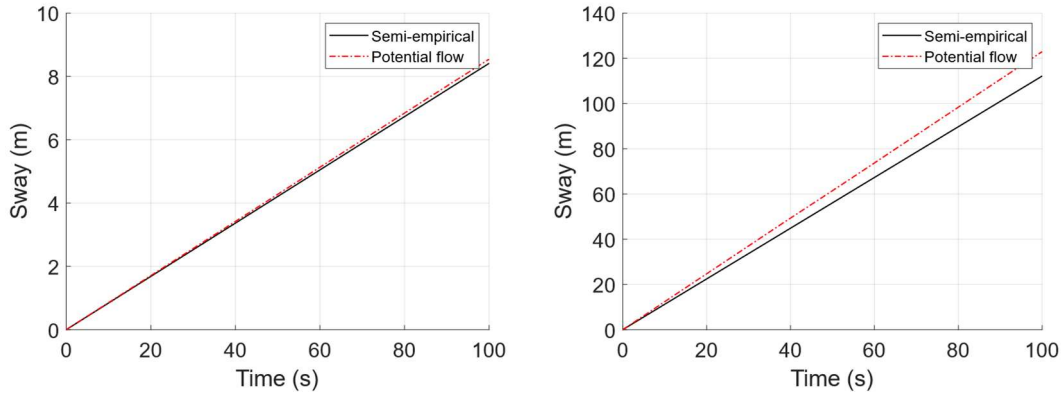


*Figure 5.4 Time-series of sway motion in case 1a with beam wind and 1DOF (sway). Base condition (left) and critical condition (right).*

A small deviation on the resulting motion for the base case and for the critical case is observed. The slight deviation in the base case of 1% and the slightly larger deviation in the critical case of 8% suggest that the difference between the results is related to a speed-related force component.

In this simulation, the forces acting are the lateral wind force and, opposing the wind force, the "manoeuvring" force described in Equation (3.14) for the semi-empirical tool and in Equation (3.24) for the potential flow tool. Note that, in the potential flow tool there is an additional force originated from hydrostatic force

imbalance (as discussed before) in the y-direction and a force resulting from the integration of the pressure around the hull which represents the force opposing the motion exerted by the fluid. The final values of the wind force for this simulation are presented in Table 5.3.

*Table 5.3 Value of the final y-component of wind force (in kN) in case 1a with beam wind and 1DOF (sway).*

| | Semi-empirical | Potential flow |
|---|---|---|
| Base condition | 0.249 | 0.249 |
| Critical condition | 44.3 | 44.0 |

Figure 5.5 represents the manoeuvring force calculated for both tools in both conditions.

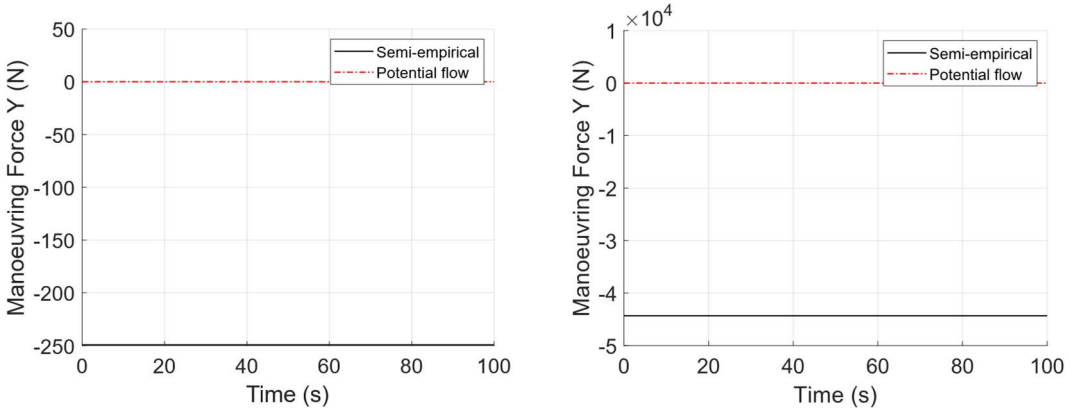


*Figure 5.5 Time-series of the manoeuvring forces in the sway direction in case 1a with beam wind and 1DOF (sway). Base condition (left) and critical condition (right).*

Note that in Figure 5.5 the manoeuvring force in the semi-empirical tool takes the exact value of the wind force in Table 5.3. The potential flow tool, however, presents very different results as part of the wind force is opposed in the potential flow by the pressure integration force that represents the transversal opposing force.

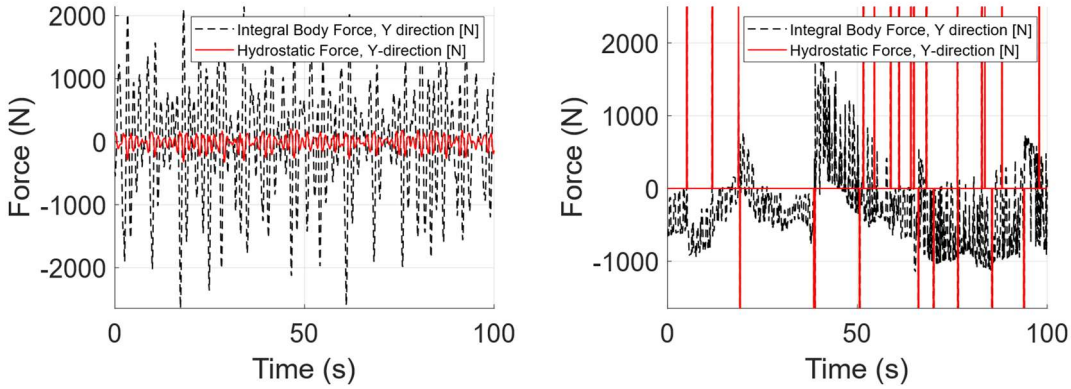


*Figure 5.6 Time-series of the hydrostatic force and for the pressure integration force in the sway direction in case 1a with beam wind and 1DOF (sway) in the potential flow method. Base condition (left) and critical condition (right).*

Figure 5.6 shows the calculated hydrostatic and the pressure integration forces from the potential flow tool. The average value of the hydrostatic force is 0.0013 kN and the average value of the pressure integration force is 0.00080 kN for the base case. This result is in line with the previous remark that the wind force is counteracted in the potential flow tool by the pressure integration forces. In the critical condition, the values obtained were 0.728 kN and 0.469 kN, respectively.

Note as well that instabilities in the hydrostatic force calculations are visible in Figure 5.6. It is also possible to observe how the sudden peaks in hydrostatic force (that reach values of up to -520 kN) cause steps in calculating another quantity - the integral body force – and consequentially in other quantities as well, such as velocity.

*Wind at 10°*

The behaviour of the ship free in yaw motion is investigated in oblique winds. Figure 5.7 shows the behaviour of the ship predicted by the semi-empirical tool for the base case (during the full simulation time). It is possible to observe the general trend of the movement of the barge, with 2 distinct moments: the first, when the barge rotates in the positive direction, with the bow rotating to starboard, towards having wind from port (beam wind) and the second, where the barge oscillates around this equilibrium position.

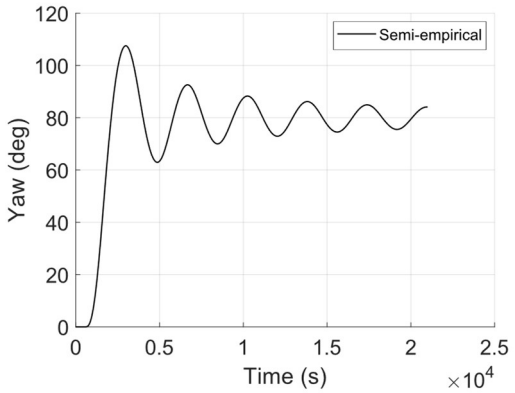


*Figure 5.7 Time-series of yaw motion in case 1a with oblique wind and 1DOF (yaw) in base condition.*

*Figure 5.8* contains the response of the vessel during the initial stage of the simulation, converging towards equilibrium position for both base and critical conditions.

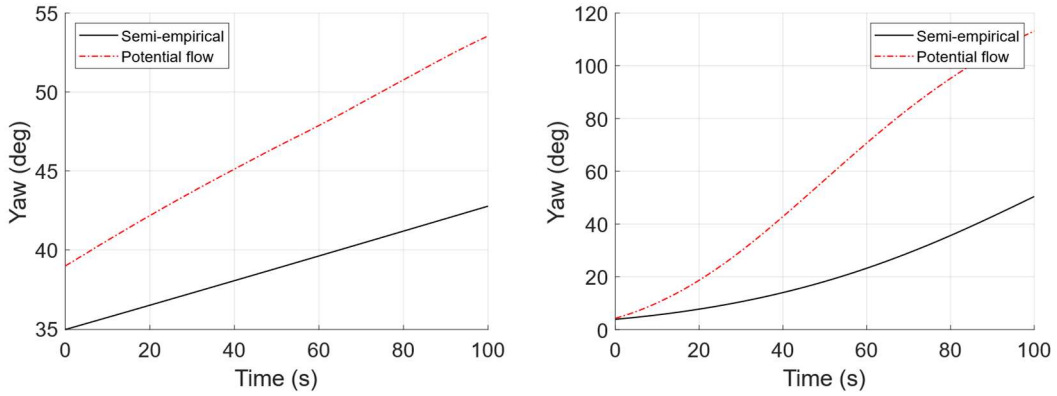


*Figure 5.8 Time-series of yaw motion in case 1a with oblique wind and 1DOF (yaw). Base condition (left) and critical condition (right).*

Figure 5.8 shows that the different methods ramp up towards a position (where wind is coming from port) with different velocities. The semi-empirical tool takes on a smaller rotation velocity for the yawing motion. This will in turn result in a slower change of the apparent wind angle (AWA) and consequently in a slower change of the wind moment. All of this contributes to the less steep yawing motion observed in Figure 5.8.

The moments acting in each of the methods for this time interval of the simulations are presented in Table 5.4.

*Table 5.4 Value of the average component of different moments (in Nm) in the yaw degree of freedom in case 1a with oblique wind and 1DOF (yaw).*

| | Semi-empirical | Potential flow |
|---|---|---|
| Manoeuvring Moment in yaw degree of freedom | | |
| Base condition | -256.1 | 0 |
| Critical condition | -10800 | 0 |
| Hydrostatic Moment | | |
| Base condition | 0 | 0 |
| Critical condition | 0 | 0 |
| Moment due to integration of pressure around the hull (potential flow) | | |
| Base condition | - | -176.0 |
| Critical condition | - | 5040 |

The values in Table 5.4 represent the resisting moment from the water to the rotating motion of the barge induced by the wind. It is possible to observe that in the semi-empirical method this opposing moment is larger, resulting in the slower rotation we observe in Figure 5.8.

It is also worth noting that the hydrostatic moment has a zero value, which means for the degree of freedom of yaw, the small rotation speeds do not introduce the complications in the potential flow method discussed for the degrees of freedom of surge and sway.

For the analysis of the second part of the simulation, the critical case is used.

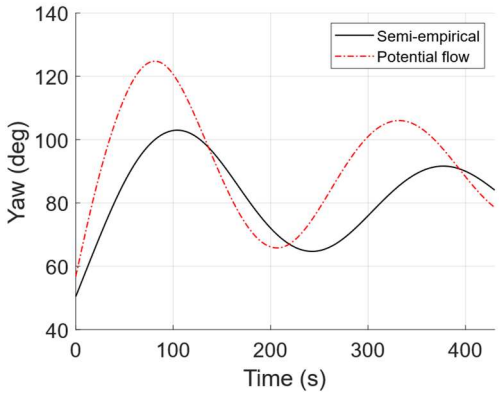


*Figure 5.9 Time-series of yaw motion in case 1a with oblique wind and 1DOF (yaw). Critical condition; second part of the simulation.*

In the second part of the simulation, presented in *Figure 5.9*, the yaw motion predicted by the semi-empirical force, and that is being "damped" by larger opposing forces, will converge quicker to the equilibrium position (barge rotated 80 degrees in the positive direction, i.e. with beam wind facing the barge from port).

In general, there is a good agreement between the results obtained with the semi-empirical method and the potential flow method when it comes to the overall motion of the barge. There are, however, differences that can be important in the context of the analysis of mooring ropes. Different velocities will result in different dynamic behaviours, which can cause to underprediction of dynamic loads of the mooring ropes.

### 5.1.2 Response to current

Response to current is analysed in the cases of head current, beam current and oblique current at 10°. For the case of head current, only surge is considered, while the other DOFs are fixed. For the case of beam current, only sway is considered. Finally for oblique current, surge, sway and yaw are considered and the coupling between these motions are taken into account - namely the couplings described in Equations (3.13) to (3.16) for the semi-empirical tool and Equations (3.23) to (3.25) for the potential flow tool. The current is applied according to both base and critical conditions, according to the values presented in Table 4.5.

The conceptual implementation of current in the semi-empirical tool represents the current as an additional speed through water, while the potential flow tool creates the effect of current by moving the world object (and hence the free surface panels) in relation to the barge.

*Head Current*

In these simulations, the aim is to compare the surge motion results derived from the employed tools. The results are shown in Figure 5.10.

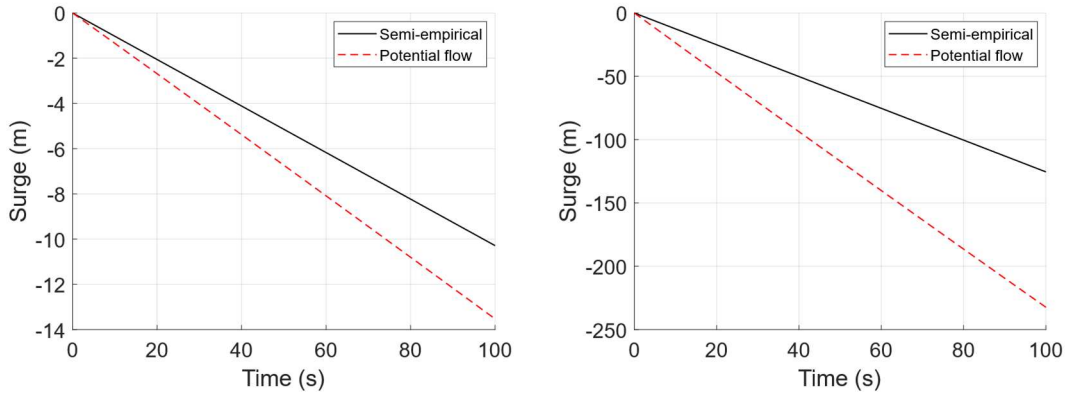


*Figure 5.10 Time-series of surge motion in case 1a with head current and 1DOF (surge). Base condition (left) and critical condition (right).*

Figure 5.10 shows the expected movement of the barge on the longitudinal direction. The difference in the slope of the curves suggests that the ship is moving with different velocities in different tools. The potential flow method results are unreasonable as the ship is seen moving with a speed larger than that of the current. In fact, a ship in 0.11 m/s current in 100 seconds should have travelled 11 m (instead of 13.54 m) in the base case and 150 m (instead of 232.43 m) in the critical case. These overpredictions of 23.1% (in the base case) and 55.0% (in the critical case) can be justified mainly by the discussed hydrostatic force imbalances due to the panelisation. Figure 5.11 shows the hydrostatic force calculated by the potential flow tool.

The semi-empirical tool presents more reasonable results, with a speed slightly smaller than the current speed. This difference between the current speed and the ship speed might be originated from the resistance interpolations in this method.

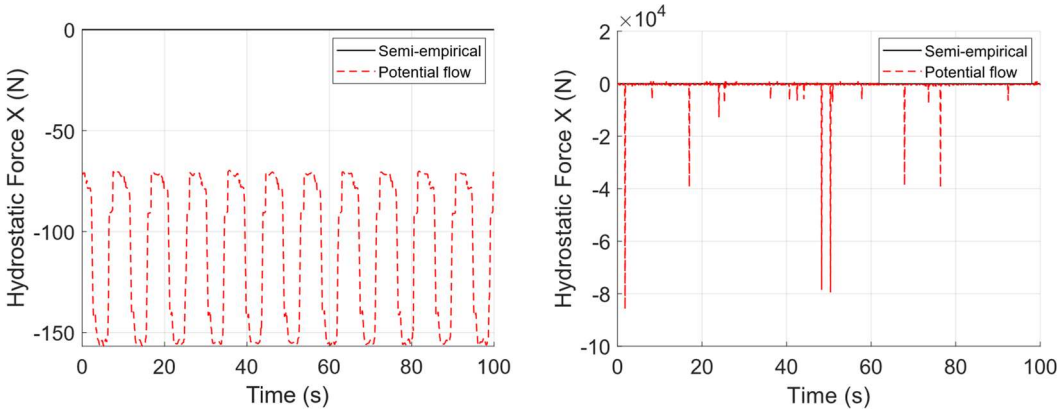


*Figure 5.11 Time-series of hydrostatic force in surge direction in case 1a with head current and 1DOF (surge). Base condition (left) and critical condition (right).*

The hydrostatic force presents a significant force in the base case (average force of -110 N) with a period of 10 seconds – unreasonable for a simulation with constant current.

*Beam Current*

Beam current was analysed considering sway unconstrained for these simulations. Figure 5.12 contains the response of the vessel to beam current in both the base and critical conditions.

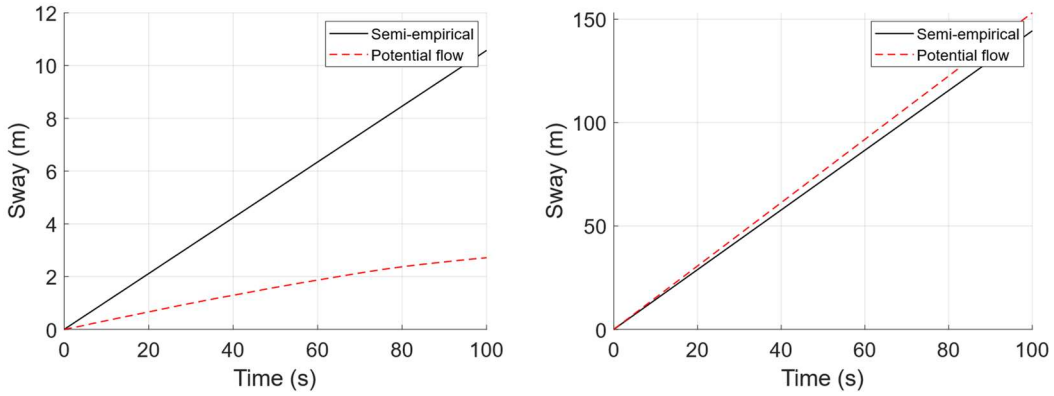


*Figure 5.12 Time-series of sway motion in case 1a with beam current and 1DOF (sway). Base condition (left) and critical condition (right).*

It is once again possible to visualize a difference between the two methods resulting possibly from a speed dependent force, as the potential flow tool underpredicted sway motion in relation to the semi-empirical tool in the base case, but slightly overpredicts in the critical case. We observe the same behaviour in the semi-empirical tool as we had observed for the head current case: the barge has almost the same speed as the current, with a slight difference coming from a force component (in this case, this force is included in the manoeuvring force module of the semi-empirical tool).

The base case result for the potential flow tool reveals an exaggerated horizontal hydrostatic force with an average value of 512 N. The transversal resisting force in the sway direction calculated via pressure integration around the hull presents an average value of 132 N, and it also opposes the motion of the barge.

Regarding the critical case, the hydrostatic force converges to zero (average value of 0.05 N) which further confirms the speculation that significant errors might raise due to hydrostatic forces imbalance due to panelisation. Note that the barge has on average a larger speed than that of current because of the oscillating nature of the hydrostatic force.

*Oblique current*

Oblique current (current from 10° on the fine port bow side) was analysed considering all the three motions we have considered so far, surge, sway and yaw and it is expected that the coupling between these motions to be visible in the results obtained. Figure 5.13 contains the response of the vessel to oblique current in both the base and critical conditions.

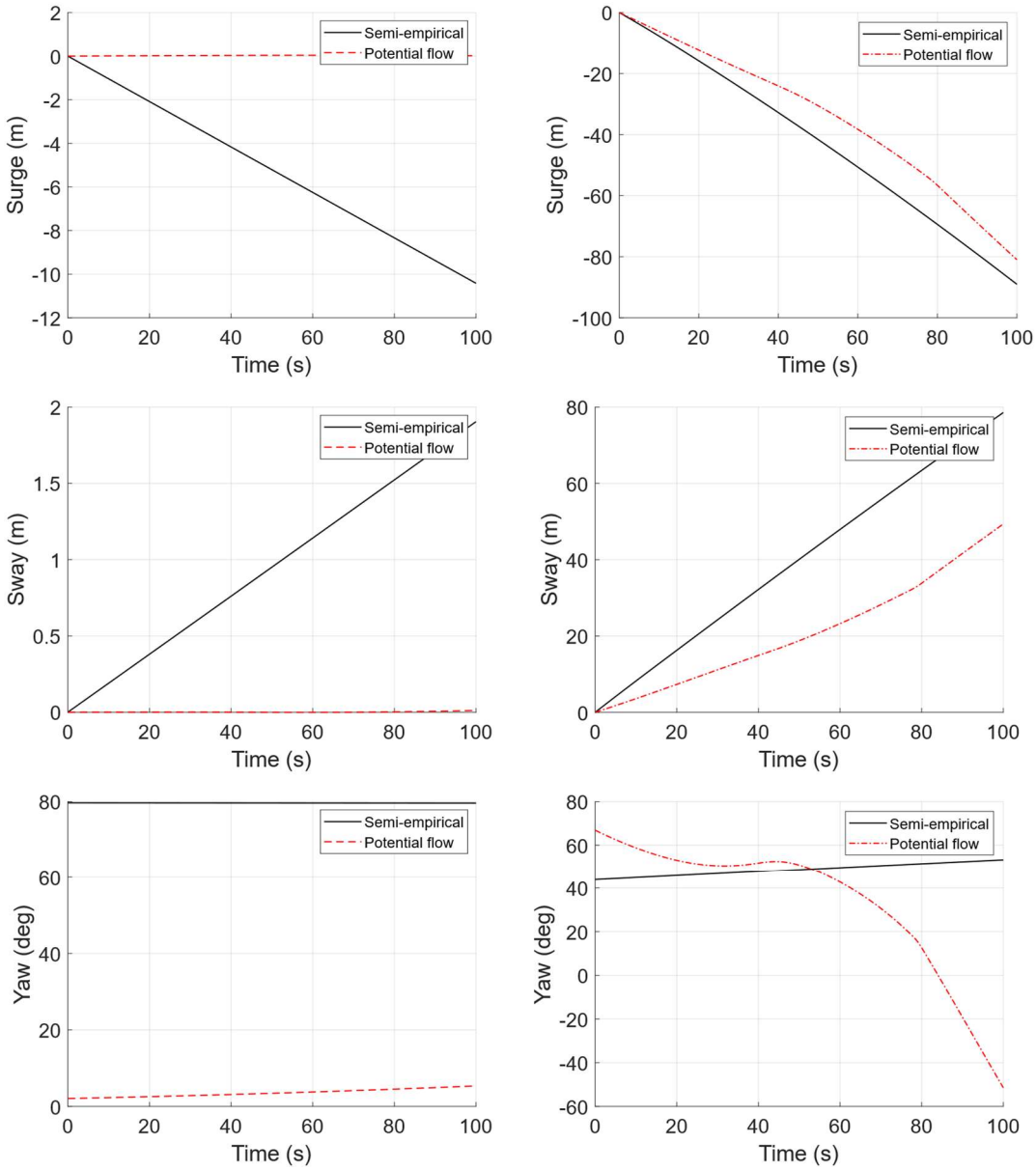


*Figure 5.13 Time-series of surge, sway and yaw motion in case 1a with oblique current and 3DOF (surge, sway and yaw). Base condition (left) and critical condition (right).*

From these simulations we can observe that the hydrostatic forces stopped the movement in the x and y-direction for the potential flow tool in the base case (total surge in the potential flow tool: 27.9 mm; total sway in the potential flow tool: 1.4 mm). Figure 5.14 shows the hydrostatic forces for the base case for the 3 DOFs.

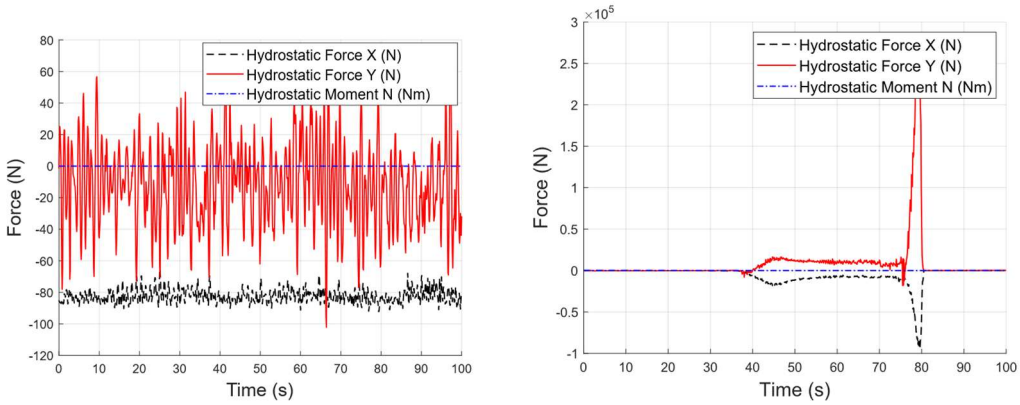


*Figure 5.14 Time-series of the hydrostatic forces in case 1a with oblique current and 3DOF (surge, sway and yaw). Base condition (left) and critical condition (right).*

From Figure 5.14 we see how the hydrostatic forces are significant for surge and sway (average values: 83 N and 12 N) and in yaw its negligible (average value of 0).

The manoeuvring forces, where the coupling is evident from the existence of the cross terms are shown in Figure 5.15.

It is possible to observe how these forces are mostly negligible to the semi-empirical tool in the base case. The force generated by the current will have the biggest component in the longitudinal direction, and the largest forces will be fall under the Resistance module and not under Manoeuvring force calculation.

Note that in Figure 5.13, the same behaviour that was observed with oblique wind is observed here: the different tools find different solutions for the stable position of the barge in relation to the wind: the semi-empirical tool presents a result where the barge is perpendicular to the current whereas the potential flow tool shows that the barge will be in line with the current.

The critical condition results for this simulation show how an instability in the simulation causes the result to be unphysical. The kink introduced by the hydrostatic forces at t=40s (cf. Figure 5.14) causes the yawing trend (to converge to yaw angle = 80°) to fail and produces the unphysical result of further rotation by the barge, where an inflexion point was expected (cf. Figure 5.13).

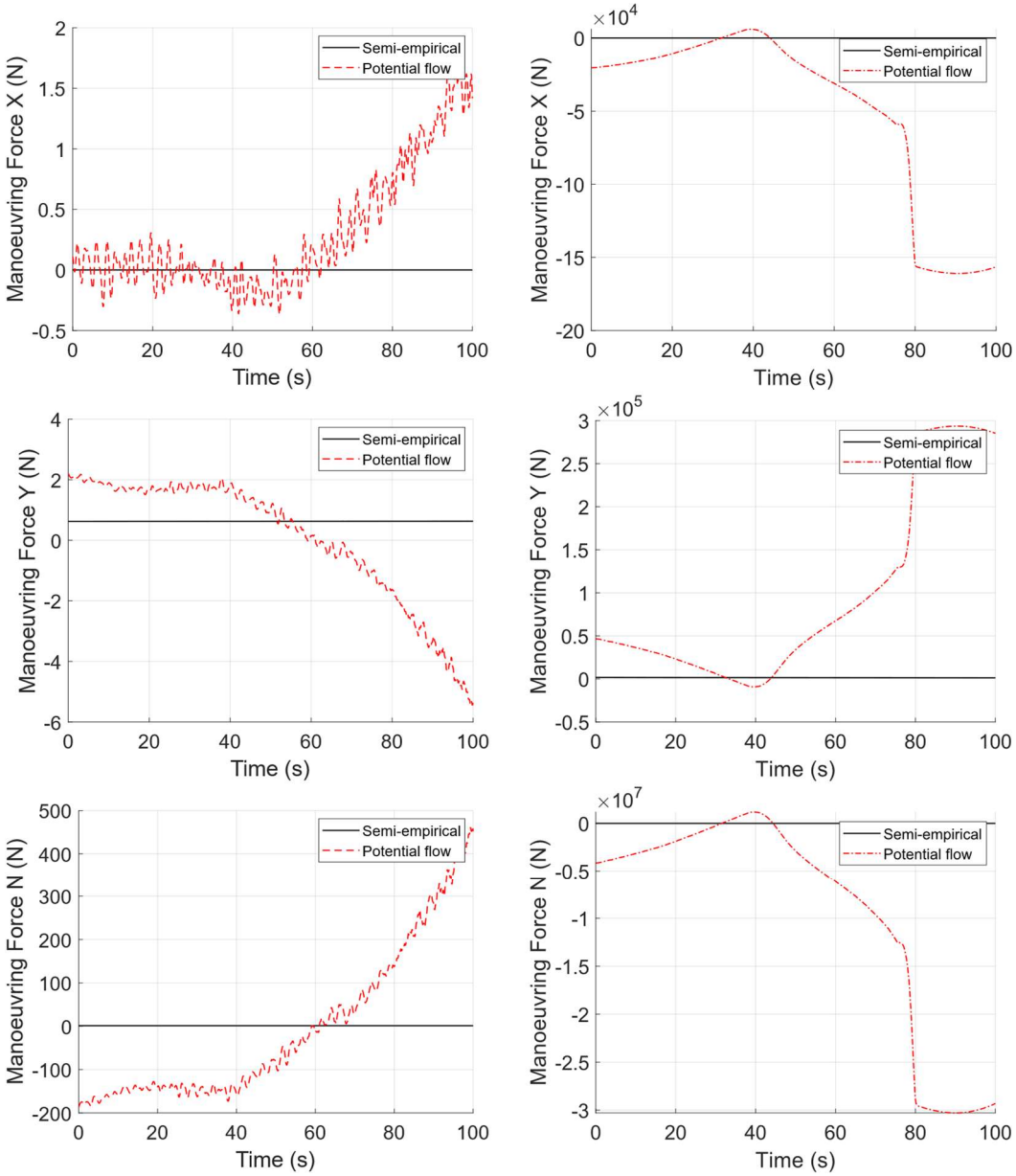


*Figure 5.15 Time-series of the manoeuvring forces in case 1a with oblique current and 3DOF (surge, sway and yaw). Base condition (left) and critical condition (right).*

### 5.1.3 Response to waves

The response of the vessel to regular waves is analysed in three different simulations identified by the considered direction, i.e. 0° (head wave), 10° (oblique wave) and 90° (beam wave). In each simulation, the base and critical wave conditions, are considered.

*Head wave*

Figure 5.16 shows the time series plot for heave and pitch motions for the barge in head waves (2DOF). The performed analysis does not consider the transient response period, instead only includes a time window in which the simulation is deemed converged, and the response of the vessel becomes rather harmonic. Running the simulations on a normal desktop computer, the potential flow

simulation took over five hours of wall-clock time to simulate three hundred seconds of physical time, while the semi-empirical code produced the results in less than a minute.

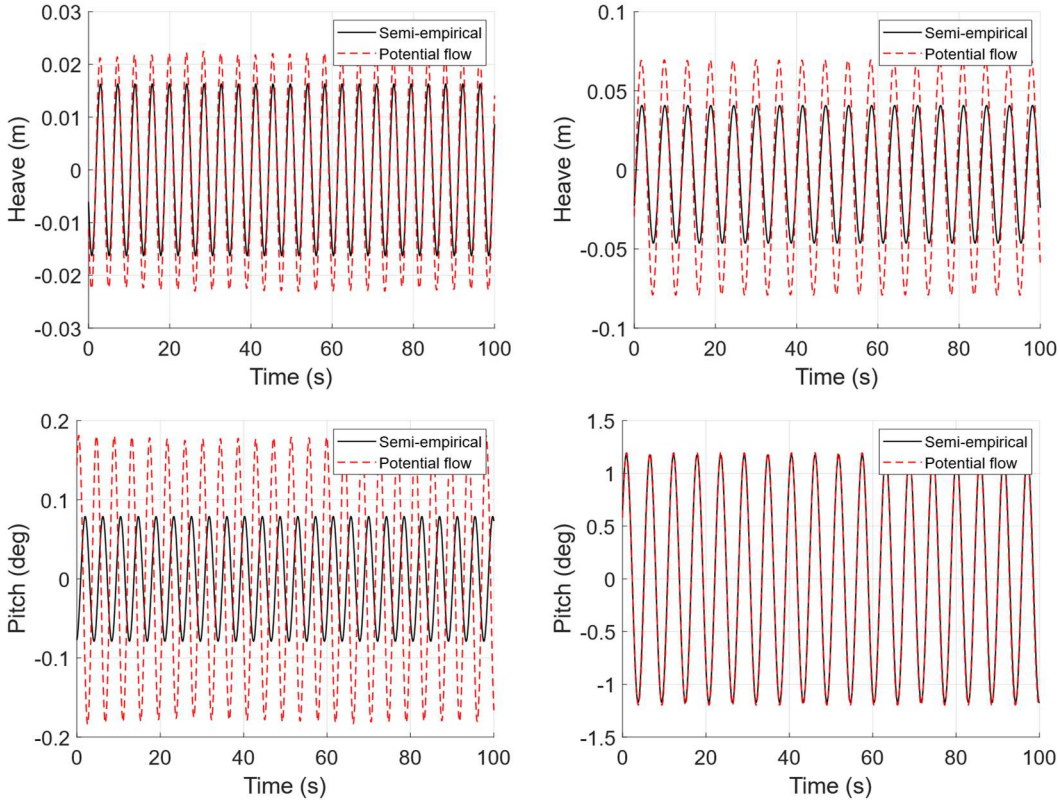


*Figure 5.16 Time-series of heave and pitch motions in case 1a with head waves and 2DOF (heave and pitch). Base condition (left) and critical condition (right).*

The results obtained for the base case present a general agreement in heave motion, with a difference of 0.006m between the peak values. The potential flow solver calculates the integral pressure acting on the wetted surface and accommodates for the diffraction and radiation effects. On the other hand, the semi-empirical method utilised strip theory and Lewis form approximations for force and added mass effect calculations and does not accommodate for the radiation and diffraction effects. The underpredicted semi-empirical heave in comparison to the potential flow method results can be attributed to these approximations.

The reduced effect of waves due to the above reasons can also be attributed to the deviations in the pitch response. However, a relatively larger underprediction is observed from the semi-empirical method. Any underprediction of the calculated forces results in a larger underprediction of the turning moment due to the lever arm. It is also seen from the velocities achieved by the barge in the pitch direction (shown in Figure 5.17), that the motion estimated using the semi-empirical tool is damped in comparison to speeds achieved in the potential flow simulations.

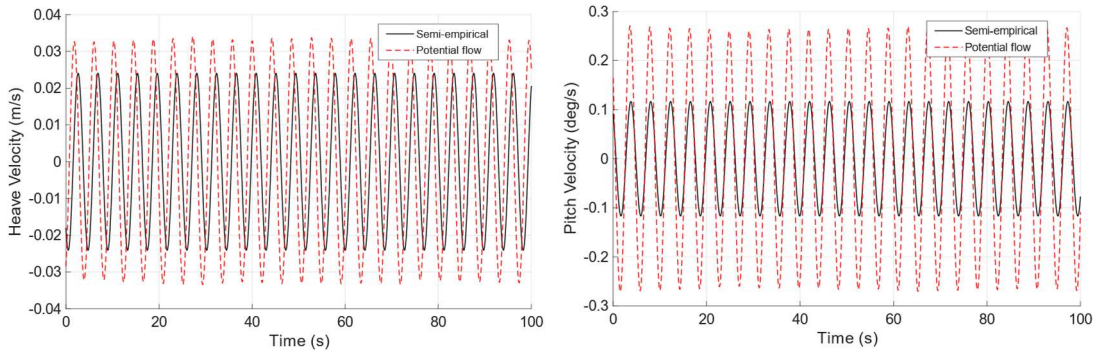


*Figure 5.17 Time series of motions velocities for case 1a with head waves and 2DOF. Heave (left) and pitch (right) velocities for base environmental condition.*

In the case of critical waves (Figure 5.16), a good match is seen in the pitch motion, but a small underprediction from the semi-empirical method in the heave motion. Even though the observations could be attributed to the effects mentioned above, the critical nature of the wave introduces effects due to resonance. This results in large pitch values, which here has matched with the prediction obtained in the potential flow solution.

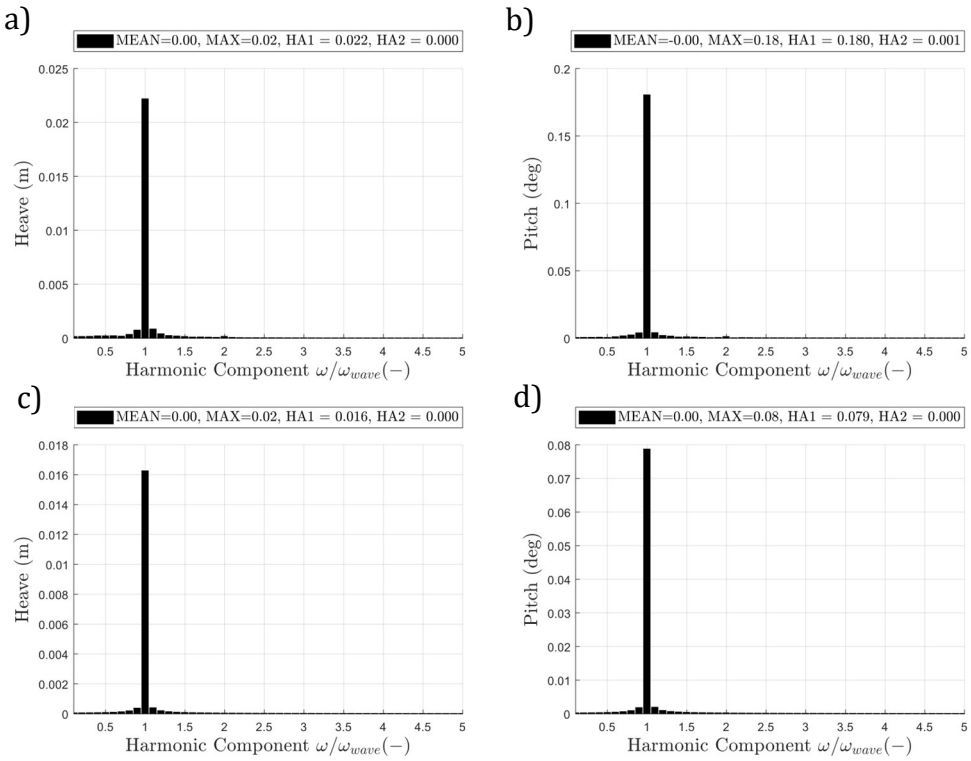


*Figure 5.18 FFT plots for case 1a in base condition with head waves and 2DOF (heave and pitch). a) and b) Potential flow method, c) and d) semi-empirical method.*

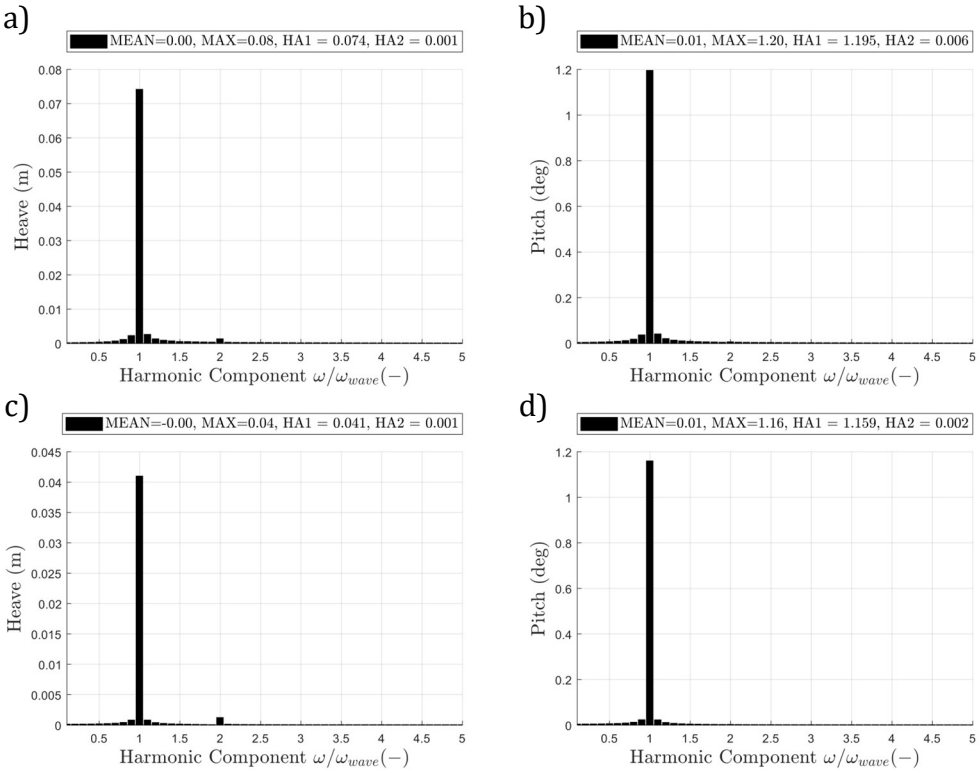


*Figure 5.19 FFT plots for case 1a in critical condition with head waves and 2DOF (heave and pitch). a) and b) Potential flow method, c) and d) semi-empirical method.*

The first harmonic amplitudes of heave and pitch motions, derived from the Fourier analysis (presented in Section 4.5), are compared in Figure 5.18 and in Figure 5.19. The results show that response follows the excitation force frequency (wave frequency) with very little spectral leakage, in which the first harmonic amplitude is the dominant one. These first harmonic amplitudes are provided in Table 5.5, which reveal that the motion responses obtained using the empirical method are slightly under-predicted compared to those of potential flow method.

*Table 5.5 First harmonic amplitudes of heave and pitch motions for case 1a in head waves.*

| | Semi-empirical method (1) | Potential flow method (2) | Difference (2)-(1) | Percentage difference wrt. (1) |
|---|---|---|---|---|
| | Base environmental condition | | | |
| Heave (m) | 0.016 | 0.022 | 0.006 | 37.5 |
| Pitch (degree) | 0.08 | 0.18 | 0.1 | 125 |
| | Critical environmental condition | | | |
| Heave (m) | 0.04 | 0.08 | 0.04 | 100 |
| Pitch (degree) | 1.16 | 1.2 | 0.04 | 3.5 |

The first harmonic amplitudes of the derived heave and pitch motions in regular head waves from strip theory that has been applied in the semi-empirical method

are comparable to the computationally intensive potential flow method results. Although, the percentage difference is high, the absolute values shows negligible differences compared to the dimensions of the barge.

Note that in both the semi-empirical and in the potential flow simulations, the same DOFs were fixed. In the results obtained we can observe to some extent the coupling that both models include between the pitch and heave motion. As discussed previously, in the semi-empirical model these motions are connected and independent from other motions, whereas in the potential flow method this is not as clear.

*Beam waves*

A similar study to that of head waves, is conducted to assess the responses of the barge in roll motion to beam waves. Base and critical waves were applied from the port side of the vessel at 90 degrees, and the motions were simulated with surge, sway, pitch and yaw constrained, hence free in 2DOFs (heave and roll). The motion response time series are shown in Figure 5.20. It can be seen from the plots for both the base and critical wave conditions that there is a good agreement in the heave response between the employed methods.

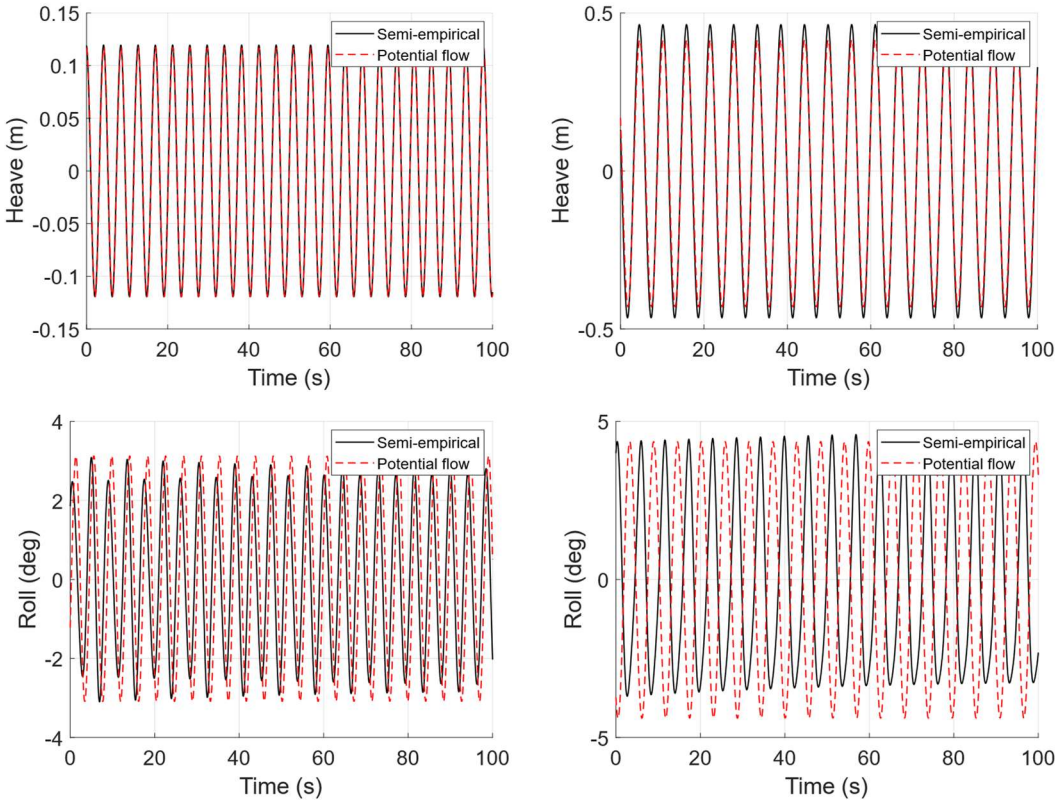


*Figure 5.20 Time-series of heave and roll motions in case 1a with beam waves and 2DOF (heave and roll). Base condition (left) and critical condition (right).*

The differences in mean (0.0002 m) and peak (0.002 m) values of calculated heave motion for both base and critical conditions do not differ significantly between semi-empirical and potential flow methods. Roll in base wave conditions is also predict to a higher conformance between the two methods. However, it is seen

from the plots that roll has an additional harmonic response in the semi-empirical model.

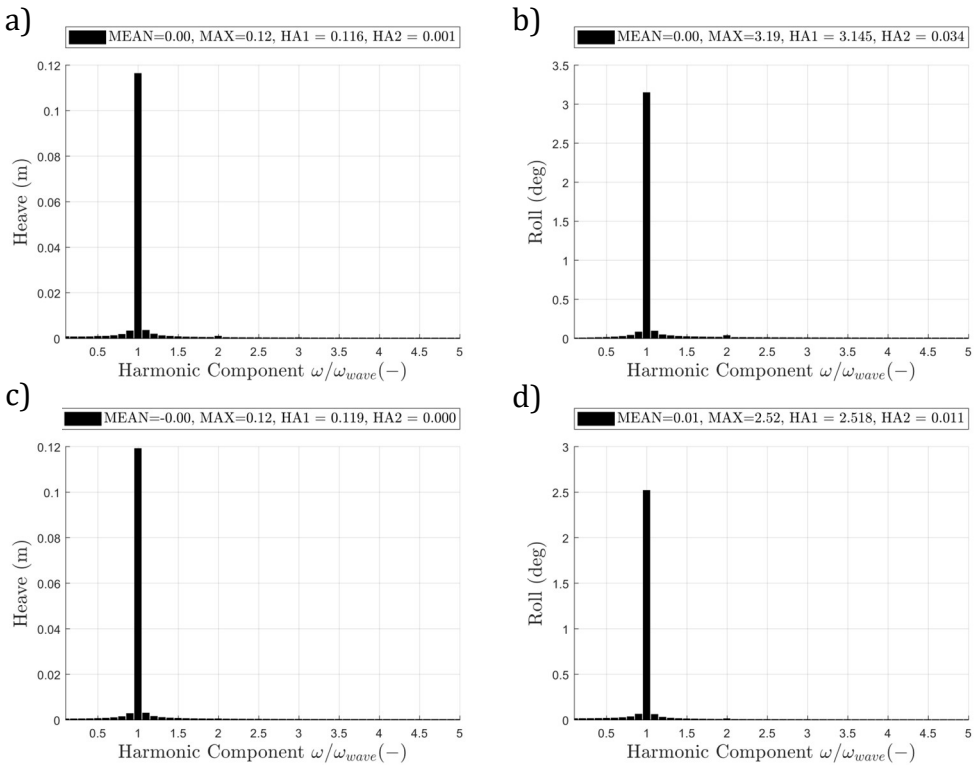


*Figure 5.21 FFT plots for case 1a in base condition with beam waves and 2DOF (heave and roll). a) and b) Potential flow method, c) and d) semi-empirical method*

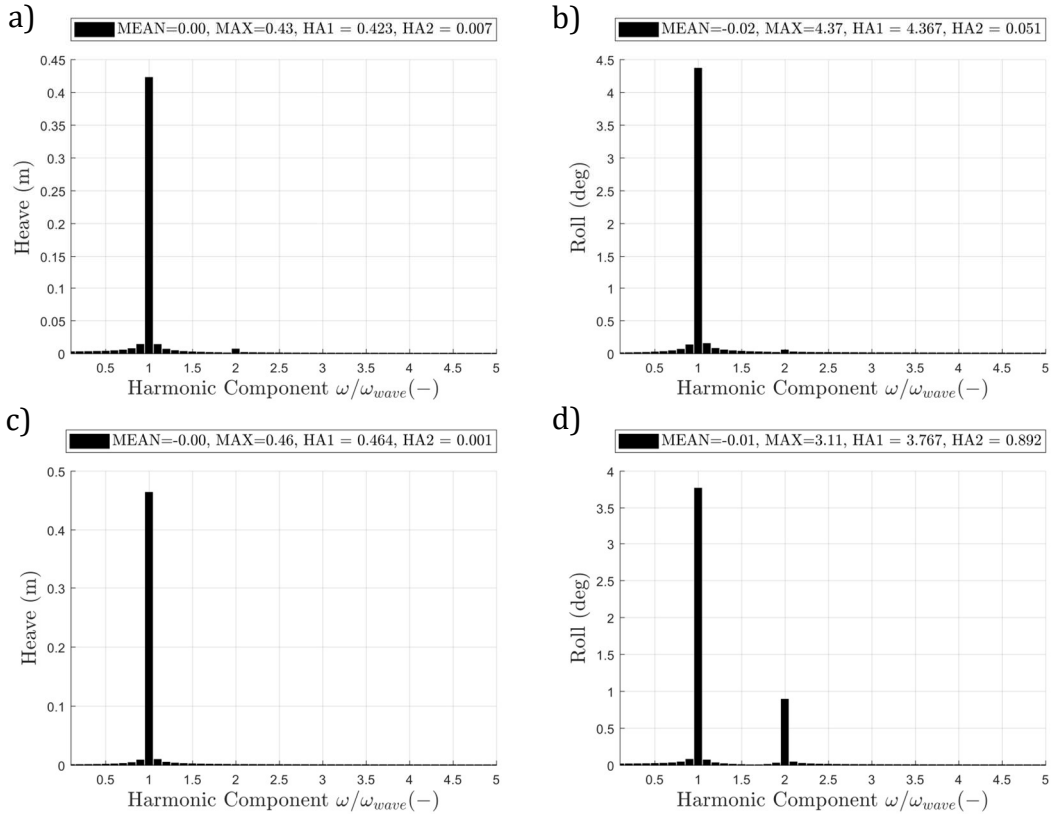


*Figure 5.22 FFT plots for case 1a in critical condition with beam waves and 2DOF (heave and roll). a) and b) Potential flow simulation, c) and d) semi-empirical calculations*

As in the case of head waves, Fourier analysis is utilized to assess the harmonic components of the motions. The results are shown in Figure 5.21 and Figure 5.22, and Table 5.6.

*Table 5.6 First harmonic amplitude responses in heave and roll for case 1a in beam waves*

| | Semi-empirical method (1) | Potential flow method (2) | Difference (2)-(1) | Percentage difference wrt. (1) |
|---|---|---|---|---|
| | Base environmental condition | | | |
| Heave (m) | 0.119 | 0.116 | - 0.003 | 2.5 |
| Roll (degree) | 2.518 | 3.145 | 0.627 | 25 |
| | Critical environmental condition | | | |
| Heave (m) | 0.464 | 0.423 | - 0.041 | 8.8 |
| Roll(degree) | 3.767 | 4.367 | 0.6 | 16 |

The first harmonic amplitudes are shown in Table 5.6 and the plots, Figure 5.21 and Figure 5.22, depict that the empirical method follows closely with the potential flow method in heave response. However, the empirical method under-predicted the roll motion in comparison to the potential flow method. This can be associated with the lever arm any additional force calculated by the potential flow solver as discussed in the case of head waves. The lever arm for the roll motion is significantly lower for roll motion.

If roll is considered in a point located at a distance $r$, the distance covered by this point, $s_r$ , can be calculated based on the angular displacement, $\delta\theta$, as,

$$s_r = r.\delta\theta_{rad} \quad . \tag{5.1}$$

This is important as in simulations with mooring lines, the winches are located away from the centreline. The angular displacement of a point at the side of the barge is 0.074 m in the base condition while in the case of critical wave is 0.127 m. This does not necessarily translate into a significant increase in the tensions in the case when a mooring line is involved due to the much larger length of the rope and due to the coupled effect of the tensions reducing the displacement. This will be further investigated in case 2.

It is also seen from the Fourier analysis that there is an additional harmonic component of roll motion in the empirical method results. This is more pronounced in the critical wave. This could be due to non-linearities introduced due to limitations in representing roll damping or due to the calculation of second order wave drift forces that introduces acceleration at a different frequency than that of the calculated force caused by the linear wave. This additional component is not considered in the potential flow solver and hence the effect is not seen in the response.

*Oblique wave*

Having explored the heave, roll and pitch responses under head and beam waves, the next comparison looks at the yaw response obtained from both the methods when the barge encounters an oblique wave. The simulation is carried out with surge and sway fixed to isolate effect on yaw motion and prevent drift. Yaw is mostly coupled with surge and sway, however the coupling with roll and heave is also investigated in this simulation. Figure 5.23 and Figure 5.24 show the response of the barge in heave, roll, pitch, and yaw for base and critical conditions respectively. Here, the transient response is shown for a better understanding of the response in yaw.

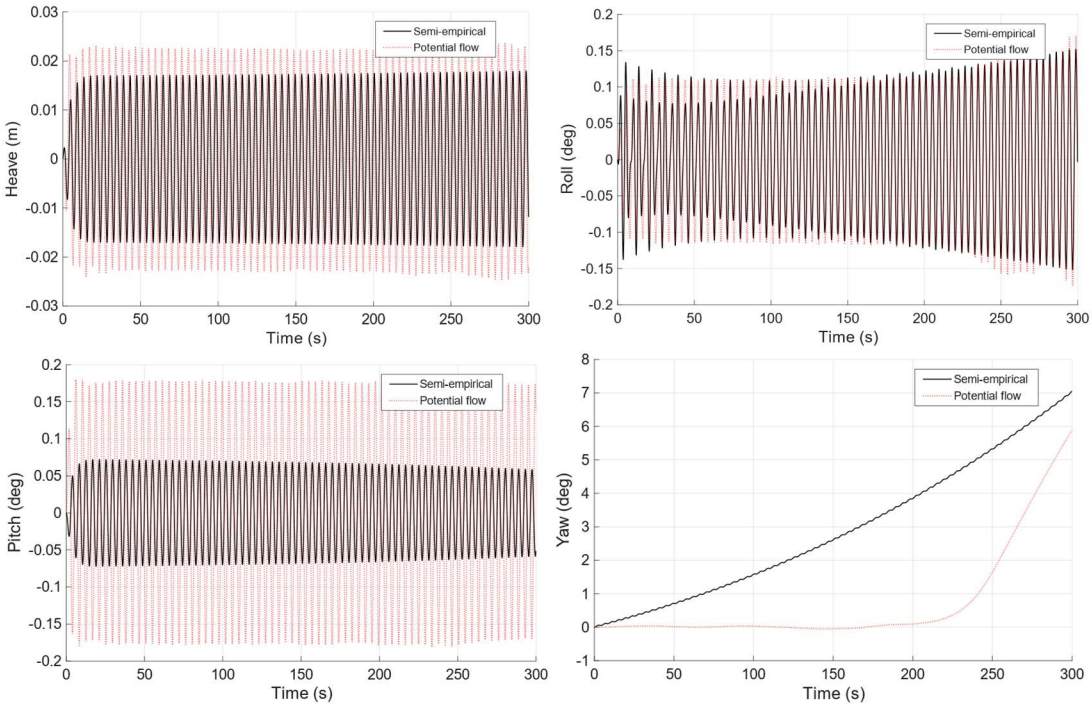


*Figure 5.23 Time-series of heave, pitch, roll and yaw motions in case 1a with oblique waves and 4DOF (heave, pitch, roll and yaw) in base condition.*

It is seen that heave, roll and pitch follow the observations made in the previous results when the yaw is within the range of a few degrees as is the case for the base wave condition. However, in the base wave condition, the yaw moment changes gradually in the semi-empirical method while, the response in the potential flow solver is rather sharp. It is also observed that the response of the barge in yaw, predicted by the potential flow solver, is completely opposite to that predicted by the semi-empirical model. The yaw moment generated determines this behaviour.

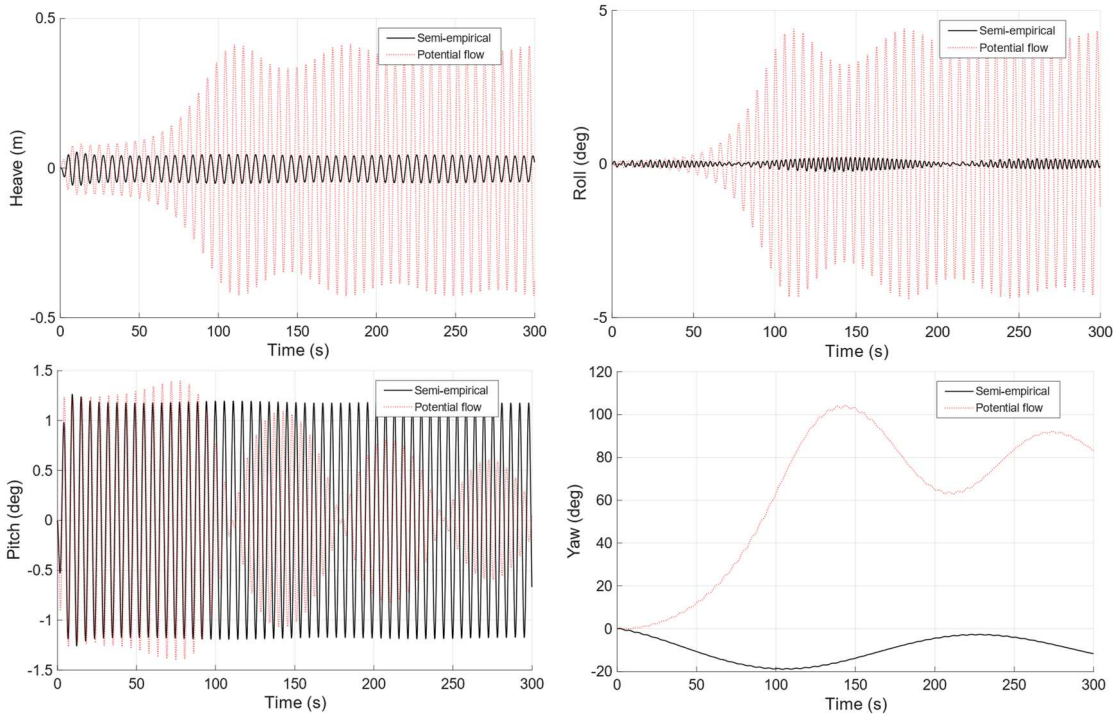


*Figure 5.24 Time-series of heave, pitch, roll and yaw motions in case 1a with oblique waves and 4DOF (heave, pitch, roll and yaw) in critical condition.*

There are several factors that can lead to the difference in yaw moment. In the semi-empirical model, the bow and stern geometry is simplified and the imbalance in the moment generated due to such a difference is not captured. A hydrostatic imbalance was also observed in the potential flow solver, which can amplify the additional yaw moment leading to further deviations. In the simplified models such effects are not captured and hence the vessel tends to align in-line with the wave rather than in a perpendicular orientation as was observed in the potential flow solver. Any imbalance in the forces is amplified in the critical wave due to the critical nature of the case and hence a sharper and quicker reaction is observed. In a mooring setup, however, this effect can be expected to be limited by the line tensions preventing extreme movement in either direction of yaw, however this will lead to different characteristics in the mooring line response.

### 5.1.4 Summary of case 1a

From the analysis of the different environmental conditions and from the analysis of the calculated responses by each of the two methods, it has been discovered some significant difference that might affect the results in more complex mooring simulations. Namely, the use of the potential flow tool in simulations with a small ship speed is prone to errors coming from miscalculation of hydrostatic force due to instabilities in the simulation.

However, most of the deviations the semi-empirical tool presented in relation to the potential flow tool were deemed acceptable, especially considering the time and computational resources spent in each of the methods.

## 5.2 Case 1b

Summary of the setup of Case 1b: a barge with simple geometry is moored using two mooring lines extending along the surge direction from the bow and stern respectively (Figure 4.4). Analyses done in this case aim to obtain confirmation of the mooring line dynamics module.

### 5.2.1 Response to environmental forces at 0°

*Wind*

In the case of head wind acting on a barge with motion constrained by the 2 lines we obtain the motions represented in Figure 5.25. Only the base case was considered.

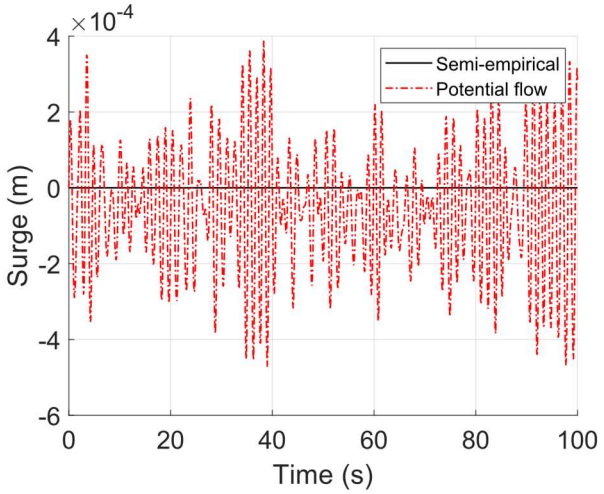


*Figure 5.25 Time-series of the surge motion in case 1b with head wind and 1DOF (surge) in base condition.*

The system at hand constitutes a spring-damper system with added damping from the resistance provided by the water. An FFT analysis was performed on the time-series predicted by the potential flow tool in Figure 5.25 and compared against the undamped natural frequency of the equivalent system simplified to spring and mass, i.e.

$$\omega_n = \sqrt{\frac{k}{m}} \ . \tag{5.2}$$

The resulting FFT graph obtained is presented in Figure 5.26.

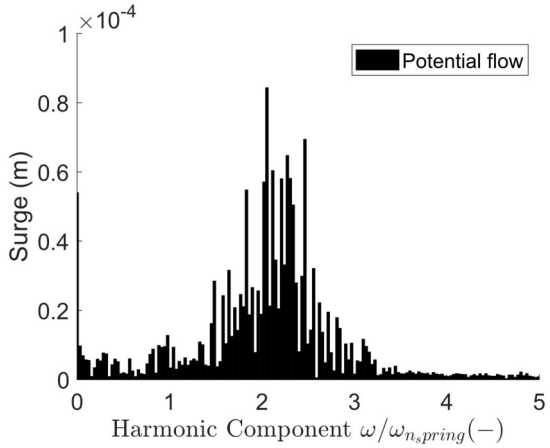


*Figure 5.26 Fourier Analysis of the time-series of surge motion predicted by the potential flow method in case 1b with head wind and 1DOF (surge) in base condition.*

In the presented Fourier Analysis, it is possible to observe a dominant frequency very close to 2 times the natural frequency of the equivalent spring mass system.

The tensions obtained in this case are represented in Figure 5.27.

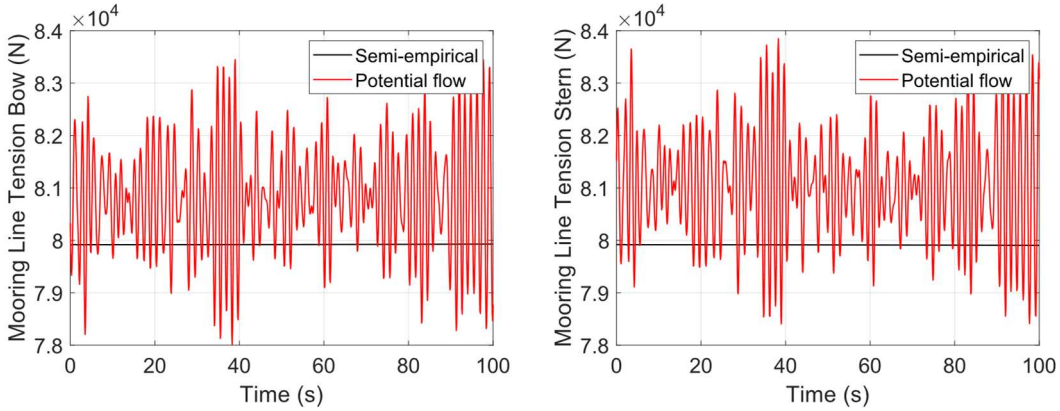


*Figure 5.27 Time-series of line tensions in case 1b with head wind and 1DOF (surge).*

The average values recorded for the tensions are shown in Table 5.7.

*Table 5.7 Value of the average tensions (in kN) obtained in case 1b with head wind and 1DOF (surge). Base Case.*

| | Semi-empirical method | Potential flow method | Difference (Absolute) | Difference (Relative) |
|---|---|---|---|---|
| Average tension - Line 1 (kN) | 79.92 | 80.81 | 0.89 | 1.1% |
| Average tension - Line 2 (kN) | 79.91 | 81.05 | 1.14 | 1.4% |
| Difference | -0.01 | 0.24 | - | - |

The difference between the tension in line 1 and line 2 should correspond to the value of the wind force. In the present case we can assume that the AWS will be constant as the surge motion is negligible. The x-component of the wind force for this case should approximately be -128 N (calculated according to Equation (2.4)), which is not captured correctly by either method.

*Current*

Base and critical currents are applied on the barge at zero heading. The vessel motions are also limited to surge, heave and pitch in the simulation setup. The response is recorded as shown in Figure 5.28 for the case of current.

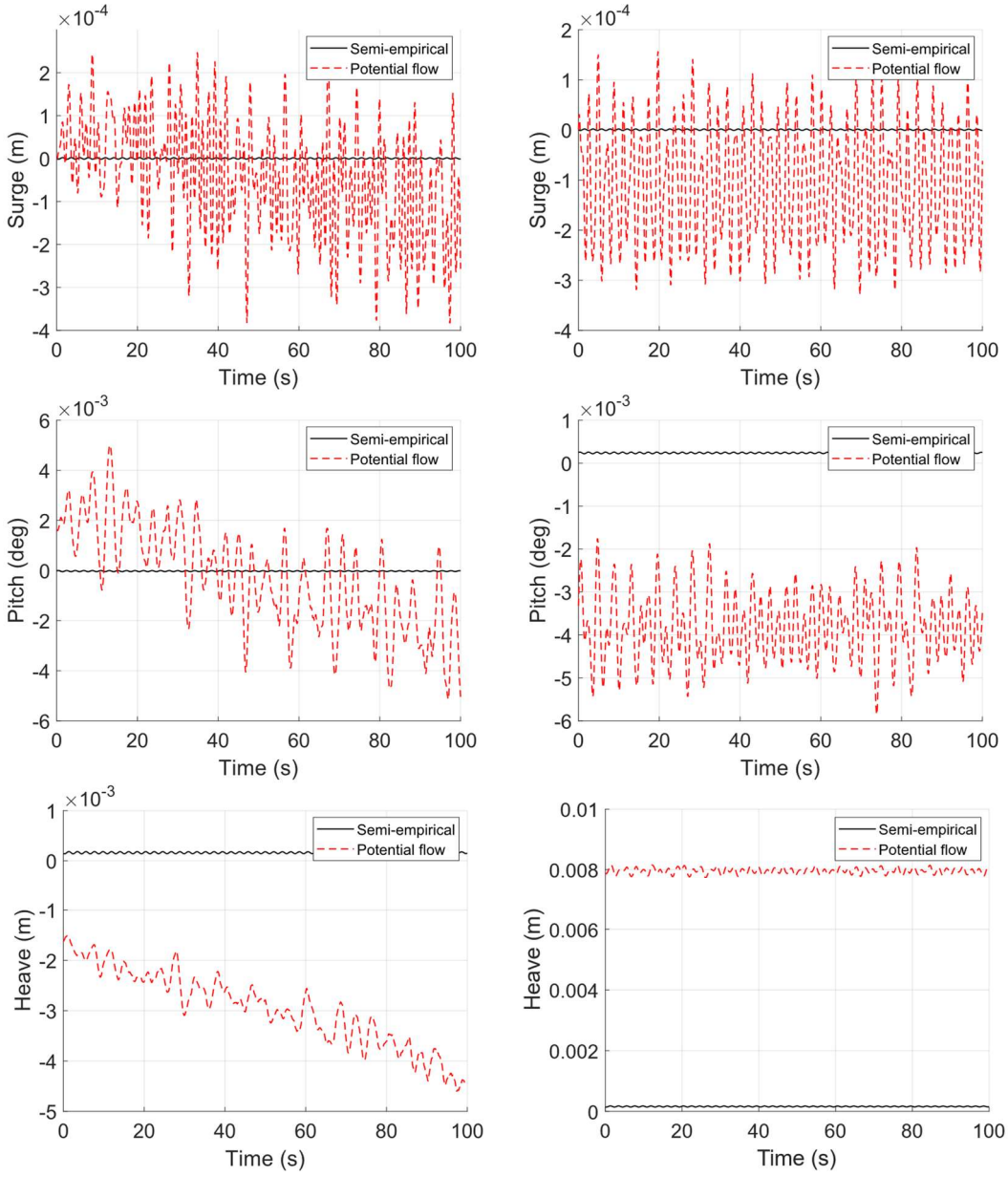


*Figure 5.28 Time-series of surge, heave and pitch motions in case 1b with head current and 3DOF (surge, heave and pitch). Base condition (left) and critical condition (right).*

The motions are comparably smaller to the ones observed in case 1a, which shows the lines were effective at stopping the movement in the barge both in the semi-empirical method and in the potential flow method. The recorded values for surge are very small – less than a millimetre – but with a reasonable result, as it is expected a negative average value of surge motion, as the barge is being pushed by the current. Heave presents some movement in the order of magnitude of the millimetres. The slight pitching moment that can be observed in this simulation can be a representation of a "lift" force that the water exerts on the barge when hitting the bow. The negative heave in the base case suggests this lifting force is dominant, while in the critical case, positive heave suggests the pretension is dominant (due to the geometry of the case: the bollards are 2.35m above the waterline, whereas the winches are defined initially 2.4 m above the waterline). Hence it is expected a slight heaving motion downwards due to the action of the lines.

The tensions obtained in the two lines are shown in Table 5.8 and in Figure 5.29.

*Table 5.8 Value of the tensions (in kN) obtained in case 1b with head current and 3DOF (surge, heave and pitch). Base Case as an example.*

| | Semi-empirical method | Potential flow method | Difference (Absolute) | Difference (Relative) |
|---|---|---|---|---|
| Maximum tension - Line 1 (kN) | 80.9 | 83.0 | 2.1 | 2.5% |
| Maximum tension - Line 2 (kN) | 78.9 | 80.8 | 1.9 | 2.3% |
| Average tension - Line 1 (kN) | 80.9 | 81.8 | 0.9 | 1.1% |
| Average tension - Line 2 (kN) | 78.9 | 79.5 | 0.6 | 0.8% |

The semi-empirical method results show a very good agreement (slight underprediction) in comparison to the potential flow method results. It is also observable in Figure 5.29 and Figure 5.28 that the motions have significantly smaller amplitude in the semi-empirical method than in the potential flow method. This might be due to the artificial damping force introduced at the beginning of the semi-empirical line simulations to stabilize the solver for these lines (cf. Section 3.1.5.1). Another reason for such instabilities in the potential flow method results might be related to the challenges involved in the free surface and ship panelization, as discussed before. The small changes of the wetted surface area and thus the small changes of the integrated pressure over this area might result in small oscillations of the motions and hence oscillation of the line tensions.

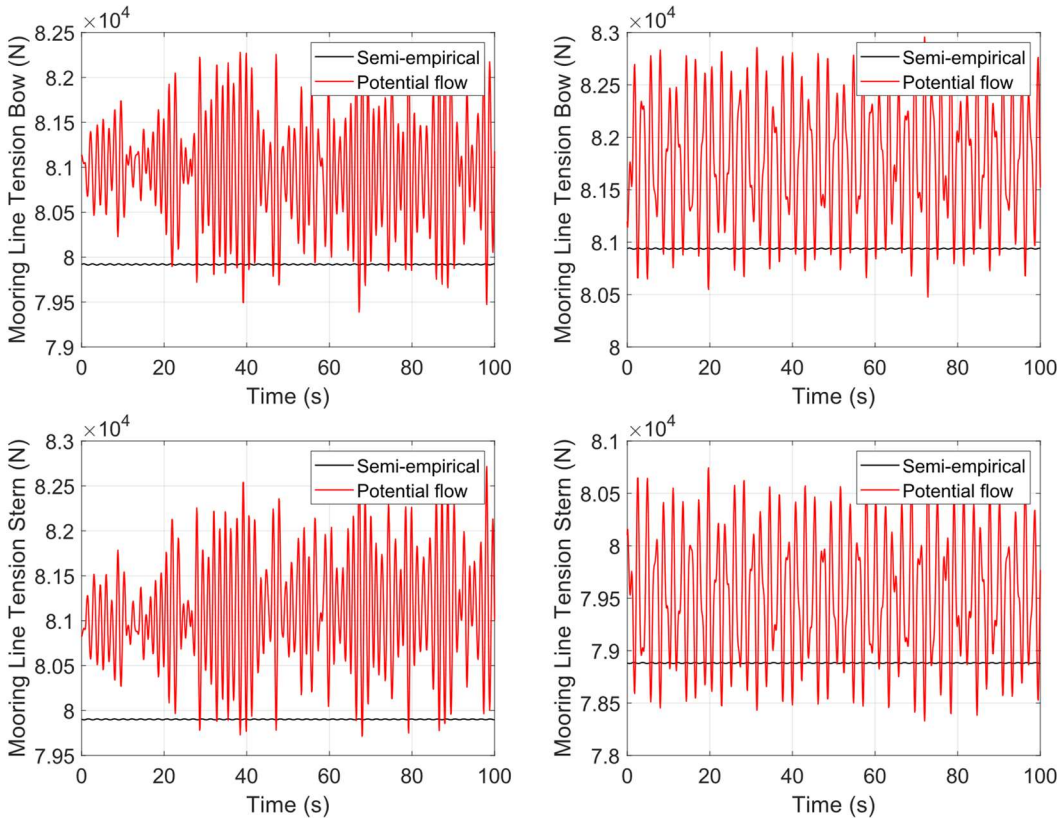


*Figure 5.29 Time-series of line tensions in case 1b with head current and 3DOF (surge, heave and pitch). Base condition (left) and critical condition (right).*

*Waves*

The two-line mooring arrangement was then subjected to a base head wave with DOFs along the vertical plane (along surge, heave and pitch). Figure 5.30 depicts the motions obtained and the line tensions.

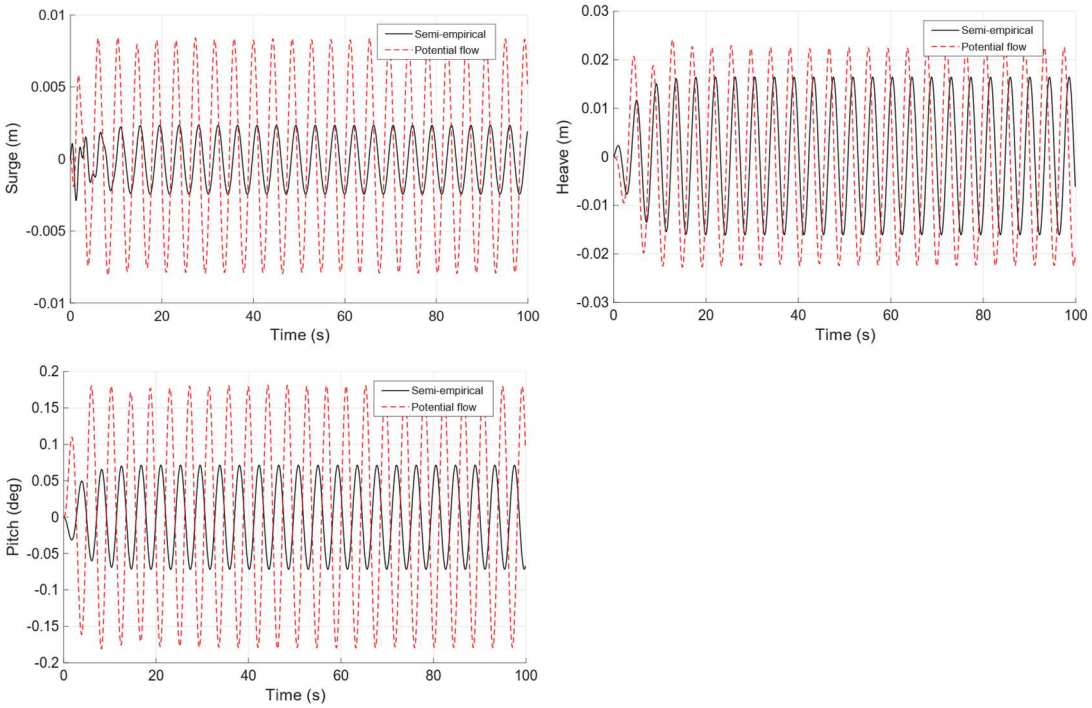


*Figure 5.30 Time-series of motions case 1b with base head wave condition*

It is seen from the Figure 5.30 that the displacements follow closely with the observations made so far, where the semi-empirical model predicts a smaller motion compared to the potential flow solver in surge, heave and pitch responses.

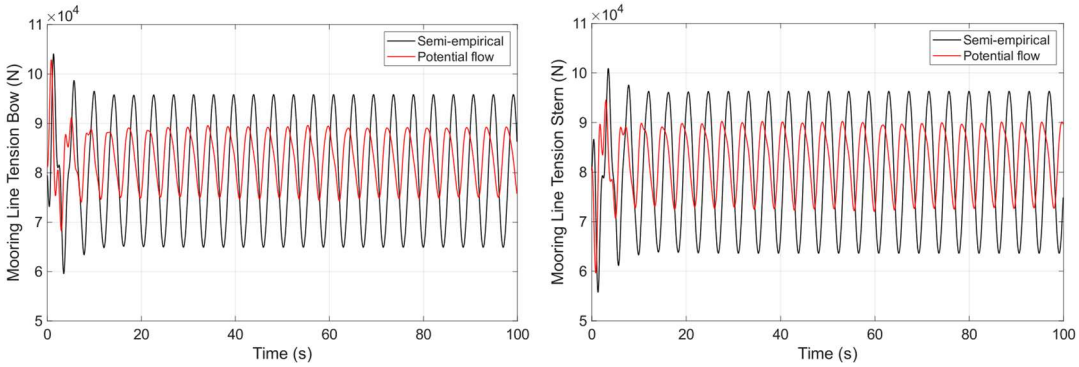


*Figure 5.31 Time-series of line tension in case 1b with base head wave condition.*

The line tension plots (seen in Figure 5.32) show a response that is contradictory to the displacement seen. The line tensions predicted by the semi-empirical model are higher than those predicted by the potential flow solver model even though the lines used are identical. However, the difference in tensions calculated are approximately 5 kN in each line. This value is not significant considering the capacity of the rope selected.

### 5.2.2 Response to forces at 10°

*Current*

Base and critical currents are applied on the barge, coming from 10° to the port side. The vessel motions are also limited to surge, sway and yaw in the simulation setup. The response is recorded as shown in Figure 5.32 for the case of current.

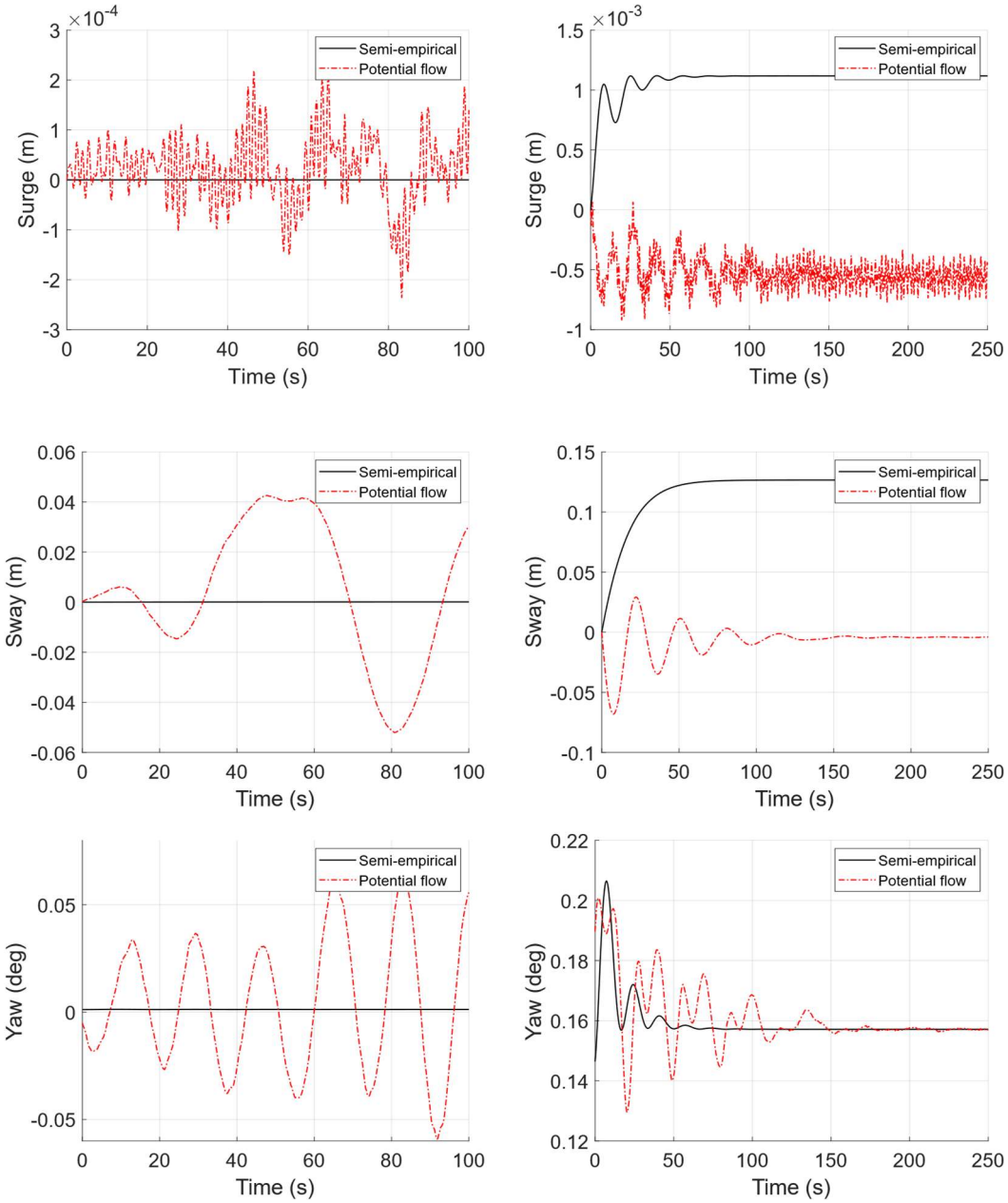


*Figure 5.32 Time-series of surge, sway and yaw motions for case 1b with oblique current condition. Base condition (left) and critical condition (right).*

From Figure 5.32 it is possible to observe that the semi-empirical tool underpredicts the resulting motion in the base case but overpredicts the amplitude of motions in the critical case in relation to the potential flow tool.

The resulting tension of the two lines are presented in Figure 5.33 and in Table 5.9, where this trend (of underprediction by the semi-empirical tool in the base case and overprediction in the critical case) follows.

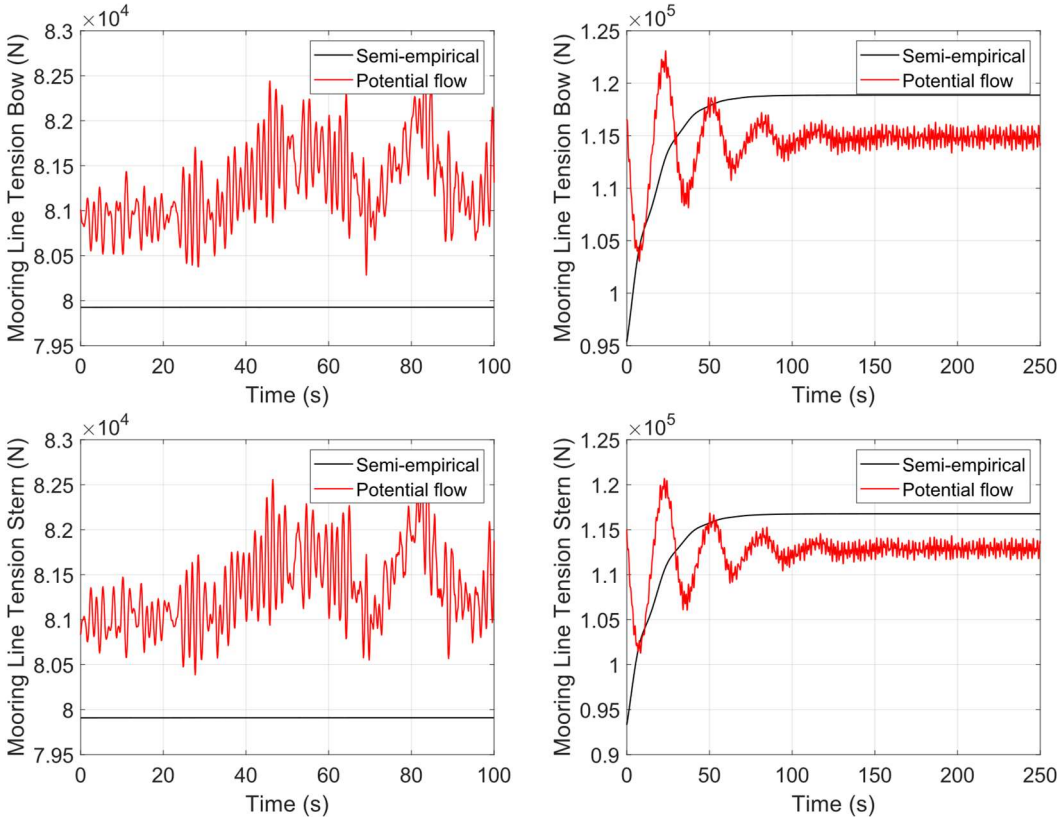


*Figure 5.33 Time-series of line tensions in case 1b with oblique current and 3DOF (surge, sway and yaw). Base condition (left) and critical condition (right).*

*Table 5.9 Value of the tensions obtained in case 1b with oblique current and 3DOF (surge, heave and pitch). Base case / critical case (kN).*

| | Semi-empirical method | Potential flow method | Difference (Absolute) | Difference (Relative) |
|---|---|---|---|---|
| Maximum tension - Line 1 (kN) | 79.93 / 118.9 | 82.75 / 123.1 | 2.82 / 4.2 | 3.4% / 3.4% |
| Maximum tension - Line 2 (kN) | 79.91 / 116.8 | 82.67 / 120.7 | 2.76 / 3.9 | 3.3% / 3.2% |
| Average tension - Line 1 (kN) | 79.93 / 117.3 | 81.27 / 114.5 | 1.34 / -2.8 | 1.6% / 2.4% |
| Average tension - Line 2 (kN) | 79.91 / 115.2 | 81.34 / 112.5 | 1.43 / -2.7 | 1.8 %/ 2.4% |

Note that these results are in line with the motions presented: the semi-empirical overpredicts motions in the base case as it presents a smaller resisting force from the lines and underpredicts the motions in the critical case as it predicts a higher tension for the lines.

The different methods find different equilibrium positions. This is evident in Figure 5.32 in the motions of surge and sway in the critical condition. This is a result of a difference in the forces generated by each method. In case 1a we saw how the semi-empirical method and the potential flow method generated different forces in the case of current. Now it is expected that these different environmental loads will result in different equilibrium positions.

It is important to mention the damping force introduced in Section 3.1.5.1 does not influence the simulation at the time that it is being analysed: it only plays a role in the semi-empirical method in the initial time steps to avoid amplification of instabilities.

### 5.2.3 Summary of case 1b

Through the analyses done in Case 1b it is possible to observe that the semi-empirical calculations fall within a reasonable reach from the potential flow simulations, especially the calculations of the line tensions that all presented less than 5% error.

Even though the achieved equilibrium positions – resulting from different environmental force calculation – the amplitude of the motions is comparable between the methods for the environmental forces coming from 0 degrees but diverge considerably in the case of the forces acting from 10° to port.

### 5.2.4 Contributions of the thesis regarding case 1b

It is important to note the contribution this thesis has had to the development of the semi-empirical tool at RISE, namely by providing a clearer overview of two important tools used in these simulations but that generate a lot of errors: the (lack of) artificial damping force and the calculation of line length.

The lack of the damping coefficient introduced in the simulation instabilities that caused the semi-empirical tool to produce results with surge amplitudes of up to 1.5 m, as shown in Figure 5.34.

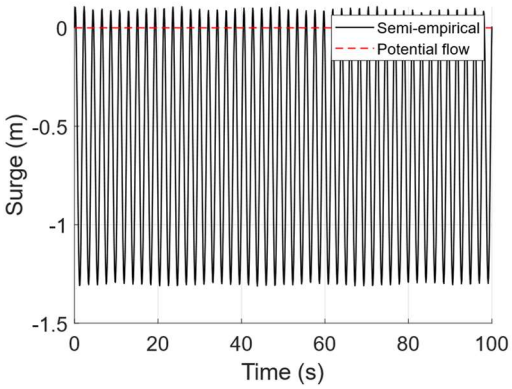


*Figure 5.34 Time-series of surge motion in case 1b (no damping coefficient and thus unphysical unstable solution by the semi-empirical method) with head current, critical condition, and 3DOF (surge, heave and pitch).*

Besides the lack of this artificial stabilizing force, the calculation of the length was not being done correctly in the initial stage of the simulations. This caused the 2 lines to have different lengths, making the problem asymmetric from the start and generating instabilities from the initial position. Figure 5.35 shows the line length calculation, namely how it was dependent on the time defined as the end of the pre simulation (in this example, the time was t= 80s).

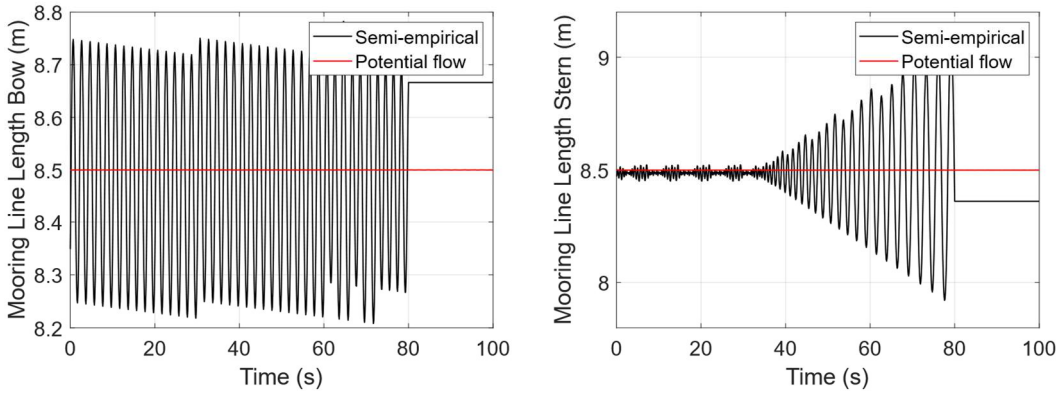


*Figure 5.35 Time-series of the line length calculation (pre simulation) in an unstable simulation of case 1b with head current, critical condition, and 3DOF (surge, heave and pitch). It is possible to see after t=80s, line length becomes constant regardless of its value.*

These two combined sources of error generated tensions that were significantly over predicted. Figure 5.36 shows an example of such exaggerated calculation.

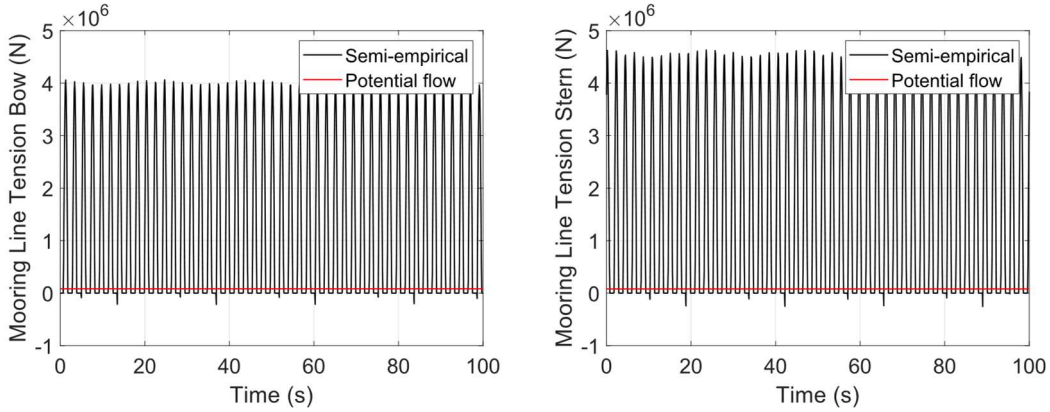


*Figure 5.36 Time-series of the mooring line tension in an unstable simulation of case 1b with head current, critical condition, and 3DOF (surge, heave and pitch).*

## 5.3 Case 2

Summary of the setup of Case 2: a barge with simple geometry is moored using four mooring lines. Analyses done in this case aim to assess mooring simulations of an arrangement closer to real life scenarios. All environmental conditions are applied simultaneously.

### 5.3.1 Response to forces at 0°

Base and critical current, wind and waves are applied from head direction, and the motion response predictions are obtained as follows.

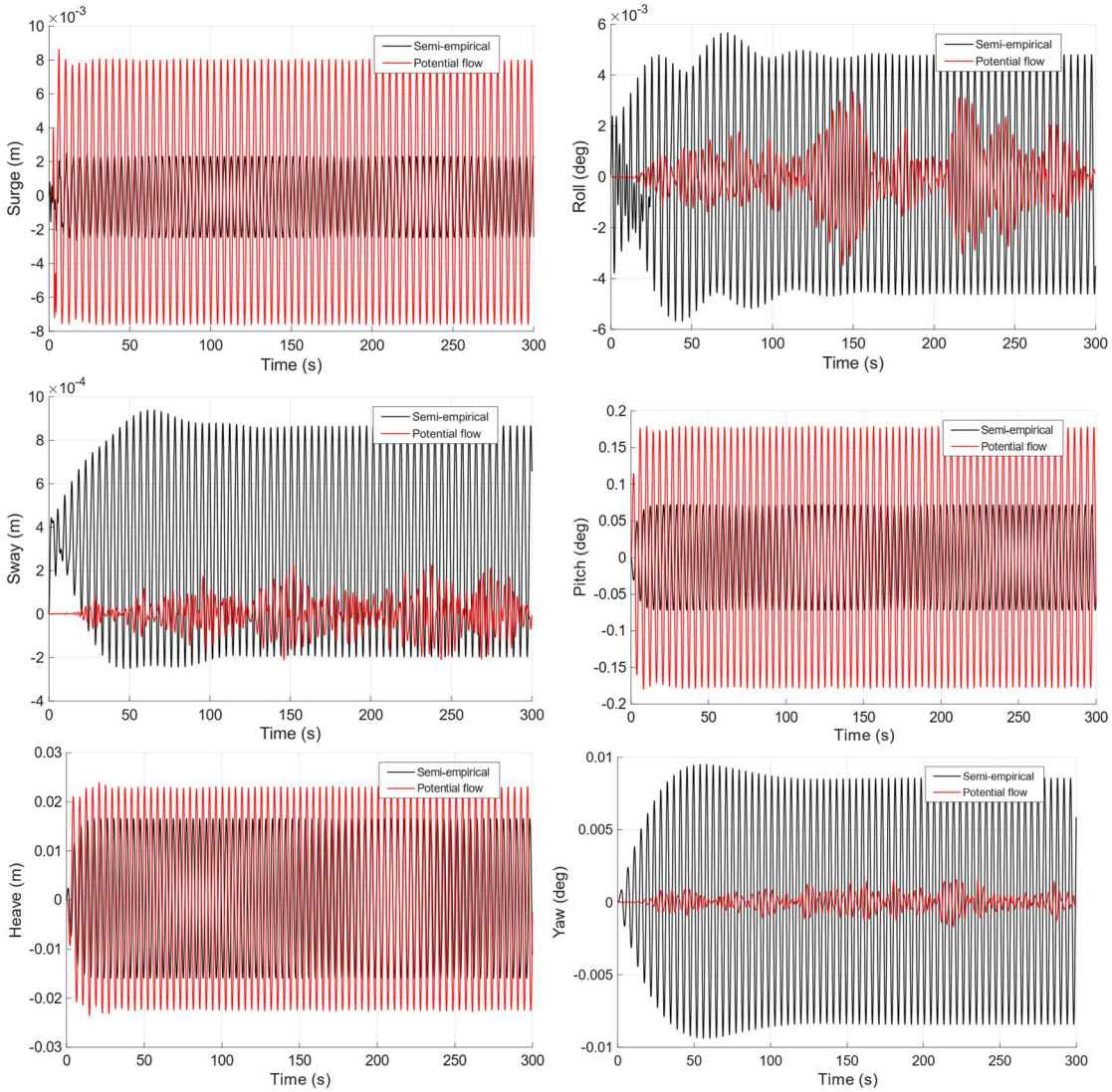


*Figure 5.37 Time-series of motion responses in case 2 with base waves, current and wind from 0° surge, sway and heave (left) and roll, pitch and yaw (right).*

The difference in results obtained for surge, heave and pitch are comparable to the responses seen in the case 1b and base wave acting from head direction (Figure 5.37). The sway response predicted by the semi-empirical method averages around 0.0003 m, while in the potential flow solver, the response averages 0 meters. The difference in peak values of sway predicted is close to zero (0.0002m). Roll and yaw predictions have an average value of 0 degrees in both potential flow simulation and semi-empirical method. The peak value differs by 0.003 and 0.007 degrees respectively with the semi- empirical tool having larger predictions. Thus, the differences in response calculated are small across all DOFs. It is also noted that potential flow predictions in surge, heave and pitch are larger while the sway, roll and yaw predictions have larger amplitudes in semi-empirical method.

With very small discrepancies in values of sway, roll and yaw responses, the major difference is seen in the surge, heave and pitch motions thus highlighting the significance of wave effects over other forces. Even though potential flow solution is computationally intensive, both method produces comparable results.

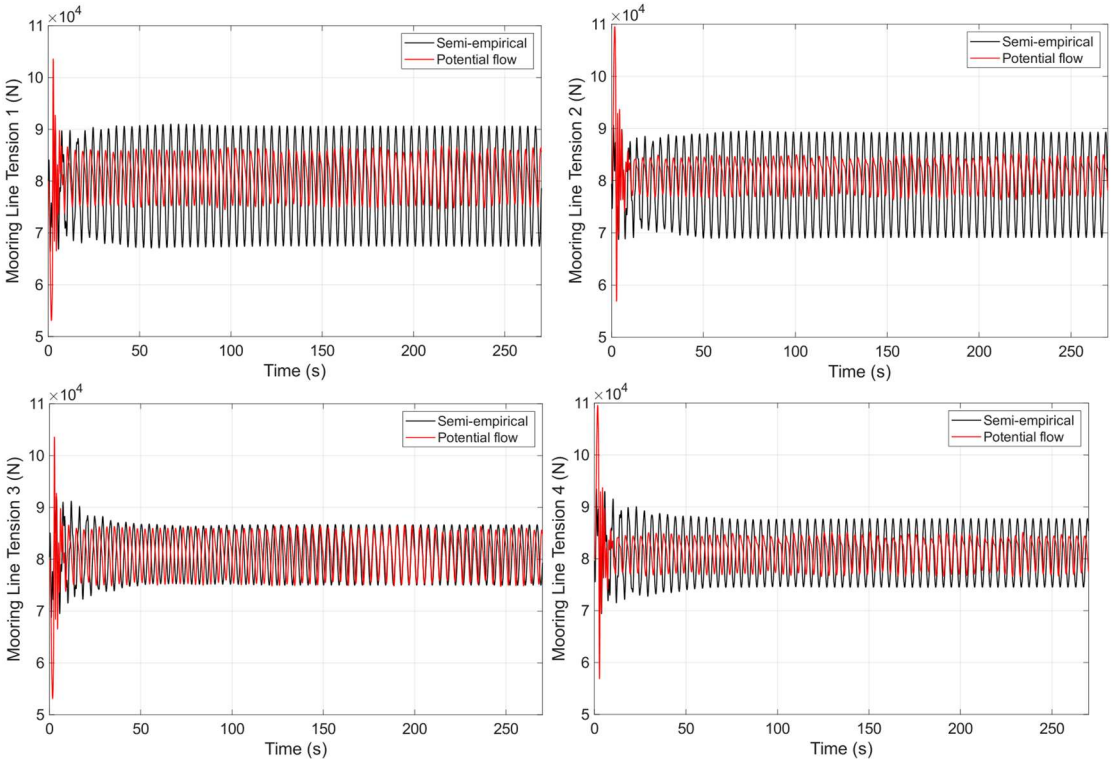


*Figure 5.38 Time-series plots for line tensions in case 2 with base waves, current and wind from 0°.*

The tensions predicted for the four lines is shown in Figure 5.38. It is seen that the peak tensions obtained for lines 1 and 2 have a difference of 5 kN between the values predicted by potential flow method and semi-empirical method with the latter being larger. The difference in tension in line 3 matches closely between the two methods, while the difference in tension in line 4 is 3 KN.

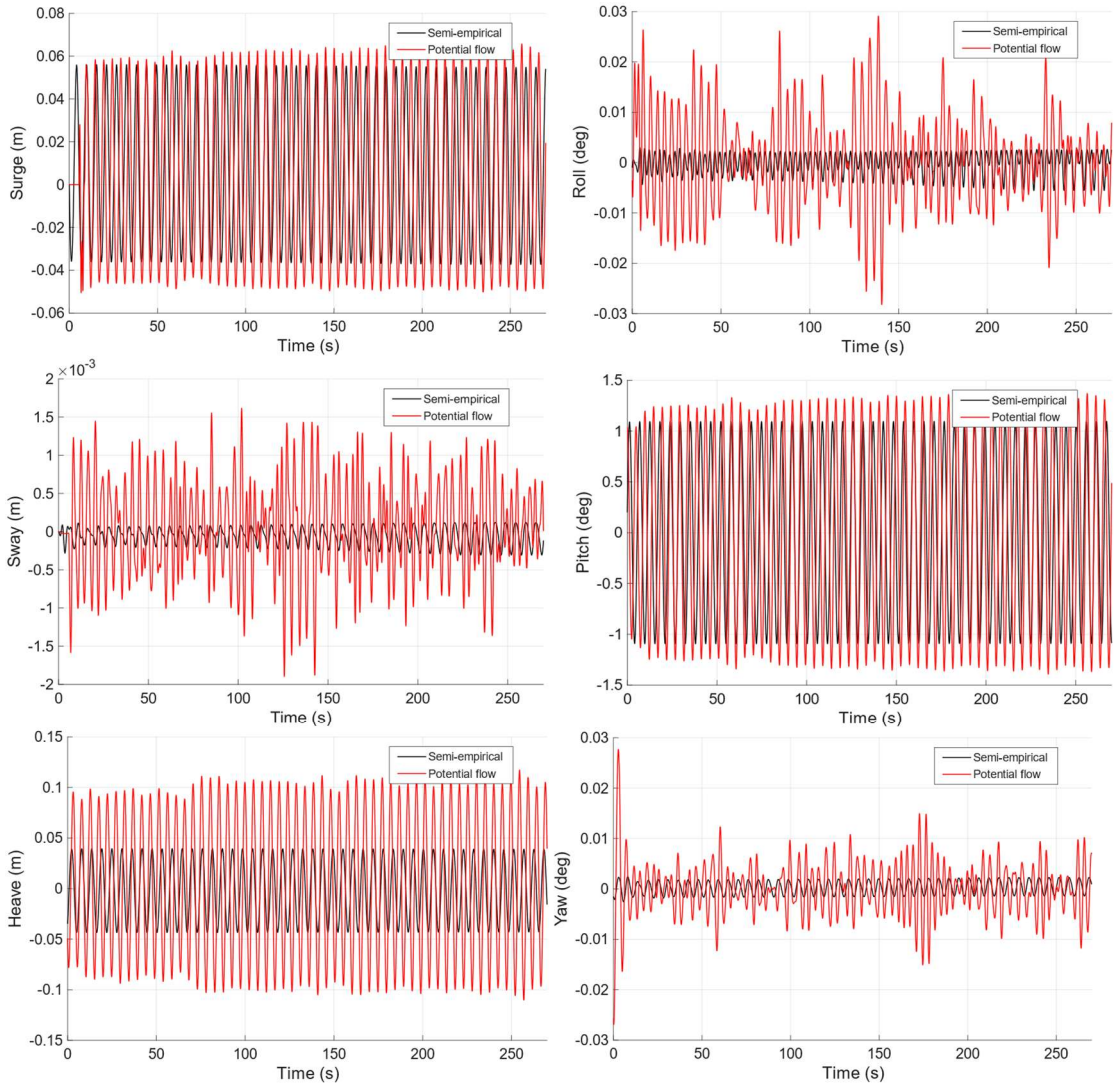


*Figure 5.39 Time-series of motion responses in case 2 with critical waves, current and wind from 0° (head) and free in 6DOF.*

Figure 5.39 shows the responses predicted when critical conditions are applied from head direction. As observed in the case of base conditions, the response in surge, heave and pitch for critical conditions are underpredicted by the semi-empirical method. However, the mean values in these responses have a very small difference in magnitude. The responses in roll, pitch and yaw are however different from the observations made in the base case. The potential flow method predicts larger values of displacement in these motions, contradictory to the observations in the base case. However, the results are rather comparable, and the largest discrepancies are seen for the peak values of heave.

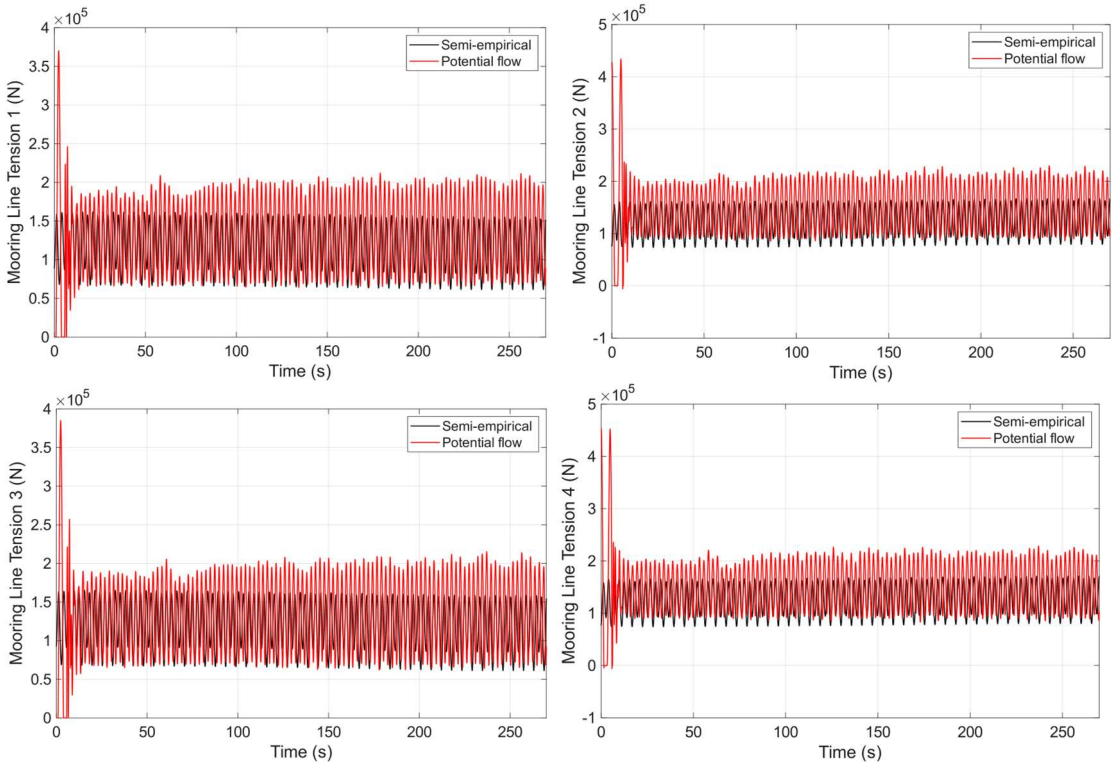


*Figure 5.40 Time-series plots for line tensions in case 2 with critical waves, current and wind from 0°.*

Figure 5.40 shows the tensions predicted for the applied conditions. It is observed that the peak tensions predicted by the potential flow tool are higher than those by the semi-empirical method by 50 kN. This is a significant difference in the line tensions. However, it has been seen from Figure 5.39, that the critical waves, current and wind generates higher displacements in the potential flow solver, and hence higher tensions are a result of that.

### 5.3.2 Response to forces at 10°

Base and critical current, wind and waves are applied from an oblique direction (10°), and the motion response predictions are obtained as follows.

The motion responses are shown in Figure 5.41 for the oblique environmental conditions. It is seen that motion responses in surge, heave and pitch are comparable to those obtained when base environmental forces were applied from zero heading. The mean sway motion predicted matches between both methods, while the peak values differ by 0.005 m. However, responses in both roll and yaw show significant differences. The response in roll is underpredicted by the semi-empirical method, with a difference of 0.075 degree in the peak values. The yaw response in unmoored simulations showed that the potential flow model showed sharper responses. However, in the moored simulation, semi-empirical tool predicts higher yaw response while the response in the potential flow method is significantly lesser.

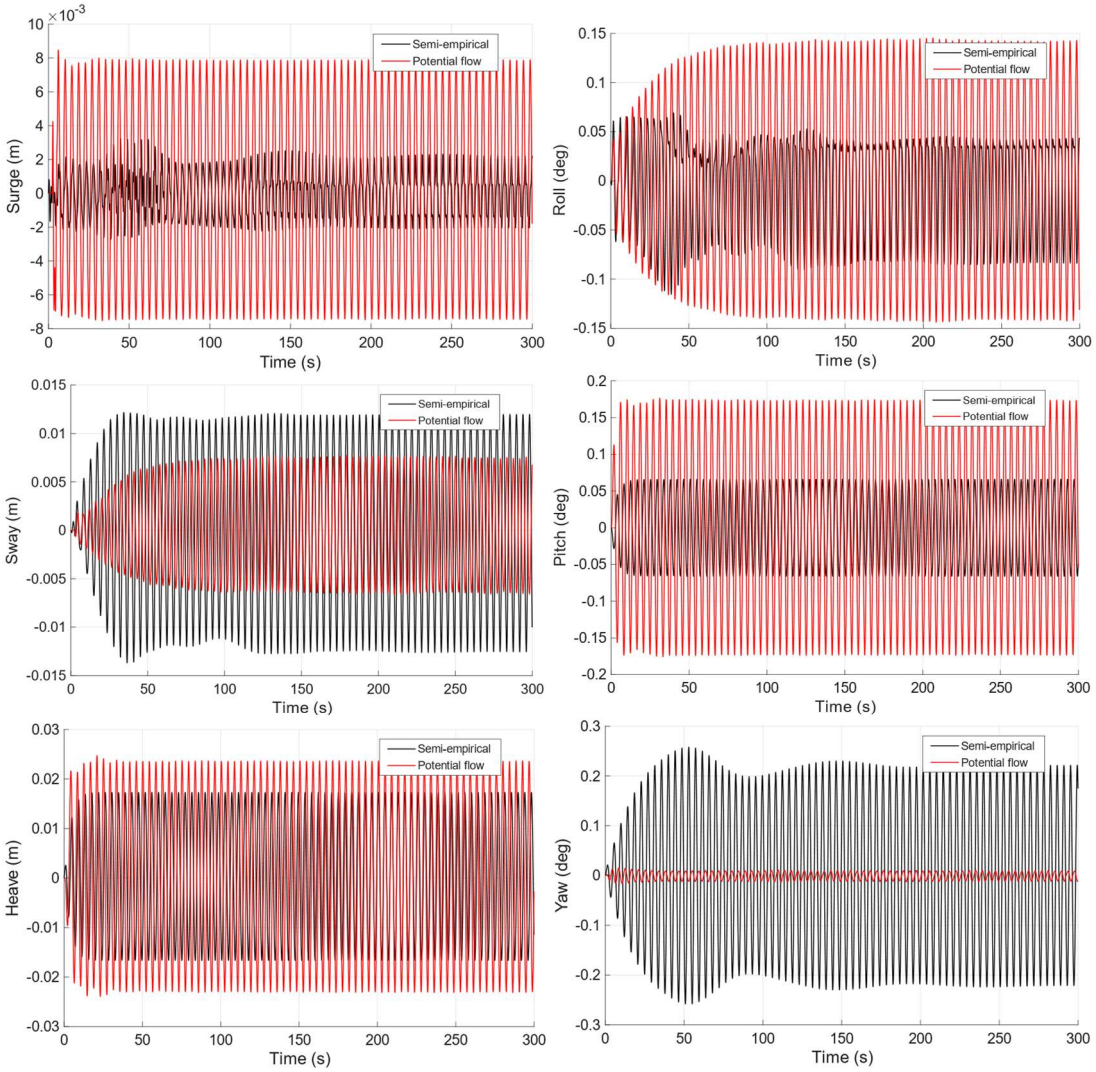


*Figure 5.41 Time-series of motion responses in case 2 with base waves, current and wind from 10° and free in 6DOF.*

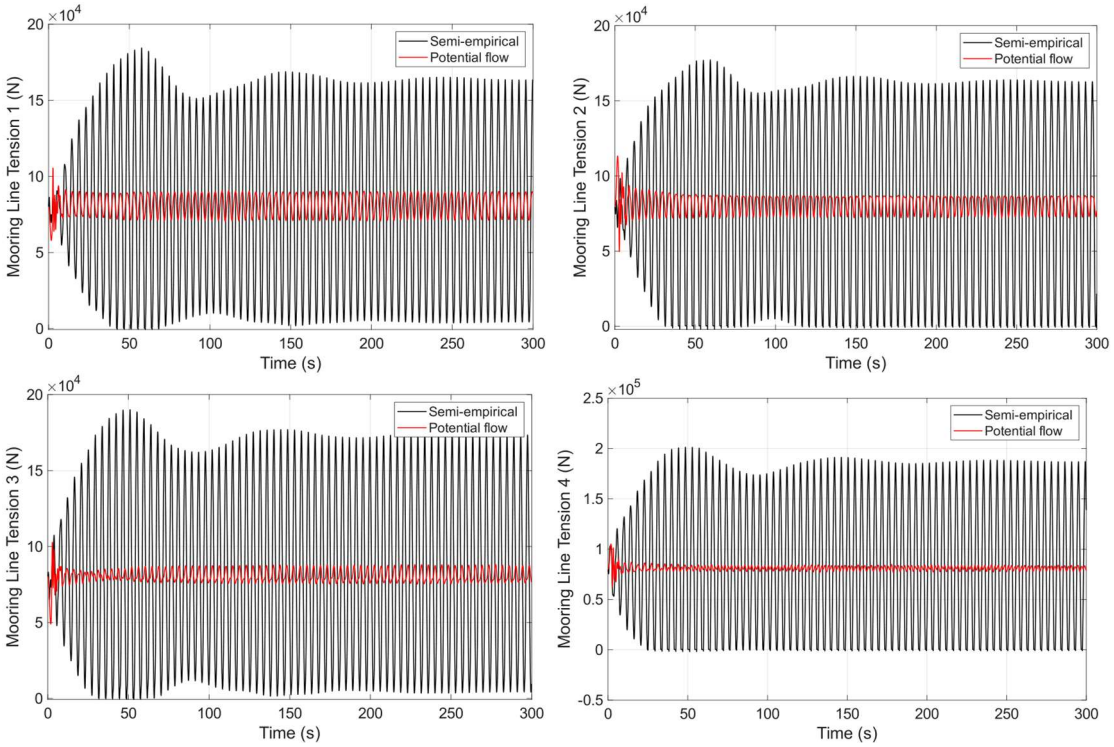


*Figure 5.42 Time-series plots for line tensions in case 2 with critical waves, current and wind from 10° and free in 6DOF.*

Figure 5.42 shows the tensions in the mooring lines, and it is seen that the tensions predicted by the semi-empirical tool are larger in all the lines. While the tensions in lines 1-3 are different across the two methods by 70-80 kN, line 4 has an even higher difference in the calculated tension 90 kN that can be attributed to the difference in yaw response obtained. As was seen from the responses observed for a freely floating barge (case 1a) in oblique environmental loads, both methods produced different responses in yaw. Here we see the effect of having such differences and highlight the importance of the accurate prediction of responses in different directions in a mooring arrangement.

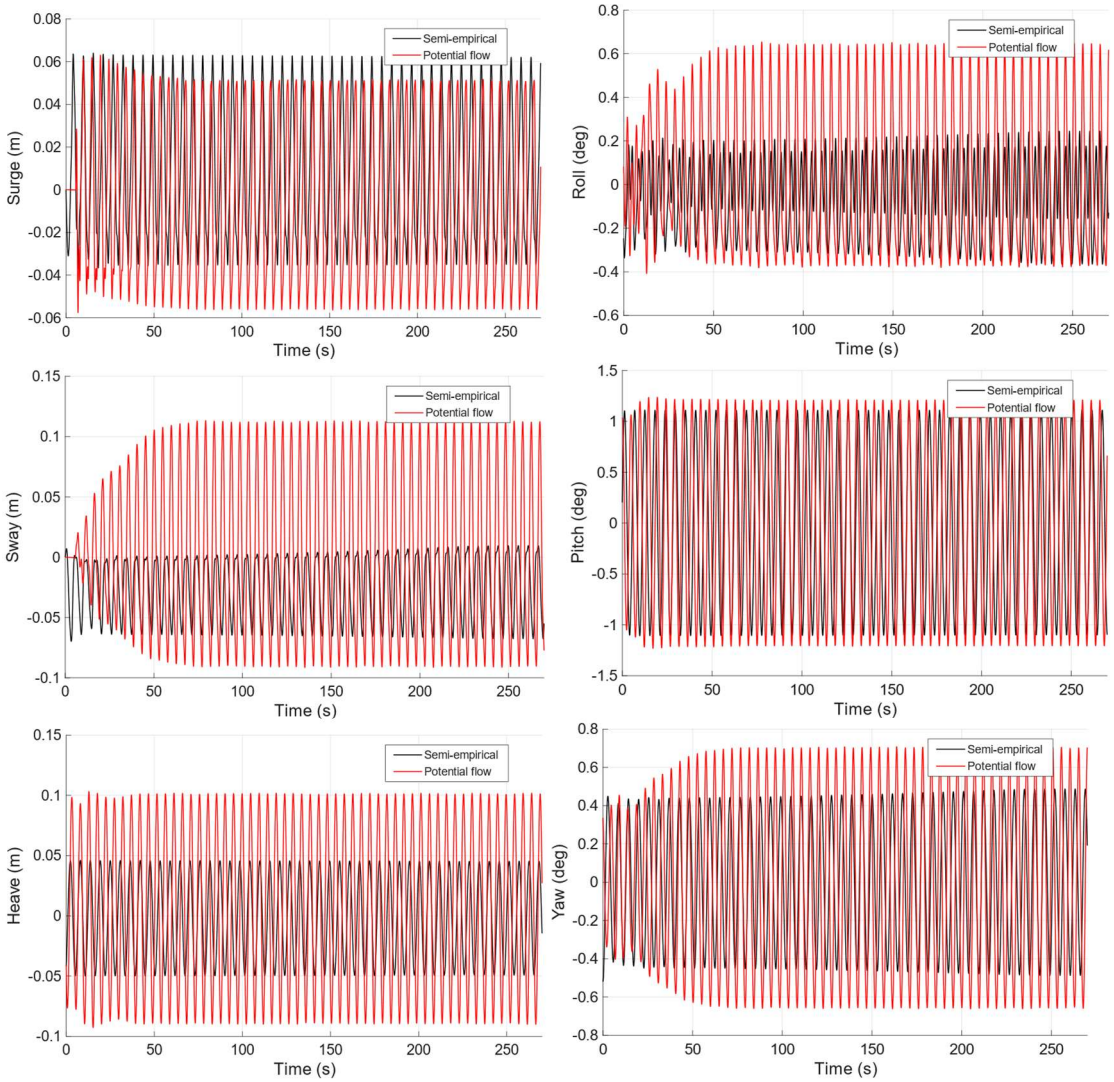


*Figure 5.43 Time-series of motion responses in case 2 with critical waves, current and wind from 10° and free in 6DOF.*

Figure 5.43 shows the responses in 6 DOFs in a critical environmental condition acting at an oblique direction. In surge, it is seen that the magnitudes of oscillation are comparable between the two methods. However, while the mean surge is close to 0 m in the potential flow solution, the surge has a slightly higher value in the semi-empirical method. Pitch and heave responses are also comparable between the two methods, even though the magnitude of heave response in potential flow solution is higher (~0.05m). A significant difference from the base condition is observed in the yaw response. This is reflective of the response obtained in the critical wave condition acting at an oblique angle in case 1a. Both in roll and sway response, the semi-empirical method produces an offset average from the origin, while in response predicted by the potential flow tool, such an offset is observed only in the case of roll with a value of 0.1 degree.

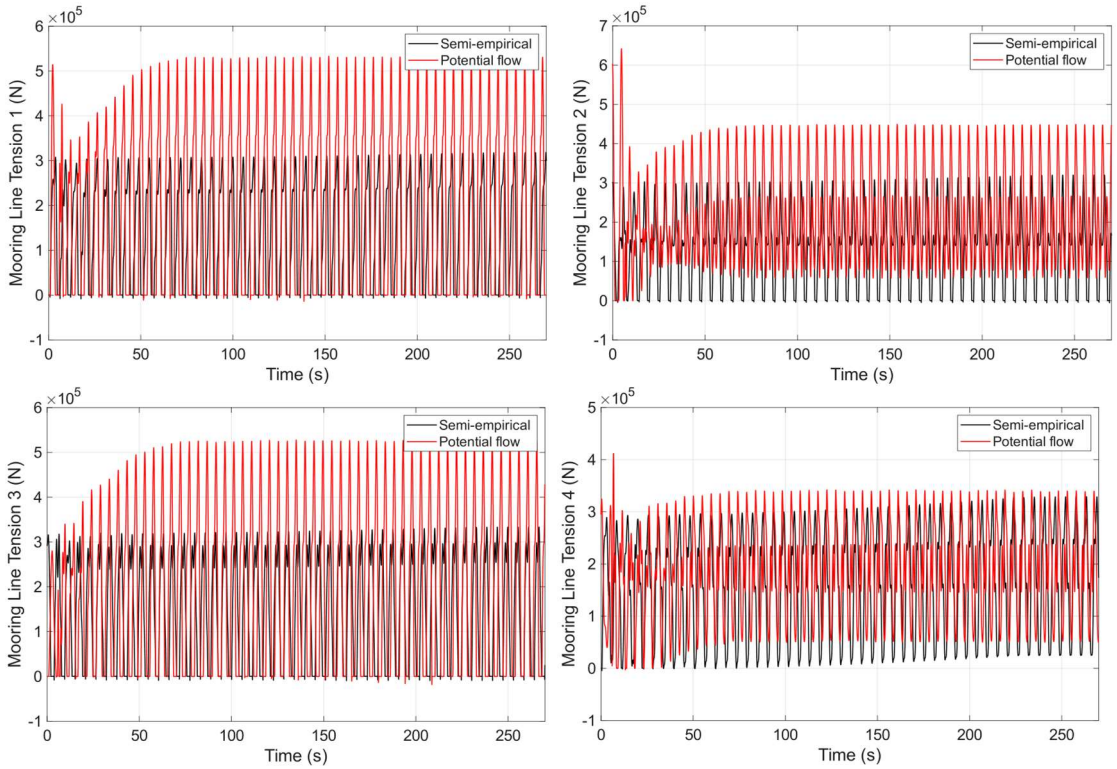


*Figure 5.44 Time-series plots for line tensions in case 2 with critical waves, current and wind from 10° and free in 6DOF.*

Figure 5.44 shows the line tensions for the arrangement assessed. It is seen that in the semi-empirical method all the lines have occurrence of snap loads, while in the potential flow solution, only lines 1 and 3 (the lines at the stern of the barge) have snap loads. The peak values of tensions obtained in lines 1 and 3 have a difference of ~200 kN as well, which presents a significant difference.

### 5.3.3 Summary of case 2

*Table 5.*10 *Difference ($T_{Potential\ Flow} - T_{semi\text{-}empirical}$) in peak and mean mooring line tensions calculated by the two methods with base and critical waves, current and wind from 0° (head).*

| | Mean Tensions | | Peak Tensions | |
|---|---|---|---|---|
| | Base | Critical | Base | Critical |
| Line 1 | | | | |
| ΔT (kN) | 3 | 20 | -5 | 50 |
| Line 2 | | | | |
| ΔT (kN) | 2 | 30 | -5 | 60 |
| Line 3 | | | | |
| ΔT (kN) | 0 | 20 | 0 | 40 |
| Line 4 | | | | |
| ΔT (kN) | 0 | 30 | -3 | 50 |

*Table 5.11 Difference ($T_{Potential\ Flow} - T_{Semi\text{-}empirical}$) in peak and mean mooring line tensions calculated by the two methods with base and critical waves, current and wind from 10° (oblique).*

| | Mean Tensions | | Peak Tensions | |
|---|---|---|---|---|
| | Base | Critical | Base | Critical |
| Line 1 | | | | |
| ΔT (kN) | 0 | 110 | -75 | 210 |
| Line 2 | | | | |
| ΔT (kN) | 0 | 70 | -70 | 140 |
| Line 3 | | | | |
| ΔT (kN) | -7 | 80 | -90 | 200 |
| Line 4 | | | | |
| ΔT (kN) | -10 | 10 | -92 | 10 |

The motion responses and line tensions predicted by both methods are comparable in the case of environmental conditions acting from head direction, both in the base and critical environmental directions. However, the with oblique environmental conditions, the response had significant differences in motion as well as the line tensions. Similarities in motion responses between oblique and beam environmental loads means that the discrepancies observed in line tensions for oblique case will be similar for beam environmental conditions as well. Table 5.10 and Table 5.11 outlines the differences in mean and peak line tensions calculated in case 2.

## 5.4 Effect of quay wall in mooring

An interesting aspect of mooring that can be explored through these simulations is the effect of having a quay wall. Potential flow simulations carried out for the case with quay (case 3, Figure 5.46) is compared with the results from case without quay (case 2). Due to lack of models that account for wave reflections and bank effects in the semi-empirical method studied, the physical phenomena related to quay wall is overlooked. Hence, the results would be identical to the cases without quay. Consequently, only the results from the potential flow method are discussed in this section.

Figure 5.45 shows the motion responses obtained from the potential flow simulations for a base environmental condition acting at zero degree, i.e., parallel to the quay and ship centreline for case 2 and 3. For case 3 (with quay), the convergence is not fully achieved yet and the simulation needs to be run for longer physical time. However, the overall behaviour of the ship can be perceived within the presented simulation results time window. It is clearly seen that adding a quay wall has resulted in more significant motion responses in all degrees of freedom. The difference is most notable in the sway, roll and yaw motions.

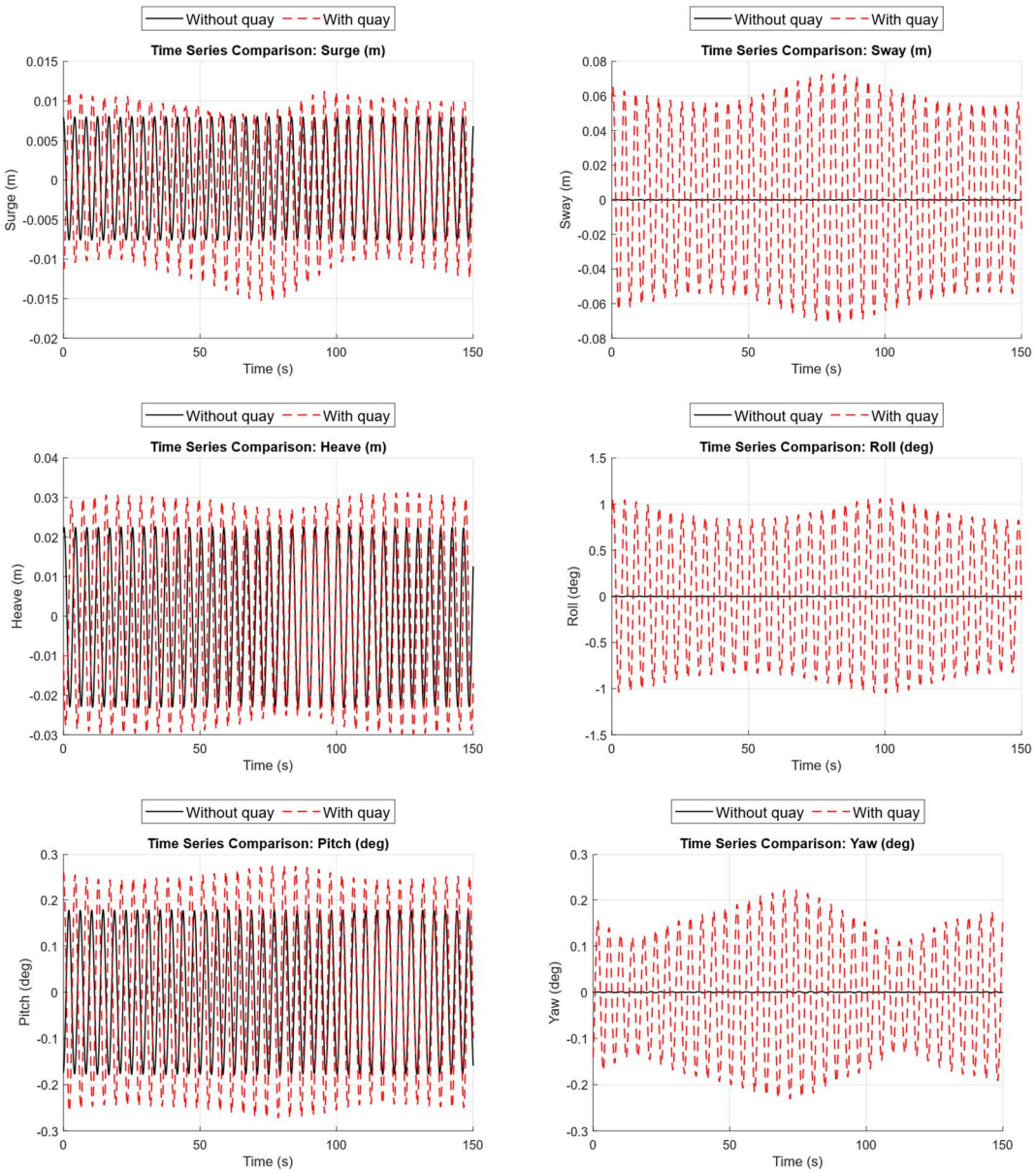


*Figure 5.45 Time-series comparison between case 2 and case 3 (without quay and with quay) with base waves, current and wind from 0°.*

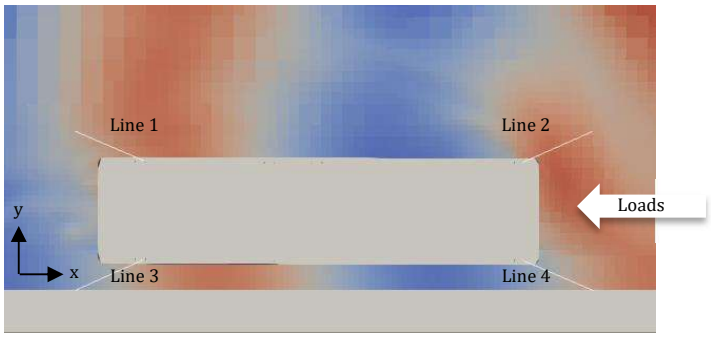


*Figure 5.46 Mooring arrangement with quay – case 3 (image from Shipflow Motions).*

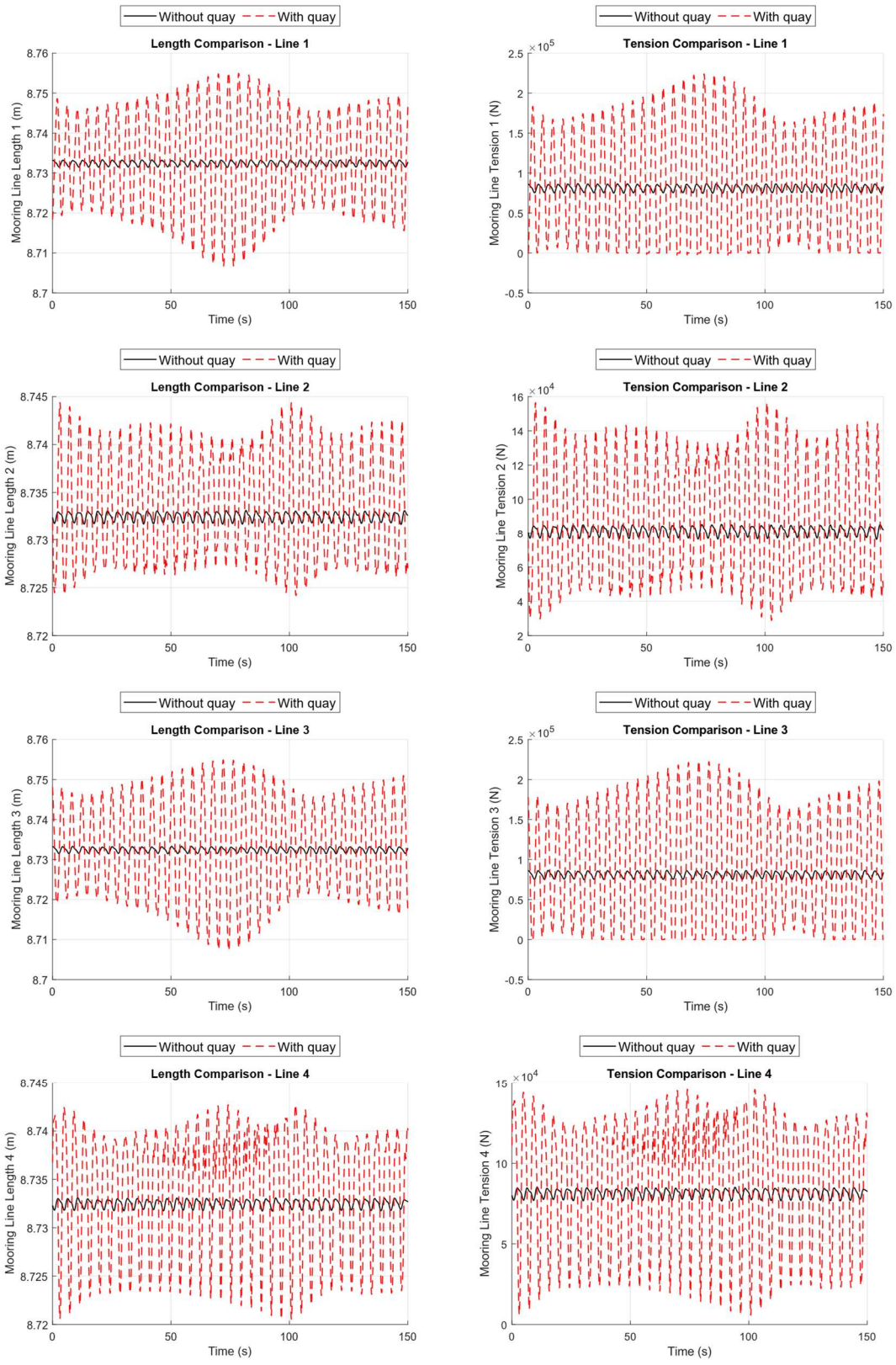


*Line length* *Line tensions*

*Figure 5.47 Time-series of lines lengths (left) and lines tensions (right) compared between case 2 (without quay) and case 3 (with quay) with base waves, current and wind from 0° (head).*

Figure 5.47 shows the line lengths and tensions corresponding to the motion responses shown in Figure 5.45. The tensions calculated in case 3 reach up to three times the value obtained in case 2 (Figure 5.47). Figure 5.48 shows a smaller time window, of the motion response and the length and line tensions of line 1 offering a closer look to understand the response.

It is seen from the plots, in Figure 5.48, that the differences in peak values for surge, heave and pitch motions are small (~0.005 m & 0.1 degrees) and the most difference is observed in sway (~0.06 m), roll (~0.7 degrees) and yaw (~0.2 degrees). In the case of line 1, these differences result in a difference of ~0.018 m, in the length calculated. The high stiffness of the mooring line causes an increase in tension of 6.3 kN even for a stretch of 0.001 m. Hence, we see a large increase in the tension. It can also be observed that the motions lead to the rope being slack (zero tension). This results in snap loads.
Although the mean value of tension in line 1 shows an increase of just ~8.5kN, the peak tensions are vital in the assessment of the mooring safety.

Similar observations have been made for loading scenarios at 10°, and the differences in peak and mean values of tensions for all the lines have been presented in Table 5.12. It is seen that there is close to 10% difference in the tensions in both 0° and 10° simulations.

*Table 5.12 Absolute and percentage differences in peak and mean mooring line tensions for simulations without quay and with quay with base waves, current and wind from 0° (head) and 10° (oblique).*

| | Peak Tensions | | Mean Tensions | |
|---|---|---|---|---|
| | 0° | 10° | 0° | 10° |
| Line 1 | | | | |
| ΔT (kN) | 137.47 | 122.63 | 8.48 | 9.43 |
| ΔT (%) | 158.21 | 135.40 | 10.45 | 11.59 |
| Line 2 | | | | |
| ΔT (kN) | 71.29 | 60.44 | 6.20 | 7.19 |
| ΔT (%) | 83.52 | 69.35 | 7.63 | 8.81 |
| Line 3 | | | | |
| ΔT (kN) | 136.66 | 126.12 | 6.07 | 7.24 |
| ΔT (%) | 157.89 | 142.91 | 7.49 | 8.96 |
| Line 4 | | | | |
| ΔT (kN) | 60.89 | 50.57 | 7.92 | 9.03 |
| ΔT (%) | 71.49 | 59.58 | 9.74 | 11.14 |

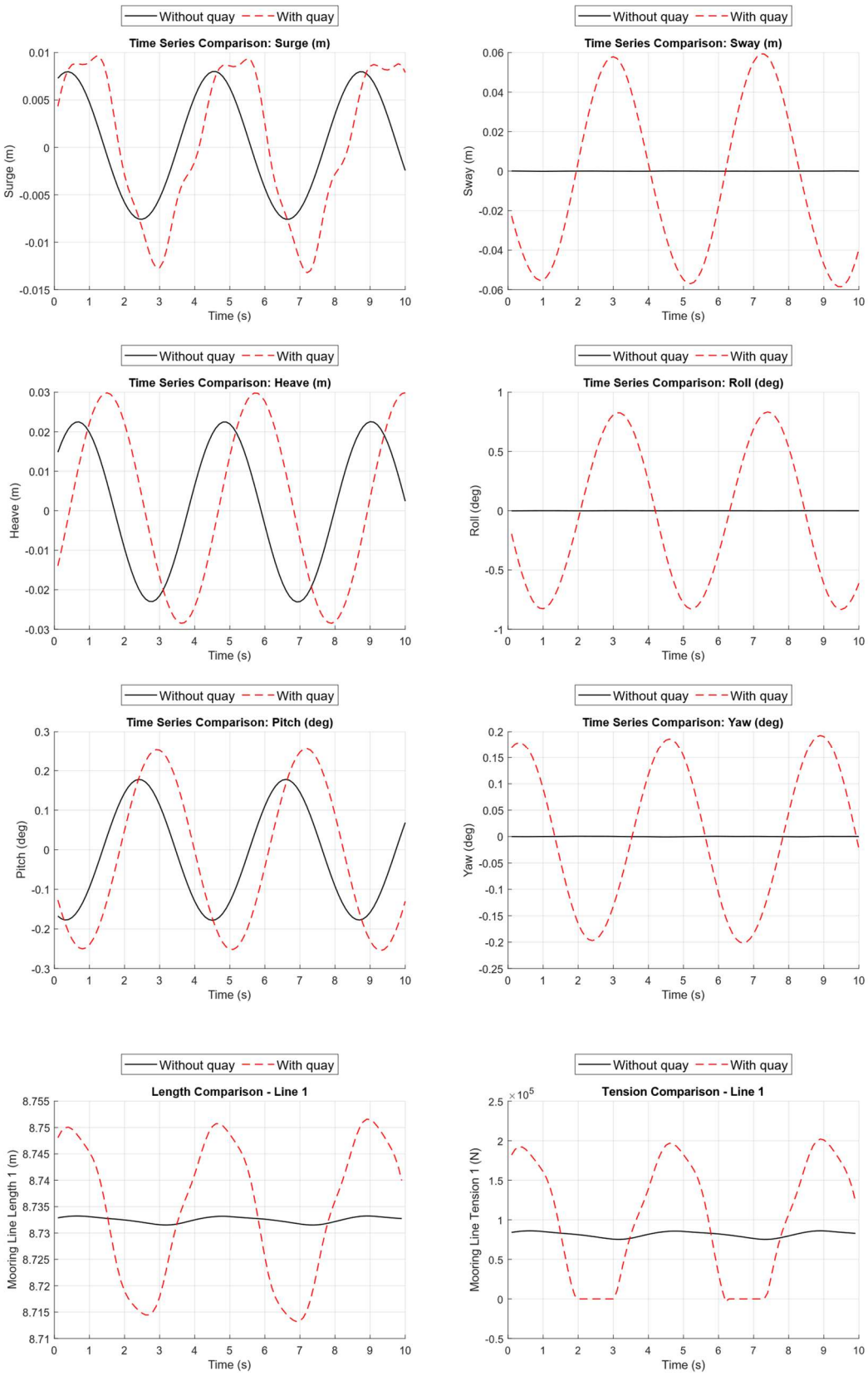


*Figure 5.48 Time-series of responses and line length (line 1 for example) compared between case 2 and case 3 with base waves, current and wind from 0° (head) and free in 6DOF.*

# 6 Conclusions

A comparative study of two time-domain simulation methods, namely the potential flow method and a semi-empirical method (based on strip theory and Lewis formulations), was carried out. The study was carried out with the intent to assess their application in predicting vessel responses and line tensions in scenarios involving just mooring lines and in scenarios with mooring lines and a quay wall in proximity.

The study conducted so far was split into two parts, firstly the comparison of the hydrodynamic modelling of the test cases and secondly the comparison of the mooring calculations performed. The hydrodynamic model based on the semi-empirical method predicted the motion responses with reasonable accuracy, matching reasonably the results obtained using potential flow method. The slight difference in the predicted response from the potential flow simulation came at the expense of significantly higher computational resources and/or simulation time. However, as experimental data is not considered, it is not possible to ascertain the true accuracy of either result. There are also several factors associated with different environmental conditions, that have been described in Section 2.2, that are not fully accounted for in either method or even in both methods studied here. This can be better understood by performing experimental validation. However, the assessment proved useful in ensuring the conformity of the methods, in laying out a base condition on which mooring assessments could be based.

It was also found from the comparison of mooring arrangements with just two mooring lines and four mooring lines that the methods produced comparable line tensions in cases with environmental conditions acting from 0° (head). However, the responses and the line tensions calculated had significant differences when environmental conditions were acting from an oblique direction.

Although simulations were not carried out for vessels moored at berth, it was found from the study of the underlying code that the semi-empirical model does not account for additional effects offered by the presence of the quay such as the bank/cushion effects or reflected waves. Hence, these effects are also to be accounted for in the code for further comparison with the potential flow simulations.

A comparison between potential flow simulation results for a vessel at open sea and that for a vessel at berth showed that the presence of a quay wall greatly influenced the calculated motion responses and line tensions. This observation highlights the significant role of quay effects on mooring arrangement and demands further investigation.

# 7 Recommendations for future work

The study gives an insight into the complexity involved in the analysis of a mooring arrangement and the challenges that are involved in developing an accurate and reliable simulation tool. There have been several factors that prevented the formulation of a conclusive study of the mooring problem. This section presents suggestions and recommendations formed based on the study's scope and limitations and furthermore based on the observations and conclusions made.

Lack of accessible experimental data has been a major limitation that prevented validation of the approaches to the mooring problem. Reliable data obtained from field tests or model experiments should be included in further studies to enable an accurate assessment of both methods. CFD simulations could also be used to form better reference results in the absence of experimental data.

The recommendations that arose from this study as to how to use the mooring line module should include the use of the damping force and of accurate line length prediction.

Additionally, both methods considered linear modelling for the line elasticity. Incorporating more advanced modelling for the line dynamics can improve the accuracy of the methods in predicting line tensions and vessel motions. Benchmarking these methods against validated tools such as Optimoor or MoodyMarine would help quantify the deviations and identify possible avenues of improvement.

The semi-empirical model does not account for any hydrodynamic phenomena that could be caused by nearby quay structures. Further studies need to be conducted to quantify and understand these effects and incorporate them into the model. The effect of having fenders on the different responses were also not included in the studies. Moreover, the thesis was limited to simple environmental conditions such as regular waves, steady current and steady wind. However, in practical applications, environmental conditions are rarely steady and have a dynamic nature. The vessel can be subjected to irregular waves, unsteady current and winds with elements of gusts, as the example used in Section 1 highlighted. Fenders are also used when vessels are moored at berth. Further studies conducted on the methods could benefit from the application of such environmental conditions and arrangements.

In conclusion, while the study provides valuable insights into two approaches to the mooring problem, further research is essential to address the current limitations and form a holistic evaluation.

# 8 References


Aarsnes, JV, Odd M. Faltinsen, and B. Pettersen. 1985. "Application of a vortex tracking method to current forces on ships." Proceedings of Proc. Conf. Separated Flow around Marine Structures, Trondheim.

Biran, Adrian, and Rubén López-Pulido. 2003. Ship hydrostatics and stability. Elsevier.

Bomze, Herman. 1974. "Analytical determination of ship motions and mooring forces." Offshore Technology Conference.

BSI. 2007. “Maritime Structures. Part 8- Code of practice for the design of Ro-Ro ramps, linkspans and walkways”. British Standards Institution.

BSU. 2025. ”Autotransporter ENDURANCE – Kontakt mit Pier/Trockendock in Folge eines Leinenbruchs in Bremerhaven am 13. März 2021”. Bundesstelle für Seeunfalluntersuchung (Hamburg). Translated title: ”Car carrier ENDURANCE – Contact with pier/dry dock as a result of a line breakage in Bremerhaven on 13 March 2021”.

Bureau Veritas. 2022. “NI691 Environmental Conditions, Loads and Induced Responses of Marine Units” | Marine & Offshore. In NI691, edited by Bureau Veritas.

Costa, Fernando Vasco. 1987. "Historical Development of Berthing and Mooring." Advances in Berthing and Mooring of Ships and Offshore Structures 146.

Dong, Guohai , Mingyu Yan, Zhenjun Zheng, Xiaozhou Ma, Zhongbin Sun, and Junliang Gao. 2022. "Experimental investigation on the hydrodynamic response of a moored ship to low-frequency harbor oscillations." Ocean Engineering 262: 2-14.

Faltinsen, Odd M. 1990. “Sea Loads on Ships and Offshore Structures”. Edited by Cambridge University Press. 1st ed. Ocean Technology Series, edited by Cambridge University Press.

Faltinsen, Odd M., and Jikun You. 2015. "A numerical investigation of second-order difference-frequency forces and motions of a moored ship in shallow water." Journal of Ocean Engineering and Marine Energy 1: 157-179.

FLOWTECH International AB. 2025. “Shipflow MOTIONS 8.0 User's Manual”.

Fylling, Ivar J, and Frank Andersson. 1988. "Simulation of Motions of Berthed Vessels-Simplified Simulation Model." Advances in Berthing and Mooring of Ships and Offshore Structures: 298-303.

Isherwood, RM. 1973. "Wind resistance of merchant ships." Trans. RINA 115: 327-338.

ISO. 2015. “Petroleum and natural gas industries — Specific requirements for offshore structures (Part 1)” - ISO 19901-1:2015.

ITTC. 2014. “Analysis of Speed/Power Trial Data”. ITTC - Recommended Procedures and Guidelines. International Towing Tank Conference.

Kaplan, Paul, and Alfred Raff. 1972. Evaluation and Verification of Computer Calculations of Wave-Induced Ship-Structural Loads. Department of the Navy (U.S. Coast Guard Headquarters, Washington D.C.).

Kuzu, Ali, and Ozcan Arslan. 2017. "Analytic Comparison of Different Mooring Systems." IAMU AGA 2017, Varna, Bulgaria.

Kwan, CT, and FJ Bruen. 1991. "Mooring line dynamics: comparison of time domain, frequency domain, and quasi-static analyses." Offshore Technology Conference.

Marine Fenders International Inc. 2025. Ocean Guard™ Standard Capacity Foam Filled Fenders. edited by Marine Fenders International. from https://www.marinefendersintl.com/wp-content/uploads/OCEAN-GUARD-STANDARD-CAPACITY-FOAM-FILLED-FENDER-Netless-Foam-Filled-Fenders.pdf. Accessed on 5/5/2025.

Maritime Injury Center. 2024. "Mooring Line Accidents and Injuries." Last Modified 2024/09/12. Accessed 2025/02/03. https://www.maritimeinjurycenter.com/accidents-and-injuries/mooring-line/.

Muga, Bruce J. 1971. "Experimental and theoretical study of motion of a moored barge." Society of Petroleum Engineers Journal 11 (3): 206-214.

OCIMF. 1977. “Prediction of Wind and Current Loads on VLCCs”. Witherby.

OCIMF. 2018. "Mooring Equipment Guidelines 4” (MEG4). https://www.ocimf.org/publications/books/mooring-equipment-guidelines-meg4.

Papanikolau, Apostolos. 2014. Ship Design – “Methodologies of Preliminary Ship Design”. Springer.

PIANC, MarCom WG-24. 1995. “Criteria for movements of moored ships in harbours - a practical guide” - PIANC. https://www.pianc.org/publication/criteria-for-movements-of-moored-ships-in-harbours-a-practical-guide/.

PIANC, MarCom WG-33. 2002. "Guidelines for the design of fender systems." Brussels, Belgium: PIANC ISBN-2-87223-125-0.

RISE. 2016. “Seaman Reference Manual”.

Rosa-Santos, P, F Taveira-Pinto, and F Veloso-Gomes. 2014. "Experimental evaluation of the tension mooring effect on the response of moored ships." Coastal Engineering Journal 85: 60-71. https://doi.org/10.1016/j.coastaleng.2013.11.012.

Soares, Carlos Guedes, and Serge Sutulo. 2011. "Mathematical models for simulation of manoeuvring performance of ships." In Marine Technology and Engineering, edited by C. Guedes Soares et al, 661-698. London: Taylor & Francis Group.

Sakakibara, Shigeki, and Masayoshi Kubo. 2008. "Effect of mooring system on moored ship motions and harbour tranquillity." International Journal of Ocean Systems Management 1 (1): 84-99.

Samson Rope. (2024). "Rope - Proton8." from https://www.samsonrope.com/mooring/proton--8. Accessed on 1/05/2025.

Sarkar, Nilarghya, and Aparna Dey Ghosh. 2022. "Comparative study on response of jacket platforms under regular waves using Airy's and Stokes' fifth-order wave theories." ASPS Conference Proceedings.

Trelleborg Marine and Infrastructure. 2020. "Fender systems - Product Brochure". In Fender Systems, edited by Trelleborg. Trelleborg.

UK P&I CLUB. 2009/01 2009. "Understanding mooring incidents". https://www.ukpandi.com/fileadmin/uploads/ukpandi/Documents/imports/13108/bulletins/2937-understandingmooringincidents.pdf.

van der Molen, W, P Monárdez, and A van Dongeren. 2006. "Numerical simulation of long-period waves and ship motions in Tomakomai port, Japan Coastal Engineering Journal 48 (1): 59-79.

Wang, Jian, and Jackyou Noh. 2022. "Calculating the Mooring Force of a Large LNG Ship based on OCIMF Mooring Equipment Guidelines." Journal of the Korean Society of Marine Environment & Safety 28 (4): 594-600.

Wichers, Johan E.W. , and Jan O. de Kat. 1991. "Behavior of a moored ship in unsteady current, wind and waves." Marine Technology 28 (5): 251-264. https://doi.org/10.5957/mt1.1991.28.5.251.

Ziylan, K, and S Nas. 2024. "A quasi-static mooring analysis approach for berthed ships." Ocean Engineering 309. https://doi.org/10.1016/j.oceaneng.2024.118488.

DEPARTMENT OF MECHANICS AND MARITIME SCIENCES
DIVISION OF MARINE TECHNOLOGY
CHALMERS UNIVERSITY OF TECHNOLOGY
Gothenburg, Sweden 2025
www.chalmers.se


CHALMERS
UNIVERSITY OF TECHNOLOGY